National Library of Canada
Bibliothèque nationale du Canada

Canadian Theses Service
Service des thèses canadiennes

Ottawa, Canada
K1A 0N4

NOTICE

The quality of this microform is heavily dependent upon the quality of the original thesis submitted for microfilming. Every effort has been made to ensure the highest quality of reproduction possible.

If pages are missing, contact the university which granted the degree.

Some pages may have indistinct print especially if the original pages were typed with a poor typewriter ribbon or if the university sent us an inferior photocopy.

Reproduction in full or in part of this microform is governed by the Canadian Copyright Act, R.S.C. 1970, c. C-30, and subsequent amendments.

AVIS

La qualité de cette microforme dépend grandement de la qualité de la thèse soumise au microfilmage. Nous avons tout fait pour assurer une qualité supérieure de reproduction.

S'il manque des pages, veuillez communiquer avec l'université qui a conféré le grade.

La qualité d'impression de certaines pages peut laisser à désirer, surtout si les pages originales ont été dactylographiées à l'aide d'un ruban usé ou si l'université nous a fait parvenir une photocopie de qualité inférieure.

La reproduction, même partielle, de cette microforme est soumise à la Loi canadienne sur le droit d'auteur, SRC 1970, c. C-30, et ses amendements subséquents.

NL-339 (r. 88/04) c

Canada

UNIVERSITY OF ALBERTA

SIMULATION OF THE DYNAMIC BEHAVIOR OF A HYDRONIC FLOOR HEATING SYSTEM

BY

SHUK-YEE HO

A THESIS

SUBMITTED TO THE FACULTY OF GRADUATE STUDIES AND RESEARCH

IN PARTIAL FULFILLMENT OF THE REQUIREMENTS FOR THE DEGREE

OF

MASTER OF SCIENCE

IN

PROCESS CONTROL

DEPARTMENT OF CHEMICAL ENGINEERING

EDMONTON, ALBERTA

FALL, 1992

National Library of Canada
Bibliothèque nationale du Canada

Canadian Theses Service
Service des thèses canadiennes

Ottawa, Canada
K1A 0N4

The author has granted an irrevocable non-exclusive licence allowing the National Library of Canada to reproduce, loan, distribute or sell copies of his/her thesis by any means and in any form or format, making this thesis available to interested persons.

L'auteur a accordé une licence irrévocable et non exclusive permettant à la Bibliothèque nationale du Canada de reproduire, prêter, distribuer ou vendre des copies de sa thèse de quelque manière et sous quelque forme que ce soit pour mettre des exemplaires de cette thèse à la disposition des personnes intéressées.

The author retains ownership of the copyright in his/her thesis. Neither the thesis nor substantial extracts from it may be printed or otherwise reproduced without his/her permission.

L'auteur conserve la propriété du droit d'auteur qui protège sa thèse. Ni la thèse ni des extraits substantiels de celle-ci ne doivent être imprimés ou autrement reproduits sans son autorisation.

ISBN 0-315-77050-3

Canada

UNIVERSITY OF ALBERTA

RELEASE FORM

NAME OF AUTHOR:	Shuk-Yee Ho
TITLE OF THESIS:	Simulation of the Dynamic Behavior of a Hydronic Floor Heating System
DEGREE:	Master of Science
YEAR THIS DEGREE GRANTED:	1992

Permission is hereby granted to the University of Alberta Library to reproduce single copies of this thesis and to lend or sell such copies for private, scholarly or scientific purposes only.

The author reserves all other publication and other rights in association with the copyright in the thesis, and except as hereinbefore provided neither the thesis nor any substantial portion thereof may be printed or otherwise reproduced in any material form whatever without the author's prior written permission.

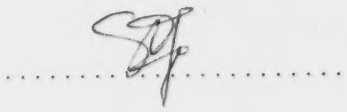

ADDRESS:

Rm 522, Chung Man House,
Oi Man Estate,
Kowloon,
Hong Kong

Date: August 19, 1992

UNIVERSITY OF ALBERTA

FACULTY OF GRADUATE STUDIES AND RESEARCH

The undersigned certify that they have read, and recommend to the Faculty of Graduate Studies and Research for acceptance, a thesis entitled

Simulation of the Dynamic Behavior of a Hydronic Floor Heating System

submitted by Shuk-Yee Ho in partial fulfillment of the requirements for the degree of Master of Science in Process Control.

.....
Dr. R.K. Wood
(Supervisor)

.....
Dr. J.D. Dale
(Mechanical Engineering)

.....
Dr. R.E. Hayes
(Chemical Engineering)

Date: August 19, 1992

To my parents and sister

Abstract

One type of heating system, common in Europe but not in North America, is the hydronic floor heating system. This type of system provides heat by circulating hot water through tubing embedded directly in the concrete floor for basement heating. For floors at other levels, usually the tubing is contained in a layer of gypsum cement on top of the subflooring.

The initial development for obtaining a dynamic model for the hydronic floor heating system involved numerical solutions for only a single pipe/tube. Simulated steady state temperature profiles and transient responses using simple models (half-pipe and one-pipe models) are given. The simple models considered only tubing in a layer of gypsum cement and did not allow for computation of outlet water temperature and backside heat loss to the soil. Since such a simple model could not represent the system installed in one of the experimental houses of the Alberta Home Heating Research Facility, a detailed model was developed. As the system in the experimental house is a composite panel consisting of gypsum cement, as the top layer, containing embedded 1.3 cm diameter tubes in a parallel layout, insulation in the middle on top of the concrete floor, a detailed model was developed to represent this system.

The full model incorporated a two dimensional unsteady state heat conduction for each layer of the composite panel. The three governing differential equations with different thermal diffusivity for each layer model equations were solved numerically because of the nonrectangular domain of the gypsum cement layer and the complicated boundary conditions. Two methods of solution, grid generation and nonuniform grids method were

considered for solving the model equations. The computation time required for the grid generation method for the simple half-pipe model was found to be more than twice the time required for the nonuniform grids approach for a transient response calculation. Furthermore, discretization of the domain because of the complex geometry using grid generation method was not an easy task. Therefore the nonuniform grids with finite difference approach was selected as the most suitable method to solve the model equations. Another alternate method of solution, the finite element approach, was also utilized to solve the full model. The computation time for the finite element approach was one-half the time required for the finite difference simulation when both programs were utilized on an IBM RISC system/6000. The finite element used only 6842 elements while the finite difference method used 19068 grid points.

For a step change in inlet water temperature from 45°C to 55°C, the initial and final steady state surface profiles and the dynamic temperatures response of the two simulation results agreed with each other in terms of trends despite a difference of about one degree Celsius in magnitude between the two simulation results. The small difference between the simulated dynamic temperature responses and the experimental responses was considered to be due to the inaccuracy of parameter values of the combined convective and radiative heat transfer coefficient and the overall heat transfer coefficient and possibly the physical properties of the gypsum cement, as demonstrated by a series of sensitivity simulations.

Two control algorithms, on-off and proportional control, were implemented experimentally for maintaining the basement air temperature in the experimental house at the desired value. A single setpoint test of the on-off and proportional control strategies was performed. No objective comparison of the performance of these two control algorithms was possible because different initial steady state basement air temperatures and different magnitude setpoint changes were used for the tests.

Acknowledgement

I would like to thank Dr. R.K. Wood for his guidance and supervision during the course of my research. In particular, I would like to thank him again for his advice on how to write this thesis and his critical proof-reading of this thesis. My gratitude is also extended to Dr. R.E. Hayes for his generosity in allowing me access to his computer facilities and his modified finite element programs. I also owe much for discussions with him about the simulation. I must take this opportunity to thank Dr. J.D. Dale who suggested me the topic of this thesis and authorized use of the experimental house for collection of experimental data. Special thanks to Mr. Mark Ackerman without whom my experimental work would not have been completed. As well, Mr. Paul Barrow, Mr. Bob Barton and Mr. Henry Sit also deserve many thanks.

My appreciation is also extended to my fellow graduate students: Mary Bourke who gave me lots of help through the course work; Sreekanth Lalgudi and S. Lakshminarayanan who entertained me for so many days and nights; Maina Macharia, Simarjit Dhaliwal, Adam Rankin, Paul Nawrocki and Wellington Kwok who gave me constant support and encouragement; Kun-Yu Kwok and Eric Lau who gave me constant spiritual support and encouraged me when I was depressed with slow progress in my research. My great appreciations are credited to my officemate, Mrs. Hong Lee, with whom I could share my problems.

Special thanks are due to: Cindy Heisler who gave me lots of support and help and my roommate, Marion Mok, who gave her spiritual support through her prayers.

Many thanks are due to my parents and sisters in Hong Kong for their constant support and encouragement over so many years. My gratitude is also extended to Mr. Stephen Ng and Mr. Sau Tsien Lim who went through many difficulties with me.

The financial support from the Department of Chemical Engineering and the Natural Sciences and Engineering Research Council of Canada is gratefully acknowledged.

I am also indebted to the Graduate Students Association which provided me a very comfortable couch so that I had sweet dreams for many nights.

Finally, I must take this opportunity to express my praise to my Lord God who has guided me through many difficulties; Jesus Christ who has strengthened me all the time and the Holy Spirit who has helped me in my weakness.

Table of Contents

1 Introduction **1**
1.1 Background 1
1.1.1 Advantages of Hydronic Floor Heating System 2
1.1.2 Disadvantages of Hydronic Floor Heating System 3
1.1.3 Controversial Issues 3
1.2 Objectives of the Study 4
1.3 Structure of the Thesis 4

2 Literature Review **6**

3 Physical System **20**
3.1 Basement Hydronic Heating System 21
3.1.1 Structure of Panel 21
3.1.2 Layout of Piping 21
3.1.3 Structure of Wall 21
3.1.4 Structure of Ceiling 25
3.2 Data Collection 25
3.2.1 Data with Two-Minute Sampling Time 26
3.2.2 Data with Ten-Minute Sampling Time 27
3.2.3 Additional Data 29
3.3 Data Conversion 30

4 Model for Hydronic Floor Heating System **32**
4.1 Descriptions of Subsystems 32
4.2 Assumptions and Boundary Conditions 34
4.2.1 Subsystem 1 : Heating Panel 34
4.2.1.1 Full Model 34
4.2.1.2 Simple Models 36
4.2.2 Subsystem 2 : Enclosure 39
4.3 Algorithms 41
4.3.1 Description of the Algorithms 41

5 Methods of Solution for the Simple Models **47**
5.1 Half-Pipe Model 47
5.1.1 Discretization and Grid Generation for the Half-Pipe Model 47
5.1.2 Solution Procedure 51
5.1.3 Comparison of Results 54
5.1.4 Evaluation of the Choices of Methods of Solution for Full Model 56
5.2 One-Pipe Model 59
5.3 Conclusion 59

6 Methods of Solution for the Full Model **64**
6.1 Finite Difference Method with Nonuniform Grids 64
6.1.1 Discretization 64
6.1.2 Governing Equations and Boundary Conditions 66
6.2 Finite Element Approach 72

7 Comparison of Experimental and Simulation Results **78**
7.1 Experimental Procedure 78
7.2 Predicted and Experimental Steady State Temperature Profiles and Dynamic Responses Temperature 80
7.2.1 First Test : Shutters Open 80
7.2.2 Second Test : Shutters Closed 91
7.3 Discussion 98
7.4 Effect of Model Parameters 101
7.5 Conclusions 115

8 Experimental Testing of Two Control Laws **116**
8.1 Experimental Equipment 116
8.1.1 Water Temperature Controller 118
8.1.2 Room Temperature Controller 118
8.2 Results 121
8.2.1 On-Off Control 121
8.2.2 Proportional Control 124
8.3 Conclusions 127

9 Summary and Future Work **128**
9.1 Summary 128
9.2 Recommendations for Future Work 130

References **131**

A Example: Calculations for the Parameter Values Used for Simulation **134**

List of Tables

2.1 Literature review of field studies of hydronic floor heating systems (excluding control studies) 7
2.2 Literature review of simulation studies of hydronic floor heating systems 11
2.3 Literature review of control studies of hydronic floor heating systems 15

6.1 The effect of the number of grids in one section on computed temperature 65

7.1 Initial steady state conditions and parameter values for simulation 79

List of Figures

3.1 The cross-sectional view of basement in the experimental house 22
3.2 The two types of tubing layout used in the experimental house 23
3.3 The cross-sectional view of the heating panel 24
3.4 Cross-sectional view of basement 25
3.5 Cross-sectional view of main floor panel and ceiling of the basement 26
3.6 Schematic diagram of water supply system 28
3.7 Interface of the computer and devices 31

4.1 Two subsystems in the experimental house 33
4.2 Labels of boundary conditions for full model 35
4.3 Labels of boundary conditions for half-pipe model 38
4.4 Labels of boundary conditions for one-pipe model 38
4.5 Dynamic response of the joist cavity temperature and glass fibre insulation underside surface temperature in response to a step change to the inlet water temperature from 45°C to 55°C 40
4.6 Flowchart for the computation of room air temperature and outlet water temperature for the full model 42

5.1 Generated grids for a rectangular domain 48
5.2 Half-pipe representation of the heating panel: Mapping of boundary values from (x,y) coordinates to a (ξ,η) coordinates 49
5.3 Mesh using grid generation 51
5.4 Mesh using nonuniform grids method 52
5.5 Notation for nonuniform grids 54
5.6 Temperature distribution for the simple model using grid generation 55
5.7 Temperature distribution for the simple model using nonuniform grids 55
5.8 The response of room air temperature for a step change in average water temperature from 50°C to 60°C 57
5.9 The response of floor surface temperature for a step change in average water temperature from 50°C to 60°C 57
5.10 Mesh using nonuniform grids for one-pipe model 60
5.11 Temperature distribution for one-pipe model 61
5.12 The response of room air temperature for a step change in average water temperature from 50°C to 60°C 62
5.13 The response of floor surface temperature for a step change in average water temperature from 50°C to 60°C 62

6.1 Grid mesh for one section of the domain of the full model 67
6.2 Heat flow at the interface of concrete and insulation layers 70
6.3 Mesh sections for the finite element method 74

7.1 Temperature profiles in the heating panel computed by the finite difference method 81
7.2 Temperature profiles in the heating panel computed by the finite element method 82
7.3 Initial steady state temperature profiles for an inlet water temperature of 45°C (first test) 84
7.4 Final steady state temperature profiles for an inlet water temperature of 55°C (first test) 86
7.5 Temperature dynamic responses for a step change in inlet water temperature from 45°C to 55°C (first test) 89
7.6 Initial steady state temperature profiles for an inlet water temperature of 45°C (second test) 92
7.7 Final steady state temperature profiles for an inlet water temperature of 55°C (second test) 94
7.8 Temperature dynamic responses for a step change in inlet water temperature from 45°C to 55°C (second test) 96
7.9 Solar radiation, upper zone air and outdoor temperatures versus time 100
7.10 Response of system temperatures to a change in the densities and heat capacities of the insulation and concrete 103
7.11 Response of system temperatures to a change in the density and heat capacity of the gypsum cement 104
7.12 Response of system temperatures to a change in the densities and heat capacities of the gypsum cement, insulation and concrete 106
7.13 Response of system temperatures to a change in the thermal conductivity of the concrete 107
7.14 Response of system temperatures to a change in the thermal conductivity of the insulation 108
7.15 Response of system temperatures to a change in the thermal conductivity of the gypsum cement 109
7.16 Response of system temperatures to a change in the thermal conductivity of the soil located under the concrete 111
7.17 Response of system temperatures to a change in the overall heat transfer coefficient 112
7.18 Response of system temperatures to a change in the combined convective and radiative heat transfer coefficient 113
7.19 System temperature dynamic responses for changes in heat loss or gain to the upper zone 114

8.1 Control signal diagram 117
8.2 Proportional action controller 120

8.3 Control performance using an on-off control law for a step change in setpoint from 25°C to 30°C 122
8.4 Control performance using a proportional control law for a step change in setpoint from 21°C to 25°C 125

List of Symbols

A	= floor surface area
$\underline{\underline{A}}$	= nine band unsymmetric matrix
$\underline{\underline{A}}'$	= seven band unsymmetric matrix
ACR	= air change rate (number of changes/hour)
Cp	= heat capacity (J/kg °C)
cycle	= length of cycle used in the proportional control
DT	= time step (s)
DX	= intervals in the x-direction for the finite difference method
DXD	= intervals between T_{ij} and $T_{i-1,j}$ for nonuniform grids
DXL	= intervals between T_{ij} and $T_{i,j-1}$ for nonuniform grids
DXR	= intervals between T_{ij} and $T_{i,j+1}$ for nonuniform grids
DXU	= intervals between T_{ij} and $T_{i+1,j}$ for nonuniform grids
DY	= intervals in the y-direction for the finite difference method
$F^{(e)}$	= force vector for every element for the finite element method
$\underline{F}$	= global vector for the whole domain for the finite element method
$\underline{\underline{F}}$	= transformed matrix of $\underline{\underline{A}}$ for LINPACK software use
$\underline{\underline{F}}'$	= transformed matrix of $\underline{\underline{A}}'$ for LINPACK software use
h	= combined convective and radiative heat transfer coefficient ($W/m^2°C$)
H	= height of the wall in the lower zone
k	= thermal conductivity (W/m°C)
$\underline{\underline{K}}$	= global matrix for the whole domain for the finite element method
$\underline{\underline{K}}^{(e)}$	= stiffness matrix for every element for the finite element method
L1	= distance between node ij and node i,j-1
L2	= distance between node ij and node i,j+1
L3	= distance between node ij and node i+1,j
L4	= distance between node ij and node i-1,j
m	= mass (kg)
$\dot{m}$	= mass flow rate (kg/s)
M	= total number of nodes in the y direction of the heating panel for the finite difference method
n	= number of nodes for an element
$\bar{n}$	= normal vector on the surface of finite element domain
nn	= total number of nodes in x-direction on the surface or bottom of the heating panel
q	= the rate of heat loss or gain (W)
R	= resistance ($m^2°C/W$)

t	= time (s)
T	= temperature (°C)
T(x,y,t)	= temperature distribution in the floor heating panel (°C)
TH	= thickness (m)
UA	= overall heat transfer coefficient multiplied by the area of the four walls in the experimental house (W/°C)
v	= test function used in the variational method
V	= volume (m^3)
Vol	= volume of each element (m^3)
x	= x-coordinate in panel
x_i	= x-coordinate of node i of an element
y	= y-coordinate in panel
y_i	= y-coordinate of node i of an element
Z	= heat transfer coefficient ($W/m^2°C$)

Greek symbols

ξ	= transformed x-coordinate in grid generation
η	= transformed y-coordinate in grid generation
ζ	= transformed z-coordinate in grid generation
ρ	= density (kg/m^3)
α	= thermal diffusivity of material (m^2/s)
Ω	= whole domain of heating panel
Ω^e	= domain of element
Γ	= boundary of whole domain
Γ^e	= boundary of element
ψ	= shape function or interpolation function
ψ_i	= interpolation function of node i in element

Subscripts

accum	= energy accumulation
air	= air in the enclosure
amb	= ambient (outdoor) temperature
aveb1	= average temperature at the bottom surface of the insulation layer
aveco	= average temperature at the bottom surface of the concrete
aveu1	= average temperature on the top surface of the insulation layer
bot	= bottom surface of the panel
ceil	= ceiling
flue	= heat exchange rate between the enclosure and the outdoor through the flue
foil	= aluminium foil
H	= upper tolerance of room air temperature setpoint

i	= index for the location of nodes, y-direction for finite difference method, x-direction for finite element method
in1	= interface between the concrete and insulation layers
in2	= interface between the gypsum cement and insulation layers
inbj (j=1,2,3)	= three different locations at the bottom surface of the insulation layer
input	= total heat energy for the complete system
inuj (j=1,2,3)	= three different locations on the top surface of the insulation layer
j	= index for the location of nodes, x-direction for finite difference method, y-direction for finite element method
joist	= joist cavity
L	= lower tolerance of room air temperature setpoint
loss	= heat transfer from the heating panel to the soil (T_{s1})
o	= updated total heat energy for the complete system required for the computation of the outlet water temperature in the iteration method
p1	= gypsum cement
p2	= insulation
p3	= concrete
r	= room air temperature (basement air temperature)
rset	= room air temperature setpoint
s1	= soil located under the heating panel
s2	= soil located around the north wall
set	= setpoint
soj(j=1,2,3,4)	= four different locations at 0.33m below the concrete
surf	= top surface of the panel
und	= backside of the insulation
up	= heat transfer from the heating panel to the enclosure
w	= water temperature at pipe surface
wi	= water at the inlet of the tubing
wo	= water at the outlet of the tubing
wset	= water temperature setpoint

Superscripts

(k)	= current discrete time

CHAPTER 1
Introduction

1.1 Background

Hydronic heating systems have been employed in Europe for several decades (Leigh, 1991b). Despite interest in hydronic heating systems in North America dating back to the late 1960's, only in the last few years has there been renewed interest in the actual installation of such systems. The two major types employ either floor or ceiling heating. However, in this thesis, only the more common hydronic heating system, with the floor surface temperature controlled by circulating warm water through pipes imbedded in a floor panel, will be considered. The heated floor surface or panel transfers heat to a room by convection and radiation. Since the controlled surface temperature is not very high, less than 28°C, (Grammling, 1985), the principle mode of heat transfer is convection. Advocates of hydronic heating systems think that conventional forced air heating systems should be replaced by hydronic floor heating system since these systems give nearly an ideal vertical air temperature profile and even heating over the entire floor area. However, there are still several drawbacks inherent to floor heating systems. This thesis is concerned with analyzing some operational and control aspects of such systems, particularly the control of such systems.

1.1.1 Advantages of Hydronic Floor Heating System

A. Thermal comfort

One of the major reasons for the renewed interest in hydronic heating systems is that such a system can provide ideal thermal comfort. Since most people have poor blood circulation at the feet and higher body temperature at the head level, personal comfort can be enhanced if the system provides a warm temperature at floor level, and cooler air temperature at the head level (Rekken, 1983). Hydronic floor heating systems meet these requirements because the floor panel is the heat source. Furthermore, unlike a conventional forced air heating system, the hydronic floor heating system gives a gentle temperature gradient from floor to ceiling. This moderate temperature gradient minimizes stratification of heated air so thermal comfort is enhanced.

B. Energy savings

Some reports have indicated that hydronic heating "can reduce energy costs by 30 percent or more with equal comfort" (Buckley, 1989). Since the whole floor surface is a large thermal delivery area, the system can operate at low water temperature due to its capacity. Moreover, since comfort can be maintained at a lower air temperature and higher mean radiant temperature with a hydronic heating system than with a forced air heating system, this lower air temperature and higher mean radiant temperature heating operation leads to lower heating demand which directly results in a reduction in energy costs.

C. Flexibility and space savings

Since systems require a warm water temperature of about 65°C, any domestic hot water source can be used. Furthermore, building space can be conserved because the actual system uses "only a few square feet of floor area for manifolding and control modules" (Friedlander, 1986).

1.1.2 Disadvantages of Hydronic Floor Heating System

A. Limitation of maximum heat load

In order to maintain human comfort at floor level, the system cannot be allowed to operate beyond the maximum surface temperature typically considered to be about 28°C. This means that regardless of the installed heating capacity the heat input is limited by the maximum panel surface temperature. It is therefore extremely important that buildings that use such systems be well-insulated so optimum temperature conditions can be maintained.

B. Limited choice of floor covering

If high resistance floor coverings are used to cover the panel, then heat transfer to the room will decrease and back losses will increase so highly conductive floor coverings should be used with a hydronic floor heating system to maximize heat transfer to the room. Dale and Ackerman (1990) report back losses from an uncovered basement floor panel, consisting of gypsum cement with imbedded tubes, with 2.5 cm thick polystyrene insulation below the panel plus 10 cm of concrete, to be 15-20 percent of the total energy input.

C. Difficulty of control

Since the heating panel stores a large amount of thermal energy, control of hydronic floor systems is not well understood. Because of the energy storage in the panel, which results in heating and cooling periods of several hours, the possibility of employing a night time set-back control strategy is very limited (ASHRAE Handbook, 1977). Furthermore, in order to avoid discomfort suitable control strategies are required to minimize temperature fluctuation.

1.1.3 Controversial Issues

As mentioned previously, one of the reasons for the growing popularity of hydronic floor heating systems is the reported energy saving compared with the energy

consumption of conventional forced air heating systems. However, Dale and Ackerman (1990), based on an experimental study, found that "neither form of heating system had a distinct advantage in terms of energy efficiency". The advertising literature for floor systems states that the air temperature will range from 24°C to 15°C. Dale and Ackerman did not find this to be the case. These workers found that hydronic floor heating "produced vertical temperature profiles that were very uniform from very near the floor to ceiling top". These experimental results confirmed similar earlier results of Algren et al., 1954. Dale and Ackerman found the maximum temperature difference between the floor and ceiling to be only about 3°C.

1.2 Objectives of the Study

The dynamic response of room air temperature for buildings heated using a hydronic floor heating system, due to the large energy storage capacity in the floor panel, either during heating or cooling is very slow. For this reason, control strategies for this type of system must differ from those of forced air heating systems. A two-dimensional unsteady state model of a heating panel is required to predict the dynamic and control behaviour of a hydronic floor heating system. Such a model is developed in this thesis. Numerical simulation results are compared with experimental dynamic data collected from one of the experimental houses at the Alberta Home Heating Research Facility to validate the model. Experimental results from a preliminary investigation of the use of different strategies for control of basement air temperature at the experimental house are included.

1.3 Structure of the Thesis

The content of the thesis is as follows.

Chapter 2 reviews studies of hydronic heating systems particularly modelling and control studies.

Chapter 3 describes the hydronic floor heating system as well as the dimensions and structure of the experimental house and its associated instrumentation.

Chapter 4 discusses the characteristics of the two simple models and of the full model, boundary conditions and parameter values for each model.

In Chapter 5, two different numerical methods of solution for the simple models are presented and simulation results from both methods compared to establish the method to be used for subsequent simulations.

Chapter 6 provides details of the two different numerical techniques that can be utilized to solve for steady state and unsteady state information using the full model.

In Chapter 7, a comparison of simulated results using both the finite element and the nonuniform grids with finite difference approach with experimental data presented. Steady state temperature profiles and the dynamic temperature responses are shown as well as simulation results to demonstrate the sensitivity of system responses to changes in parameters and physical property values.

Chapter 8 contains the results of the preliminary evaluation of different control strategies for the experimental house. Experimental results to demonstrate the performance of on-off and proportional control algorithms are given.

A summary of the work, results and recommendations for future work are provided in Chapter 9.

CHAPTER 2
Literature Review

During the 1940's, there was strong interest towards the use hydronic floor heating system, mainly due to its cost efficiency. In the early stages of development most studies, summarized in Table 2.1, were concerned with the dynamic response of the heating system through field studies. Some investigations were concerned with thermal control strategies and implementation, as well as the benefits and advantages of such systems. Later as development progressed, Hulbert et al. (1950) used analytical solutions to describe the heat flow within a heated panel under steady state conditions. During the 1970s and 1980s, several simulations studies on transient response of hydronic heating system were conducted. A brief description of the studies, listing assumptions, limitations and methods of solution for each model can be found in Table 2.2. Recently, MacCluer (1989) proposed a new control strategy called flux modulation to provide instantaneous response to changes of internal and external disturbances. A summary of his work as well as that of previous investigations of other workers is provided in Table 2.3.

Table 2.1
Literature review of field studies of hydronic floor heating systems (excluding control studies)

Author(s)	Date	Nature of Study
A.B. Algren	1948	**Scope:** Insulation within a footing wall and none in the other in a house with no basement. **Results:** **i)** The heat lost through the uninsulated footing was much greater than through the other wall. **ii)** The effect of the insulation was negligible for the summer period because the insulated footing wall had similar heat lost to the one uninsulated wall.
J.M. Ayres B.W. Levy	1948	**Scope:** Investigated the temperature gradient from floor to ceiling. **Results:** **i)** Uniform air temperatures occurred from 0.3 m above floor to 0.3 m below ceiling.
A.B. Algren Ben Ciscel	1949	**Scope:** Studied the transient response of floor heating system. **Results:** **i)** The response of room air temperature lagged the panel surface temperature by 1.25 hour. **ii)** In contrast to common belief, the mean radiant temperature (MRT) and room air temperature differed by only about 1°C.

C.M. Humphreys C.V. Franks L.F. Schutrum	1951	**Scope:** Determined the order of magnitude of backward heat loss for heating panel (slab) and studied effectiveness of insulation to reduce heat loss. **Four houses** -- Each equipped with "slab on grade heating". Each slab was 0.1 m in thickness, with a vapour barrier below the slab. The material and / or the configuration of the material differed for each installation as follows **No.1** -- Gravel fill of 0.48 m in depth. **No.2** -- Hollow clay tile of 0.1 m thickness on 0.36 m of gravel fill. **No.3** -- Cellular glass block of 0.05 m thickness below vapour barrier for entire floor and on top of foundation; gravel fill to a depth of 0.36 m. **No.4** -- Cellular glass block of 0.05 m thickness only 1.07 m in width around house perimeter and on inside of frame wall; gravel fill of 0.48 m depth except 0.43 m below perimeter glass block. Heating coil: sinuous, 0.01 m copper tubing spaced at 0.23 m centres. **Results:** **i)** House #4 had the lowest heat loss to the ground. **ii)** Results were not reliable because of different sizes of family and different floor coverings in the four houses.
F.W. Hutchinson D.L. Mills L.J. La Tart	1951	**Scope:** Investigated how much back heat loss to the ground in a hydronic floor heating system. **Results:** **i)** Edge and back heat losses were found to be about 30 percent of total heat input. **ii)** It was concluded that insulation was required with that type of heating system.

Z. Zhang	1986	**Scope:** Performed transient experiments on a radiant panel ceiling system. The system consisted of 0.01 m copper tubes, at 0.15 m spacing, embedded in a plaster ceiling. The supply-return lines were run parallel and counterflow to each other. **Results:** **i)** For a step increase in supply water temperature, the ceiling temperature was not uniform during the transient period. **ii)** Varying the supply water was a much better control strategy than varying the flow rate because the change of flow rate had almost no effect on the local ceiling temperature. **iii)** Response of the ceiling surface temperature to a step change in supply water temperature was exponential in nature. **iv)** Air stratification using this heating system was found to be less than with a forced air heating system with continuous air circulation. **v)** The response of room air temperature was almost same as those of wall and floor temperatures during a heating transient period.

J.D. Dale M.Y. Ackerman	1990	**Scope:** The performance of one house, equipped with both hydronic floor heating system and a forced air heating system, was studied. **Results:** **i)** The hydronic floor heating did not prove to be better than the forced air heating system in terms of energy efficiency. **ii)** Vertical temperature profiles were quite uniform from the floor to ceiling. The biggest difference was found to be 0.5°C to 1.0°C "from very near the floor to very near the ceiling". **iii)** Floor heating was more effective than forced air heating "in counteracting the cold currents falling off the windows". **iv)** It took longer for the floor heating system than the forced air system to increase the air temperature by a specified amount. The same behaviour was noted for a desired drop in temperature. **v)** Because of the slow heating and cooling rate, the schedule for night setback was different from that used for forced air heating systems. For the hydronic system, the setpoint was decreased earlier in the evening and restored to the original value earlier in the morning than usual. **vi)** Basement heat losses were 45 percent higher when using the hydronic system versus the forced air heating system.

Table 2.2

Literature review of simulation studies of hydronic floor heating system

Author(s)	Date	Nature of Study
L.E. Hulbert H.B. Nottage C.V. Franks	1950	**Scope:** Developed analytical solutions, using superposition, for heat flow in panel heating. **Assumptions:** two dimensional steady state conditions;pipes were uniformly spaced;no edge effects;each pipe represented as a line source. **Method of solution:** **i)** The temperature field in the slab was described by the superposition of source and linear components. **ii)** For the source component, each pipe was considered to be a line source in an infinite medium. **iii)** For the linear component, it was assumed that no heat source existed with uniform one dimensional heat flow between two isothermal surfaces. **Limitations:** **i)** In order to neglect variation of surface temperature, the theory was applied only to the certain ratios of D to L for specific ratios of b to L which were shown in the following **b/L** — **Max. D/L** 0.15 — 0.10 0.30 — 0.30 0.50 — 0.80 where b = distance between centre of pipe and slab surface L = slab thickness D = pipe outer diameter **ii)** All line sources were considered to be at the same temperature.

H.B. Nottage C.V. Franks L.E. Hulbert L.F. Schutrum	1953	**Scope:** An extension of the 1950 paper concerned with an experimental study of "slab on grade" heating. Pipes located at underside of slab, with tangent earth contact. **Assumptions** for mathematical analysis and electronic analog studies to determine thermal resistance: **i)** no heat loss to the earth and treated as semi-infinite medium. **ii)** no edge effects. **Limitations:** restricted to specified ratios investigated. The different ratios of "slab on grade" heating configurations studied were **s/L** — **D/L** 0.8 to 2.7 — 0.0625 to 0.125 1.6 to 4.0 — 0.250 2.7 to 5.0 — 0.313 where s = pipe spacing L = slab thickness D = pipe outer diameter Slab to earth thermal conductivity ratios of 0.60 and 1.16 were studied for all configurations.

R.E. Hogan	1979	**Scope:** Developed a numerical model to analyze the performance of hydronic floor heating system. The model included half enclosure with half heating panel, one exposed wall, "perimeter insulation, perimeter slab footing and the ground both below and adjacent to the enclosure". **Boundary Conditions:** **i)** Convection and radiation from a heated panel surface to the enclosure. **ii)** Undisturbed earth temperature at a depth of about 7.62 m. **iii)** Left and right boundaries perfectly insulated. **Assumptions:** **i)** Mean water temperature was used to compute the heat input to the enclosure. **ii)** Only two dimensional unsteady state heat transfer was considered. **iii)** The circular pipe cross section was described by hexagonal shape. **iv)** The thermal resistance of the pipe was considered to be negligible. **Results:** **i)** The discrepancy between simulated and experimental results was very large because of a lack of sufficient data for the operating conditions. **ii)** The trend of the simulated results agreed with experimental results.
Z. Zhang M.B. Pate	1989	**Scope:** Developed a new method "for designing hydronic panels with embedded tubes". The method employed a semi-analytical correlation to relate the supply water temperature and panel heat output to the physical characteristics of the panel. **Assumptions (for a floor heating system):** **i)** the underside of the panel is well insulated. **ii)** the tubes are located at the bottom of the panel. **iii)** temperature gradient in the water flow direction is negligible. **Limitations:** **i)** steady state only. **ii)** heat losses underside of the slab ignored. **iii)** applied to the bare panel only, i.e. homogeneous medium. **iv)** restricted to inlet water temperatures less than 90°C.

C.R. MacCluer	1989	**Scope:** Modelled a slab and a conventional thermostat to investigate the flux modulation control strategy. **Assumptions:** One dimensional heat conduction;no edge or back loss from the slab;uniform heat source located at bottom of slab;thermostat modelled by proportional gain in order to obtain a linear approximate model of the hydronic system. **Method of solution:** Analytical.

Table 2.3
Literature review of control studies of hydronic floor heating systems

Author(s)	Date	Nature of Study
A.B. Algren E.F. Snyder J.S. Locke	1953	**Scope:** Three different types of buildings were installed with different control systems respectively. **Results:** **i)** The results were not justified because each house had a different setup of panel systems such as different sizes of pipes and pipe spacings. **ii)** Fluctuation of panel surface temperature was reduced and room air temperature was quite stable by continuous pump operation. **iii)** Boiler reset action based on ambient temperature showed a better performance in controlling the heat supply to the room than using a fixed boiler temperature.
A.B. Algren E.F. Snyder R.R. Head	1954	**Scope:** Discussed different control strategies and the factors affecting control performance. **Problems:** The difficulty in maintaining a constant air temperature is increased if the house has a big window which allows solar radiation input to the room. **Suggestions:** **i)** In order to detect the solar intensity through the window glass, a solar compensator and outdoor sensor should be used to reset boiler temperature. **ii)** The most suitable location of the sensor is inside the compensator.
C.R. MacCluer M. Miklavcic	1989	**Scope:** Proposed a new flux modulation control strategy considered to be more robust than temperature modulation. The flux modulation strategy used just a simple thermostat with an anticipator as a controller. This simple controller provided an excellent setpoint tracking by determining the effective boiler operation time which was a function of the difference of room air temperature and setpoint. **Results:** Simulation results showed that the flux modulation was more robust to parameter drift than temperature modulation. Temperature modulation could induce instability because of the poor design parameters.

C.R. MacCluer	1989	**Scope:** Compared the performance of flux modulation for air temperature control with that of temperature modulation in response to step changes and sinusoidal variations of indoor and outdoor temperatures. **Results:** **i)** For a step change of indoor temperature, temperature modulation brought the system to the operating point if all control parameters were accurate. **ii)** For the same step change as **i)**, temperature modulation could not bring the system to the operating point if the control parameters went beyond the tolerable values. **iii)** The performance of the air temperature control system using a flux modulation strategy in response to a step change of indoor temperature was good even though the control parameters were not correct. **iv)** The flux modulation was still very robust to design flaws when the system was subject to sinusoidal variations of ambient temperature.

J.D. Dale M.Y. Ackerman	1990	**Scope:** Evaluated hydronic floor heating using three different control strategies for the system installed in an experimental house. **The three strategies were:** **#1:** On/off thermostat control: "An air temperature sensing thermostat operated a motorized valve" to be open or closed. **#2:** Proportional on/off control with ambient temperature reset: a proportional controller modulated the percentage on-time of the motorized valve in response to room air temperature error. Reset boiler control used reset slope to modulate the supply water temperature in response to the change in ambient temperature. **#3:** Water temperature in the lower zone was determined by heat demand in the upper zone. The lower zone valve was modulated proportionally with the room air temperature error. Circulation of water in the lower zone was still maintained even when the lower zone supply valve was closed. **Results:** **i)** The room air temperature was maintained to setpoint with these three control strategies respectively. **ii)** The strategy #3 was the most sensitive to the reset rate. An incorrect reset rate would cause the house to be too warm or too cool.
C.R. MacCluer	1990	**Scope:** Compared by simulation the performance of a flux modulation control strategy versus outdoor reset temperature modulation. **Results:** **i)** In response to step changes in indoor and outdoor temperatures, outdoor reset control was found to provide better control performance in tracking the setpoint than the flux modulation control strategy. **ii)** For highly insulated enclosure, neither form of modulation had a advantage in response to a sinusoidal ambient temperature. **iii)** For modestly insulated enclosure, the flux modulation was found to be more effective in tracking setpoint than outdoor reset control under daily sinusoidal ambient temperature.

C.R. MacCluer	1991	**Scope:** Simulated air temperature control using outdoor reset control with three refinements and then evaluated the performance of three control systems. **Three refinements considered:** **i)** flow inhibition:stopped circulation when energy demand was met. **ii)** reset slope modulation:reset slope was modulated by air temperature. **iii)** offset modulation:the intercept of the reset curve was modified in proportion to indoor temperature. **Results:** **i)** In response to step changes of indoor and outdoor temperatures, the performance of outdoor reset with flow inhibition in tracking the setpoint was worse than that of outdoor reset without refinement. **ii)** In response to sinusoidal change of outdoor temperature, the performance of outdoor reset with flow inhibition in tracking the setpoint was better than that of outdoor reset without refinement. **iii)** Outdoor reset with slope modulation did have improvement in response to sinusoidal variations of outdoor temperature, however, the system would become unstable at the period of large energy demand. **iv)** The advantages of outdoor reset with offset modulation were that "stability was unaffected by load" and some improvements in performance were achieved provided that careful design and installation were made.

S.B. Leigh	1991a 1991b	**Scope:** Compared the performance of proportional flux modulation in response to disturbances and variations of indoor temperature with that of outdoor reset control with indoor temperature offset in two chambers. Each chamber having dimensions of 2.44 m by 2.44 m by 2.44 m was installed with these two control strategies respectively. **Results:** **i)** The indoor temperature was maintained quite stable at the operating point by these two control strategies respectively. **ii)** After an internal load disturbance was introduced (decrease in room air temperature), the outdoor reset control was found to have slower response to the disturbance than proportional flux modulation. **iii)** The response of both systems to internal heat generation was very similar.

Chapter 3
Physical System

Interest in hydronic floor heating systems has been revived since 1980 because of suggested potential energy savings versus forced air heating system and also because of potential improvement in thermal comfort. However, operating results of studies of hydronic floor heating systems cannot be compared to those of forced air systems because room occupancy, size of the enclosure and the physical configuration are different. Moreover, advertising claims that hydronic floor heating systems can increase thermal comfort and reduce energy consumptions has not been proved. For the above reasons, the Department of Mechanical Engineering at the University of Alberta undertook a study funded by Alberta Energy, Energy Conservation in Building's Program, to evaluate the performance of a hydronic floor heating system and make a comparison of this system with a forced air heating system in terms of energy savings for the same building.

There are six experimental bungalow style houses located at the Alberta Home Heating Research Facility. Details concerning these experimental houses are available from the Department of Mechanical Engineering (Gilpin et al., 1980). Data were collected from the only experimental house equipped with a hydronic floor heating system and a forced air heating system. The forced air heating system was conventional. A central heater and fan with duct work to distribute the air at the perimeter of the above grade floor and ceiling level of the basement. In this thesis, the hydronic heating system is the main concern. The experimental house is divided into two zones, upper (main floor) and lower zone (basement). Only the basement system is considered in this study.

The general structure of the basement is typical with the basement walls surrounded by soil, except for the top portion which is above ground level. A cross-sectional view of the basement is given in Figure 3.1.

3.1 Basement Hydronic Heating System

3.1.1 Structure of Panel

The heated panel consists of three layers of materials which have different thermal properties. The top layer is a 5 cm thick layer of gypsum cement, the middle layer is 2.5 cm thick extruded polystyrene insulation of RSI 0.88. The lower material is the original 10 cm thick concrete floor. The insulation below the gypsum cement is used to reduce the amount of heat loss to the soil.

3.1.2 Layout of Piping

The gypsum layer contains two separate loops of 1.27 cm inside diameter and 1.6 cm outside diameter polybutylene tubing embedded, each containing a total of 70 m with the configurations as shown in Figure 3.2a. The spiral bilifary pattern, shown in Figure 3.2b, is used on the main floor. The second loop in the basement is not very regular because the pipe needs to curve around the staircase leading from the main floor to the basement while the first loop is quite regular with a tubing spacing of about 0.3 m. Because of its regularity, the first loop with the parallel tubing configuration is chosen for model development. A cross-sectional view of the heating panel showing the tubing embedded in the gypsum cement is shown in Figure 3.3.

3.1.3 Structure of Wall

The 20 cm thick basement wall, as can be seen from Figure 3.1, is on the outside covered with a 5 cm layer of RSI 1.76 rigid polystyrene insulation. The wall is 2.26 m high with 0.4 m of the wall above ground level as shown in Figure 3.4.

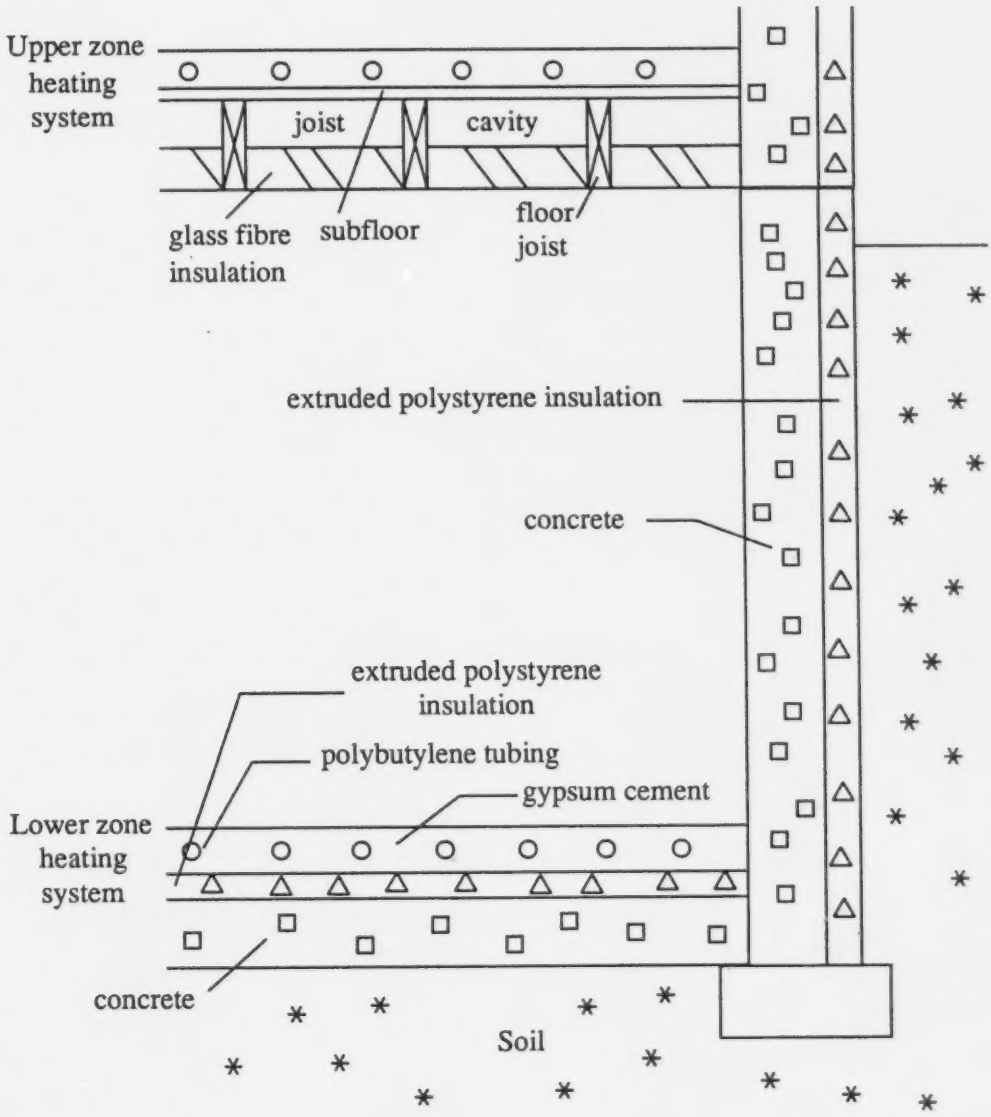

Figure 3.1 The cross-sectional view of basement in the experimental house

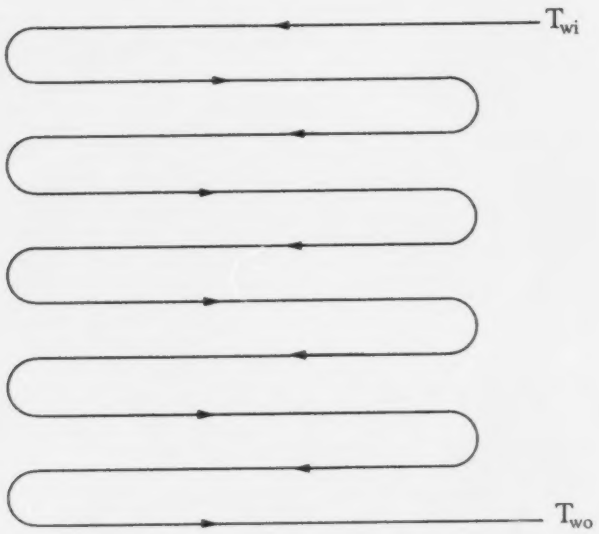

(a) Layout in the lower zone

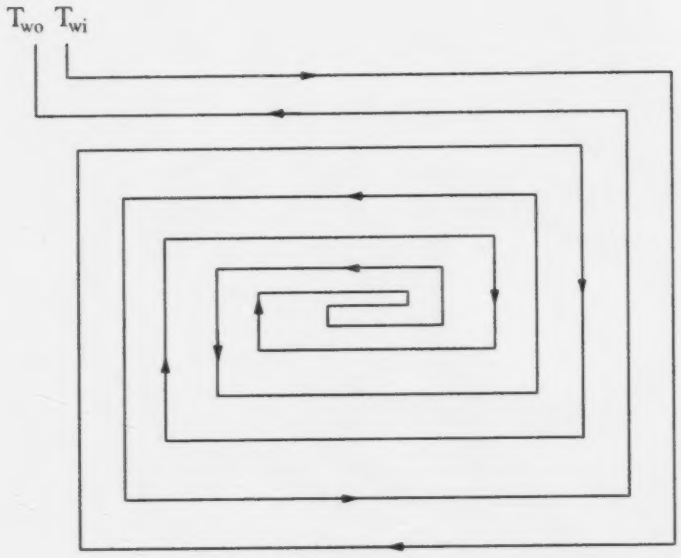

(b) Layout in the upper zone

Figure 3.2 The two types of tubing layout used in the experimental house

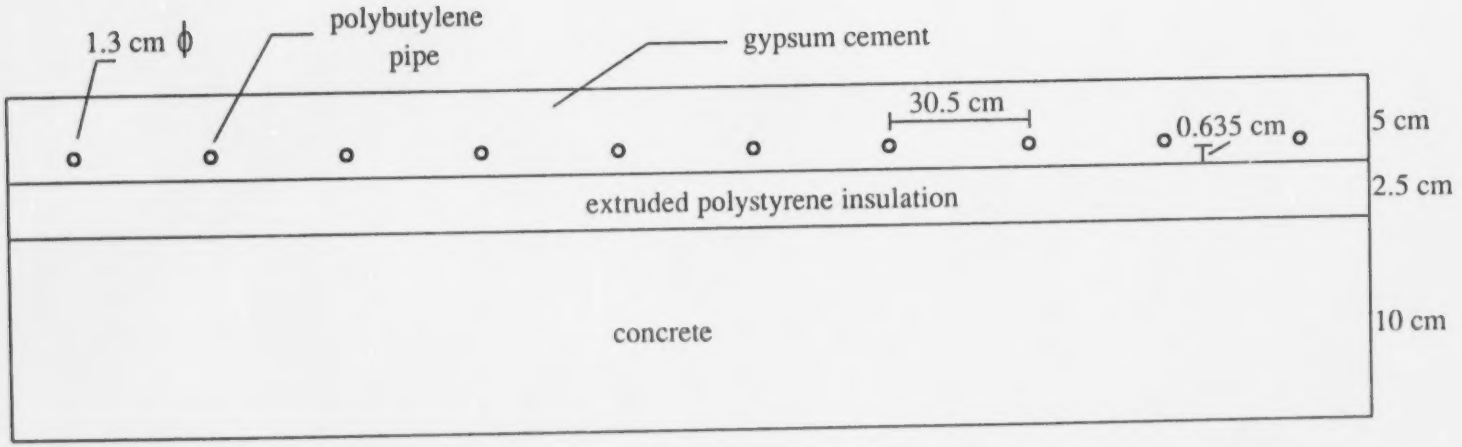

Figure 3.3 The cross-sectional view of the heating panel

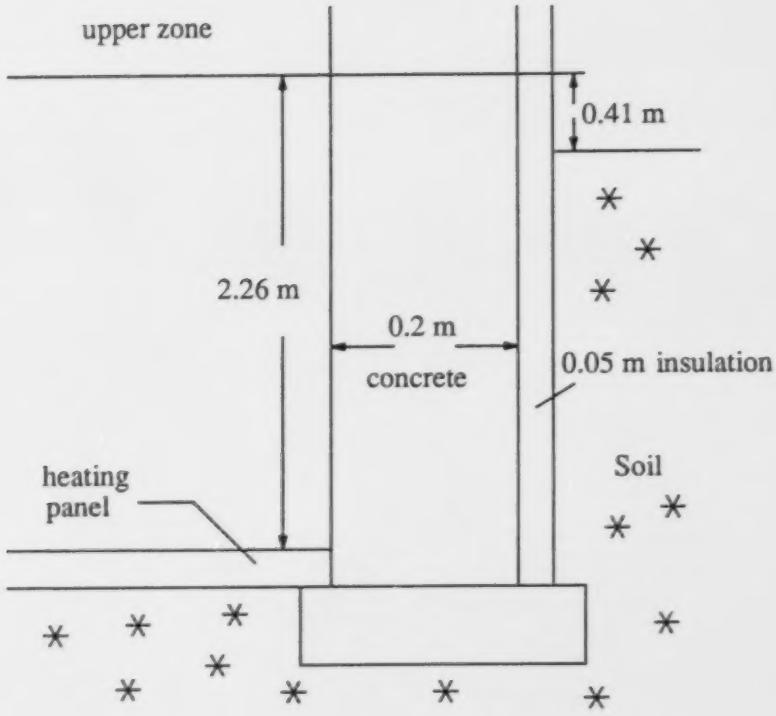

Figure 3.4 Cross-sectional view of basement

3.1.4 Structure of Ceiling

A cross-sectional view of the heating panel and floor of the upper zone which is the ceiling of the basement is shown in Figure 3.5. As can be seen glass fibre insulation (RSI 2.11) is installed in between the floor joists and covered by reflective foil on the top. An air gap exists between the foil and the subfloor (1.6 cm plywood) of the upper zone. Three separate loops of polybutylene tubing are embedded in the 5 cm layer of gypsum cement located on top of the subfloor.

3.2 Data Collection

A Sciemetric Instruments data logger and IBM XT computer continuously (24 hours per day, 7 days per week) collect data from the experimental house. Such data as

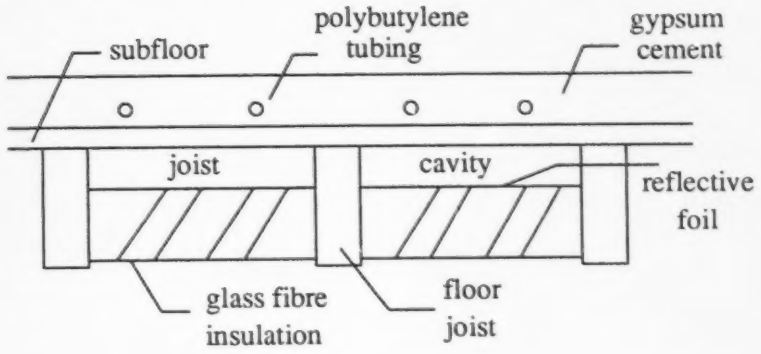

Figure 3.5 Cross-sectional view of main floor panel and ceiling of the basement

room air temperature in the upper and lower zones, temperature drop across the insulation in the basement floor heating panel, floor surface temperature, ambient temperature, soil temperatures north of the house and under the concrete are required for model. The two data logging devices have different sample rates with the computer collecting data every two minutes and the data logger every ten minutes. The data collected by the two separate devices are described in the following material.

3.2.1 Data with Two-Minute Sampling Time

i) Ambient outdoor temperature: This thermocouple and all others are Type T (copper-constantan). The thermocouple which measures ambient outdoor temperature is installed one metre above ground level, in the instrumentation shelter located on the north side of the experimental house.

ii) Basement air temperature: A thermocouple is located one metre above the centre of floor surface.

iii) Basement zone water inlet and outlet temperature: The thermocouples for measuring the inlet and outlet water in the tubing are located at positions 3 and 4 as shown in Figure

3.6. The thermocouples are installed through the wall of the tubing and have direct contact with water to obtain accurate measurements of water temperature.

iv) The water temperature entering the 10 kW rated electric boiler and leaving the hot water tank: The thermocouple measurements, with the thermocouple in the water, are taken at positions 1 and 2 as presented in Figure 3.6.

v) Water flow rate in circuit: The flow is measured by Validyne venturi meters at positions 5 and 6 shown in Figure 3.6 and the rates logged by the computer. As can be observed, a bypass circuit exists but when flow to the panel is required, the Erie motortrol on-off electric valves at position 7 and 11 are fully open while Erie electric valve at position 10 is closed.

vi) Status: The current status of the valves, Grundfos pump, and power to the boiler is logged every two minutes, with each device assigned the following designations

Valve (position 11): $2^0 = 1$

Valve (position 7): $2^1 = 2$

Valve (position 10): $2^2 = 4$

Pump (position 12): $2^3 = 8$

Boiler (position 14): $2^4 = 16$

If the current status is 27, the flow is to the heating circuit that is, the boiler and the pump are on and the electric valves, at positions 7 and 11, are open.

3.2.2 Data with Ten-Minute Sampling Time

There are 52 data values stored by the ten-minute data logger. Some of the data values are the same as those logged by the computer system at the two minute sample interval. Data required to analyze the dynamic response of the system but not scanned by Sciemetric Instruments data logger are

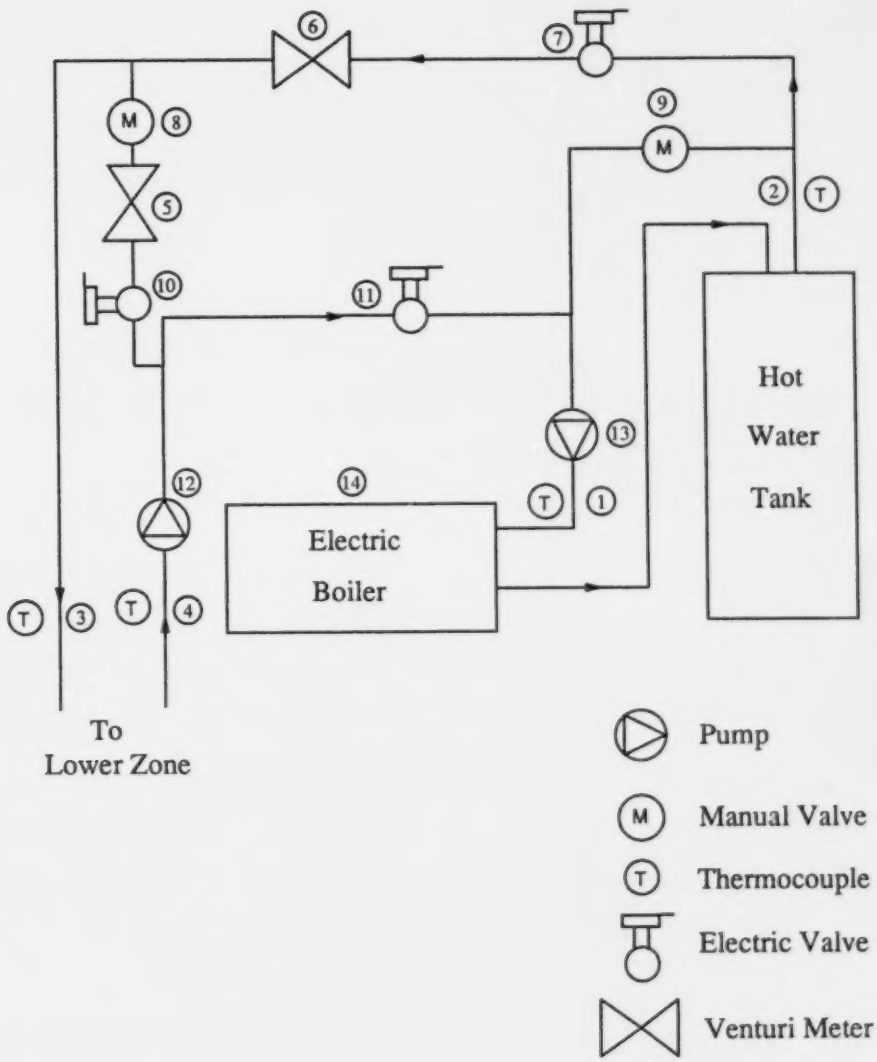

Figure 3.6 Schematic diagram of water supply system

i) Floor surface temperature: Five thermocouples, in a star pattern, located around the centre of the floor. The experimental floor surface temperature is computed as the average the readings of these five thermocouples which are taped on the surface of the floor.

ii) Temperature difference across the insulation of the heating panel: Three pairs of thermocouples are used to measure the temperature on each side of the insulation so that the amount of backside heat loss can be estimated. One thermocouple is installed at the interface between the gypsum cement and insulation and the other at the interface of the insulation and concrete.

iii) Joist cavity temperature: A thermocouple located in the space between the reflective foil on top of the insulation and the underside of the subfloor measures this temperature.

iv) Temperature at the backside of the glass fibre insulation: A thermocouple installed at the underside of the glass fibre insulation measures this temperature. The difference between this temperature and the joist cavity temperature estimates the amount of heat loss through the ceiling of the basement.

3.2.3 Additional Data

In addition to the data that is obtained from the data logger or computer, the values collected manually are

i) Soil temperature under the heating panel: Four probes, each with six thermocouples located between the north wall and the centre of the floor. The first thermocouple is 0.33 m below the concrete and the other five thermocouples are located at depths of 0.3 m from the previous thermocouple.

ii) Soil temperature north of the house: Three probes with three thermocouples each installed 0.33 m, 1.83 m and 6.1 m from the wall. The first thermocouple is 0.61 m below the soil surface, the second one is 0.61 m deeper and the third another 0.46 m deeper than the second thermocouple.

3.3 Data Conversion

The IBM XT computer is used not only for recording the output from the thermocouples and flow rate measurements but also for sending control signals to the three valves, pump and boiler. The signals of the thermocouples (μV) and venturi meters (V) are transmitted to an A/D converter which converts the analog signals into digital form. These digital data accessed by the control program determine the on-off state of the valves, pump and boiler. The code for the on-off state of the devices is then sent to the parallel printer port to drive the Crydom D2W202F. The solid state relay in each Crydom is physically connected to its associated device as shown in Figure 3.7. When a logic 1 is assigned to a particular device, a five volt signal is sent through the parallel port to energize its relay which in turn closes the AC circuit and power is then delivered to that particular device.

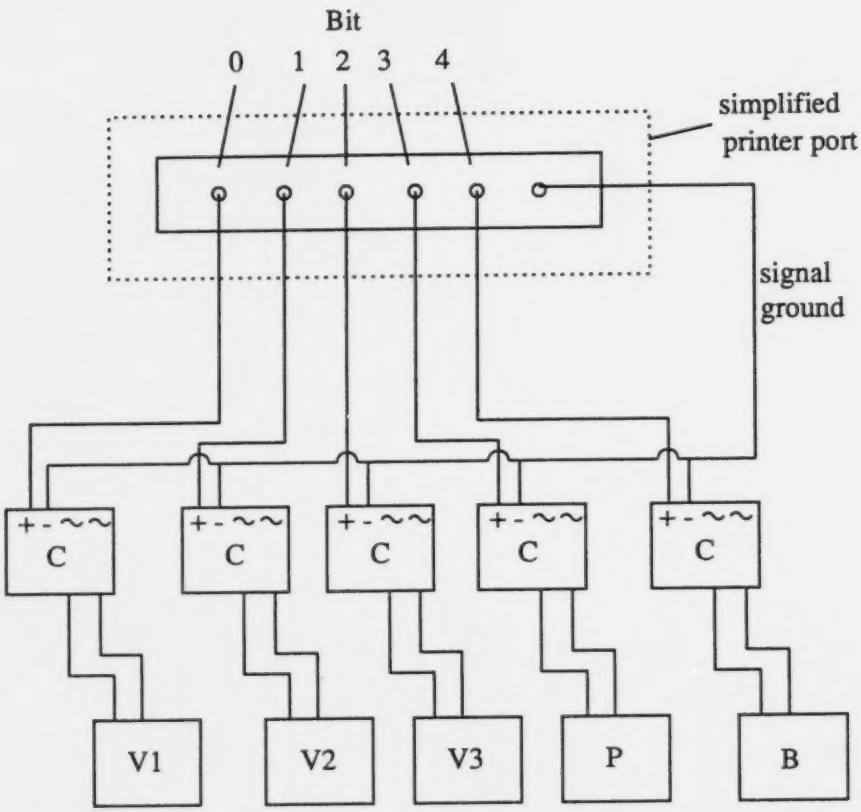

V1, V2, V3 — Electric Valves

P — Pump

B — Electric Boiler

C — Crydom D2W202F

Figure 3.7 Interface of the computer and devices

Chapter 4
Model for Hydronic Floor Heating System

A wide variety of different models for analyzing the steady and unsteady state of hydronic heating systems have been presented in the literature as discussed in Chapter 2 but none of the models are suitable for studying the dynamic behaviour of the system installed in the experimental house used in this study. This is because the models are not general and many involve simplifying assumptions which are not applicable for the system under investigation. Because of the limited instrumentation in the experimental house, in order to understand the dynamic response of the system, a model of the system is developed to investigate the transient responses of the complete system.

4.1 Descriptions of Subsystems

Generally speaking, two subsystems form a hydronic floor heating system. One of the subsystems is the heating panel itself and the other is enclosure, as shown in Figure 4.1. These two subsystems are coupled. The amount of upward heat flow from the heating panel is balanced by the energy accumulation in the air in enclosure and the amount of heat loss from the enclosure to the surroundings. In this study, the storage effect of the walls is ignored. Although it is possible to include in the model the energy storage in the walls, since instrumentation was not installed to determine temperatures this effect was not considered in this work. In the material that follows, the assumptions and boundary conditions for each subsystem will be discussed.

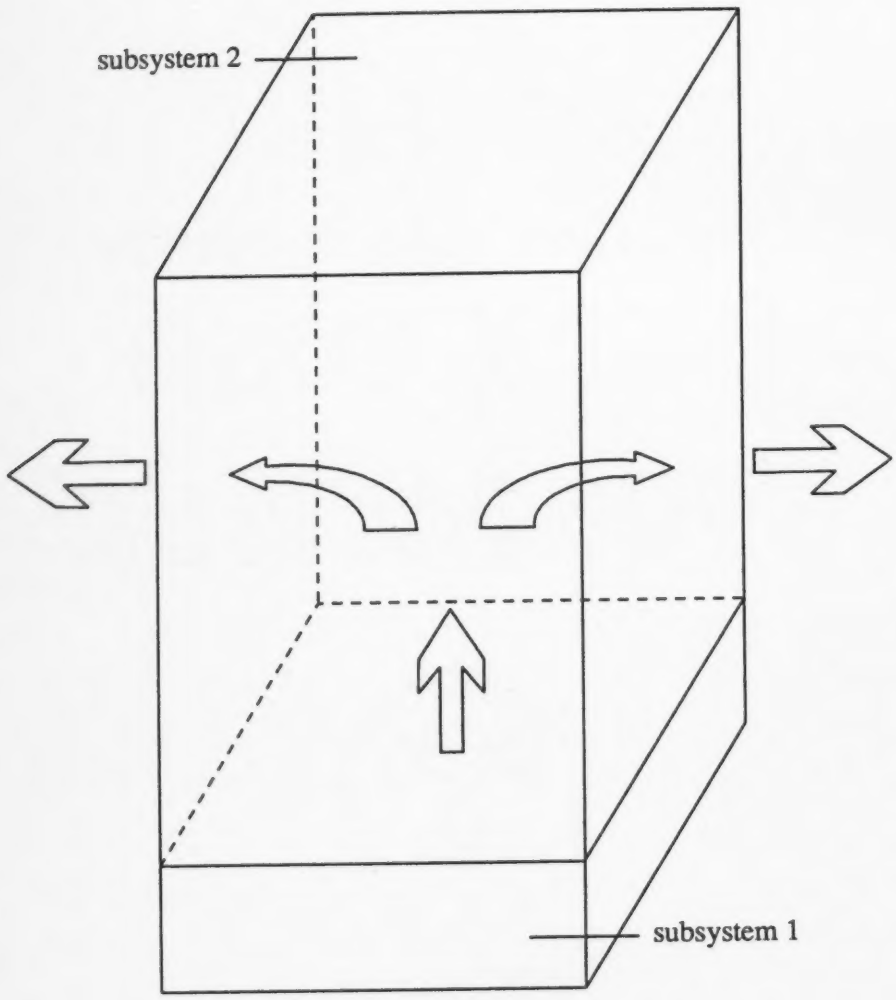

Figure 4.1 Two subsystems in the experimental house

4.2 Assumptions and Boundary Conditions

4.2.1 Subsystem 1 : Heating Panel

The details of the heating panel have already been shown in Figure 3.3. The two different models used to describe this subsystem are the simple and the full model.

4.2.1.1 Full Model

The heating panel of the system consists of three layers of materials; the gypsum cement which contains the embedded tubes, insulation and concrete are shown in the Figure 4.2. As mentioned in Chapter 3, two separate loops of 1.27 cm polybutylene tubing are installed in the heating panel. Only the heating panel containing the parallel configuration of polybutylene tubing is considered in this work. A cross-sectional representation of this loop of parallel configuration tubing can be viewed as 10 holes located at 0.64 cm from the bottom surface of the gypsum cement layer. The descriptions of the parameters, assumptions and boundary conditions for the full model are presented in the material that follows. For convenience, in this material, and for the balance of the thesis, the notation of the temperature in the solid T(x,y,t) is abbreviated as T. The detailed calculations for the parameter values given in the material that follows can be found in Appendix A. In reviewing these boundary conditions, the reader should make reference to Figure 4.2. It is noted that all the parameter values and measurements mentioned in this chapter are applicable only for the first dynamic test that is with the shutters for the windows on the main floor of the house not closed (shutters open).

i) Boundary condition on AD and EH: It is assumed that there is no heat loss from the left and right hand sides of the heating panel.

$$\frac{\partial T}{\partial x} = 0 \qquad (4.1)$$

ii) Boundary condition on AH: The conductive heat flow from the heating panel is equal to the heat flow in the soil by conduction.

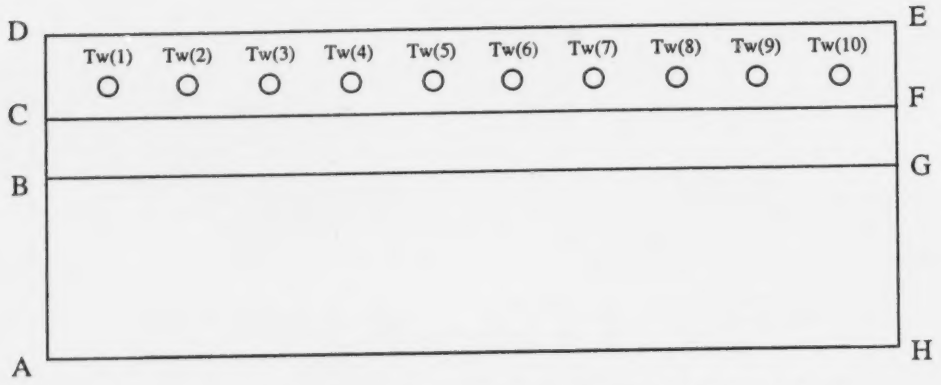

Figure 4.2 Labels of boundary conditions for full model

$$k_{p3}\frac{\partial T}{\partial y} = k_{s1}\frac{\partial T_{s1}}{\partial y} \tag{4.2}$$

The thermal conductivity of concrete (k_3), taken from ASHRAE handbook (1977), is considered to be 1.731 W/m°C and from steady state data, using the soil temperature 0.33 m below the concrete, the thermal conductivity of the soil under the heating panel was estimated to be 0.5145 W/m°C. It should be noted that the horizontal variation in soil temperature over a 48-hour period at the first thermocouple location below the concrete floor does not differ by more than 2°C, so an average of the four temperature values was used for the calculation.

iii) Boundary condition on DE: Heat flow at the panel surface is equal to the convective and radiative heat transfer from the panel surface to the room.

$$k_{p1}\frac{\partial T}{\partial y} = h \bullet (T_{surf} - T_r) \tag{4.3}$$

Based on the initial and final steady state values in the first open loop test, the basement air temperature increased from 25.8°C to 30.5°C and the panel surface temperature from 28.5°C to 33.5°C. The rate of total energy input for the complete system increased from 2459 W at the initial steady state to 2965.84 W at the final steady state. The increase in the temperatures and rate of total energy input caused the h value to increase by about 2

W/m²°C from the initial steady state h value of 15.45 W/m²°C. Even though the h value increased slightly, the value of 15.45 W/m²°C was used for all calculation. The panel surface temperature was considered to be the average of the surface temperature measurements. The thermal conductivity of the gypsum cement in the top layer of the heating panel was taken from the specifications of FORTA-FILL® gypsum concrete to be 0.62 W/m°C. The procedure employed to calculate basement air temperature will be shown in Section 4.3.

iv) Boundary condition at $T_w(i)$: Dirichlet boundary conditions are imposed on the circumference of the ten holes.

$$T_{@i} = T_w(i) \qquad (4.4)$$

$$i = 1, 2, \cdots 10$$

Based on the parallel tubing layout shown in Figure 3.2a, the temperature at the first hole, T_1, is considered to be the inlet water temperature and T_{10}, the temperature at the tenth hole the outlet water temperature. Linear interpolation is used to establish the pipe temperature for the intermediate holes. Using a value of the inlet water temperature, the outlet water temperature is computed from the algorithm as shown in Section 4.3.1.

v) Boundary condition on CF, BG: Since the finite difference and finite element solution techniques treat these two boundary conditions in different ways, the details will be discussed in Chapter 5.

4.2.1.2 Simple Models

A. Half-pipe model

In the simple model of the floor heating system, the panel is considered to be only a layer of gypsum cement containing the tubes. The main difference between the simple model and the full model is that there is no computation of the outlet water temperature and no backside heat loss considered in the simple model. Prediction of the dynamic response using the full model requires more computation time than the simple model

because the outlet water temperature has to be solved iteratively in the full model and the number of grids used in the full model are more than the number used in the simple model.

The "half-pipe model" representation with labelled boundaries, is shown in Figure 4.3. The assumptions and boundary conditions used for the simple model are the following.

i) Boundary condition on AB, CD and EF: By symmetry, the boundary conditions are considered to be

$$\frac{\partial T}{\partial x} = 0 \tag{4.5}$$

ii) Boundary condition on BC: The temperature at the pipe surface is considered to be constant.

$$T = \text{constant} \tag{4.6}$$

and at the average of the inlet and outlet water temperatures.

iii) Boundary condition on AF: Heat loss from the underside of the panel is considered to negligible even though the heat loss can be up to 25 percent of the total heat input in an actual installation.

$$\frac{\partial T}{\partial y} = 0 \tag{4.7}$$

iv) Boundary condition on DE: Heat conduction to the panel surface is equal to the convective and radiative heat transfer to the room.

$$k_{pl} \frac{\partial T}{\partial y} = -h \bullet (T - T_r) \tag{4.8}$$

B. One-pipe model

The purpose of using a one-pipe model is to validate the accuracy of the numerical solution compared with the solution for the half-pipe model. The shape of the domain with boundary conditions is shown in Figure 4.4.

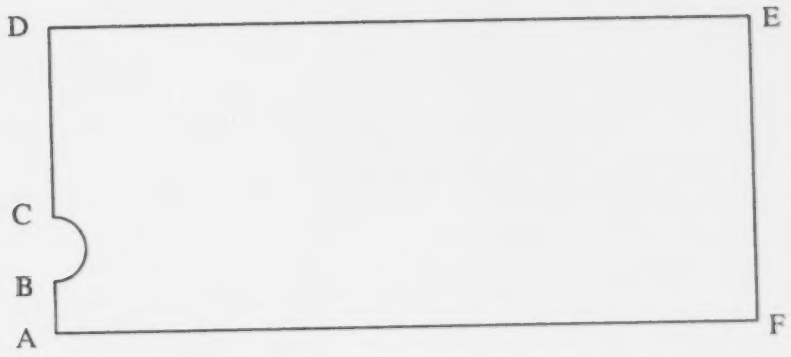

Figure 4.3 Labels of boundary conditions for half-pipe model

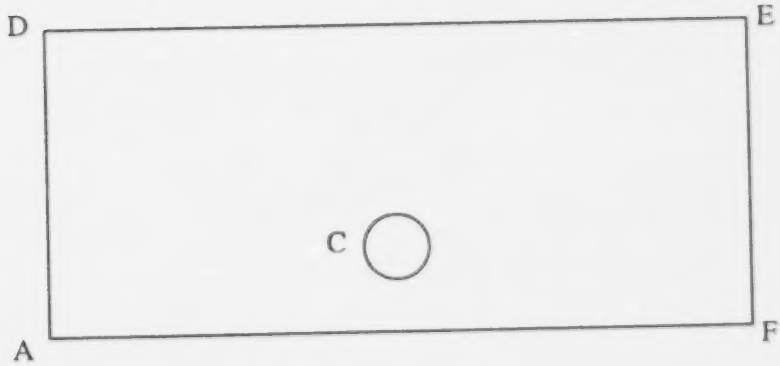

Figure 4.4 Labels of boundary conditions for one-pipe model

i) Boundary condition on AD and EF: Same as boundary conditions AB, CD, and EF in half-pipe model.

ii) Boundary condition on DE: No change.

iii) Boundary condition on AF: No change.

iv) Boundary condition on BC: No change.

4.2.2 Subsystem 2 : Enclosure

The second subsystem is assumed to be coupled to the heating panel subsystem through the combined convective and radiative heat transfer coefficient at the interface of the two subsystems. In this study, subsystem 2 is the basement space of the experimental house, excluding the heating panel. The dynamic response of basement air temperature, T_r (t) will be investigated by solving the unsteady state heating panel energy balance equation in conjunction with the room energy balance. The room energy balance is expressed as

$$h \bullet A \bullet (T_{surf} - T_r) = m_{air} \bullet Cp_{air} \bullet \frac{dT_r}{dt} + q_{ceil} + UA \bullet (T_r - T_{s2}) + ACR \bullet Cp_{air} \bullet V_r \bullet \rho_r \bullet (T_r - T_{amb}) \quad (4.9)$$

The term on the left hand side of the equation represents the rate of total energy input to the enclosure and the first term on the right hand side of the equation is the energy accumulation in the basement air. The next term is the ceiling heat loss/gain and the third term on the right hand side of the equation is the rate of heat loss to the surrounding soil. The last term in equation (4.9) allows for the heat exchange rate between the enclosure and the surrounding, through the flue, due to the air change rate (ACR) which is 0.2 per hour.

The ceiling heat loss or gain is computed by the following equation

$$q_{ceil} = k_{ceil} \bullet A_{ceil} \bullet (T_r - T_{joist}) \quad (4.10)$$

with T_r and T_{joist} time-varying during the heat-up or cool-down period. Experimental data plotted in Figure 4.5 shows that the difference between T_r and T_{joist} is quite constant so it

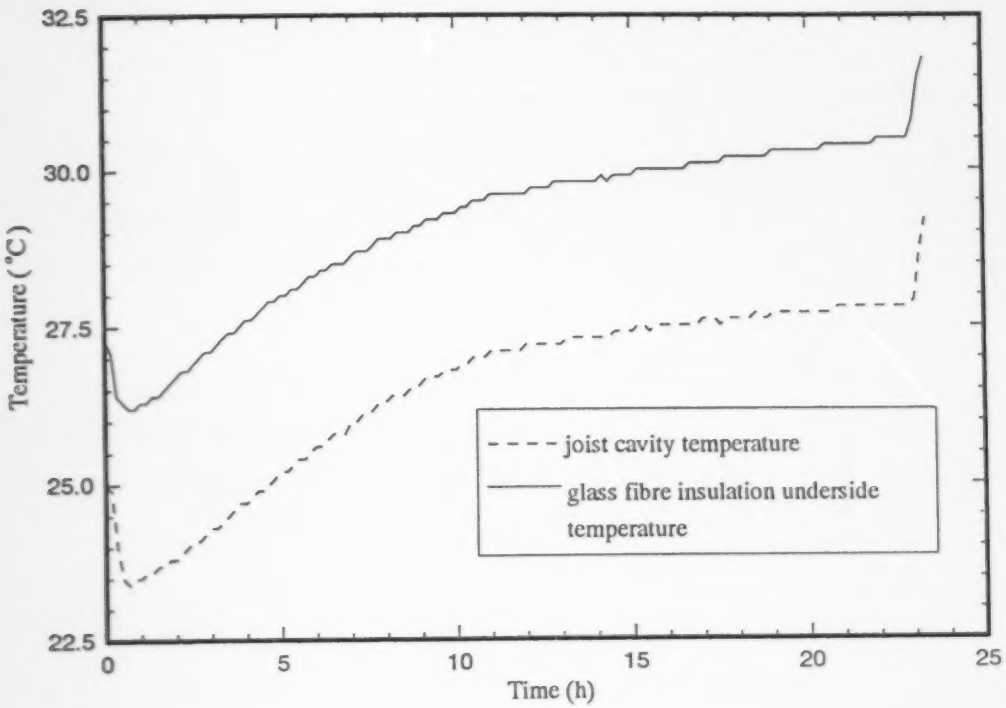

Figure 4.5 Dynamic response of the joist cavity temperature and glass fibre insulation underside surface temperature in response to a step change of the inlet water temperature from 45 °C to 55 °C

is appropriate to consider the amount of heat loss through ceiling to be constant. However, the amount of heat loss/gain varies with different tests according to operating conditions and ambient temperature. As shown in Figure 3.1, only a small portion of the basement is exposed to the outdoor ambient temperature and so this small amount of heat loss is ignored. Therefore, the temperature difference driving force for the overall heat transfer coefficient is the difference between the basement air temperature and the soil temperature around the walls. This soil temperature was taken to be the average of the three temperatures 0.3 m away from the north wall.

4.3 Algorithms

The unsteady and steady state governing equations which will be discussed in detail in the next chapter are the two-dimensional heat conduction equations. Since a different thermal diffusivity is required for each different layer of the heating panel as well as complicated boundary conditions in the full model, the transient response predictions cannot be obtained by an analytical solution. Consequently, the model equations are solved numerically. Regardless of the method of numerical solution employed, the basic algorithm for computing the average floor surface temperature, outlet water temperature and basement air temperature are the same. The flowchart for the algorithm used in the full model is shown in Figure 4.6.

4.3.1 Description of the Algorithms

In order to predict the dynamic response, all parameters and steady state variables are required so the steady state values of the basement air temperature and the outlet water temperature are required. However, since the basement air temperature and the outlet water temperature are variables in boundary conditions BC, DE and $T_w(i)$, where i = 1,2, ..., 10, the steady state values of these two variables cannot be solved for directly. The iterative solution is initiated by assuming some reasonable values for the basement air

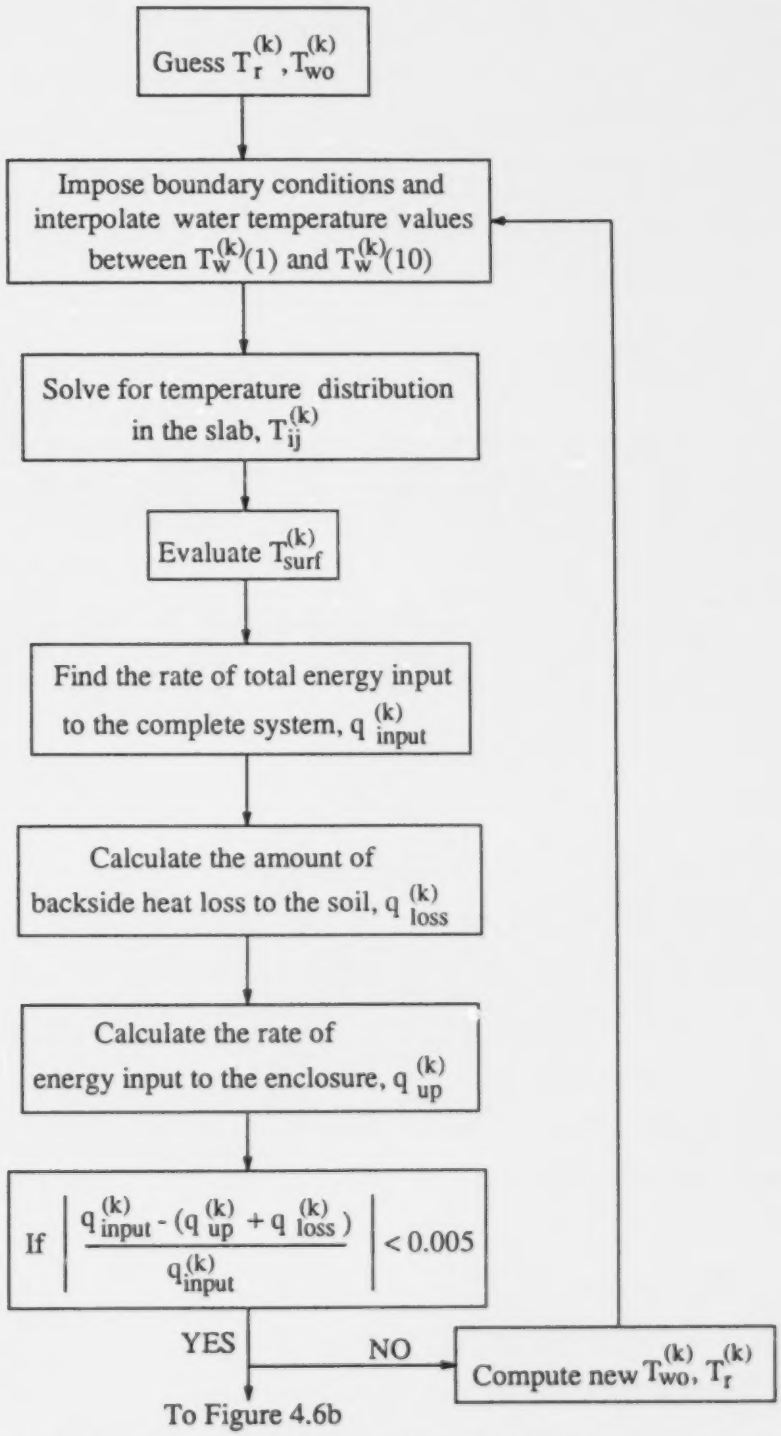
Guess $T_r^{(k)}$, $T_{wo}^{(k)}$
Impose boundary conditions and interpolate water temperature values between $T_w^{(k)}(1)$ and $T_w^{(k)}(10)$
Solve for temperature distribution in the slab, $T_{ij}^{(k)}$
Evaluate $T_{surf}^{(k)}$
Find the rate of total energy input to the complete system, $q_{input}^{(k)}$
Calculate the amount of backside heat loss to the soil, $q_{loss}^{(k)}$
Calculate the rate of energy input to the enclosure, $q_{up}^{(k)}$
If $\left| \frac{q_{input}^{(k)} - (q_{up}^{(k)} + q_{loss}^{(k)})}{q_{input}^{(k)}} \right| < 0.005$
YES
NO
Compute new $T_{wo}^{(k)}$, $T_r^{(k)}$
To Figure 4.6b

Figure 4.6a Flowchart for the computation of room air temperature and outlet water temperature for the full model (continued)

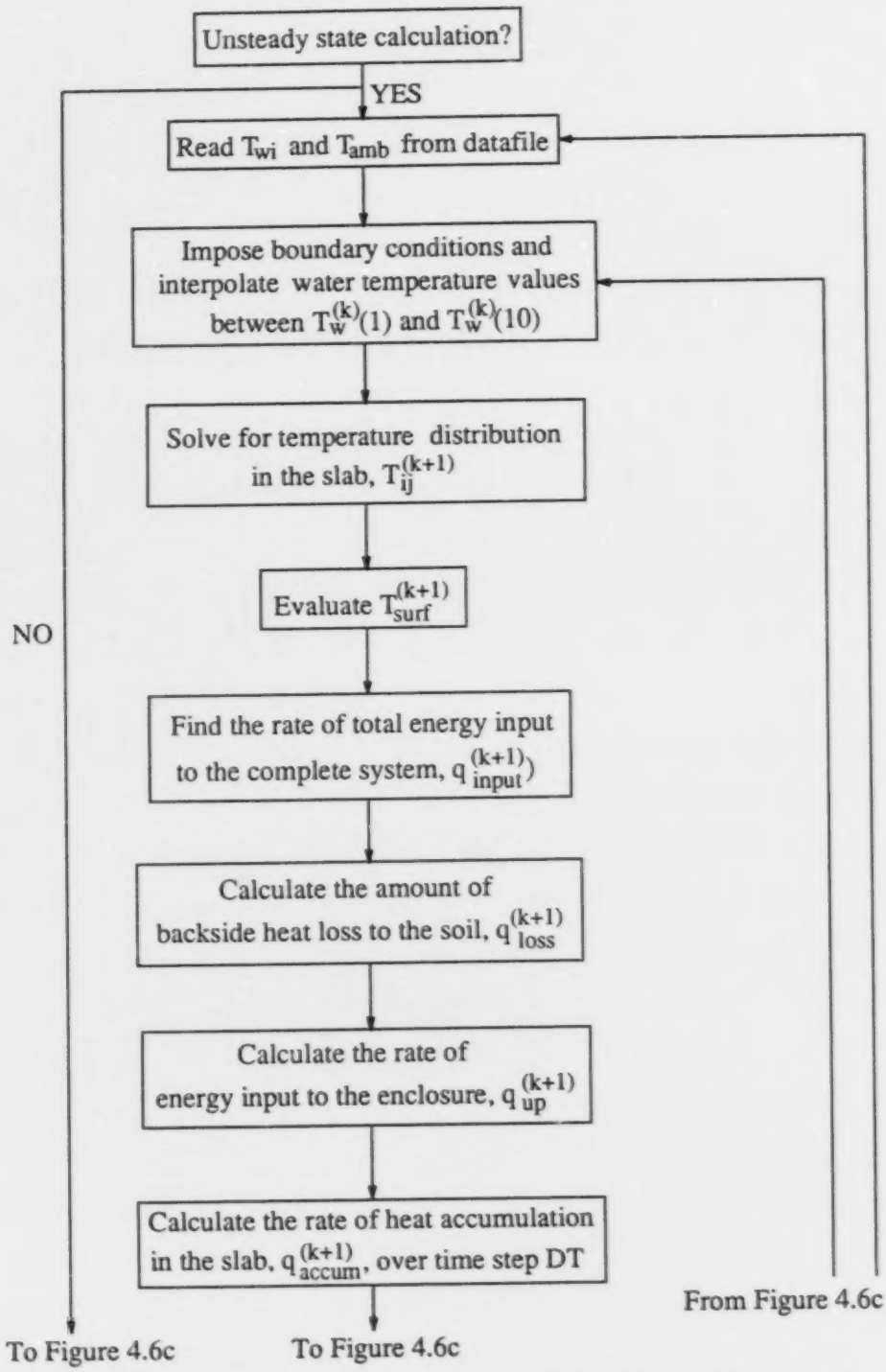
Unsteady state calculation?
YES
Read T_{wi} and T_{amb} from datafile
Impose boundary conditions and interpolate water temperature values between $T_w^{(k)}(1)$ and $T_w^{(k)}(10)$
Solve for temperature distribution in the slab, $T_{ij}^{(k+1)}$
Evaluate $T_{surf}^{(k+1)}$
NO
Find the rate of total energy input to the complete system, $q_{input}^{(k+1)}$)
Calculate the amount of backside heat loss to the soil, $q_{loss}^{(k+1)}$
Calculate the rate of energy input to the enclosure, $q_{up}^{(k+1)}$
Calculate the rate of heat accumulation in the slab, $q_{accum}^{(k+1)}$, over time step DT
From Figure 4.6c
To Figure 4.6c
To Figure 4.6c

Figure 4.6b Flowchart for the computation of room air temperature and outlet water temperature for the full model (continued)

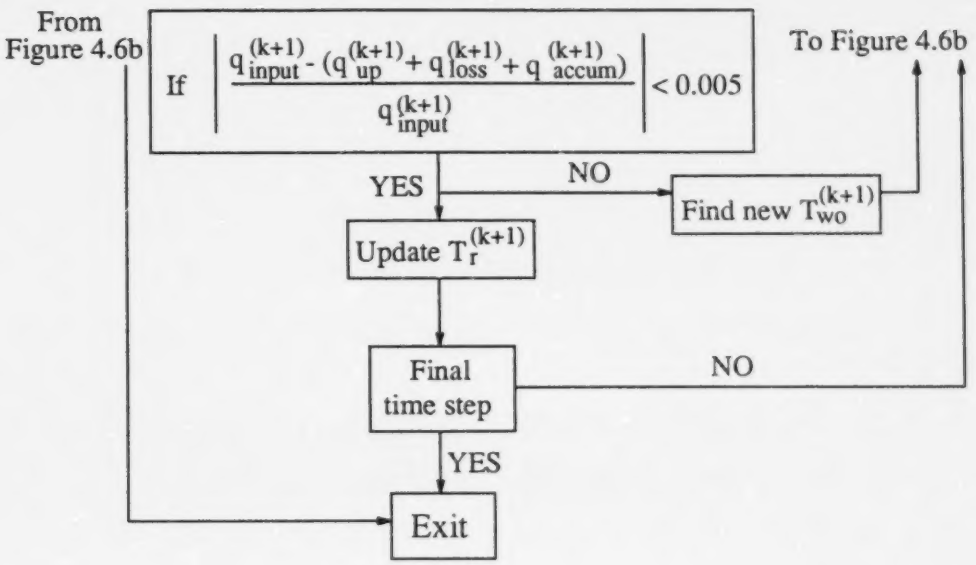

Figure 4.6c Flowchart for the computation of room air temperature and outlet water temperature for the full model

temperature and outlet water temperature in the boundary conditions. With these boundary conditions, the two-dimensional heat conduction problem can be solved for the temperature distribution in the slab, and the average floor surface temperature is calculated using the following expression

$$T_{surf}^{(k)} = \sum_{j=1}^{nn} \frac{T_{Mj}^{(k)}}{nn} \tag{4.11}$$

The next step in the algorithm is a check of the energy balance to determine if the sum of the rate of total energy input to the room and rate of backwards heat loss to soil is equal to the rate of total energy input for the complete system assuming no energy loss from the ends of the heating panel. The expressions for these three energy terms are

rate of total energy input for the complete system

$$q_{input}^{(k)} = \dot{m}_w \bullet Cp_w \bullet (T_{wi}^{(k)} - T_{wo}^{(k)}) \tag{4.12}$$

rate of backside heat loss to the soil

$$q_{loss}^{(k)} = k_{soil} \bullet A \bullet (T_{ij}^{(k)} - T_{sl})_{@\, i=1} \tag{4.13}$$

where the bottom surface of the floor is labelled as i=1

rate of energy input to the enclosure

$$q_{up}^{(k)} = h \bullet A \bullet (T_{surf}^{(k)} - T_r^{(k)}) \tag{4.14}$$

The sum of $q_{loss}^{(k)}$ and $q_{up}^{(k)}$ is

$$q_o^{(k)} = q_{loss}^{(k)} + q_{up}^{(k)} \tag{4.15}$$

The relative error of $q_{input}^{(k)}$ and $q_o^{(k)}$ is

$$error = \frac{q_{input}^{(k)} - q_o^{(k)}}{q_{input}^{(k)}} \tag{4.16}$$

If the relative error is greater than 0.005, it is considered that the overall energy balance is not satisfied with the initial guessed values of basement air temperature and outlet water temperature. New trial values of the basement air temperature, $T_r^{(k)}$ and the outlet water temperature, $T_{wo}^{(k)}$, used for the next iteration are calculated from

$$T_{wo}^{(k)} = T_{wi}^{(k)} - \frac{q_o^{(k)}}{\dot{m}_w Cp_w} \tag{4.17}$$

$$T_r^{(k)} = \frac{h \bullet A \bullet T_{surf}^{(k)} - q_{ceil} + UA \bullet T_{s2} + C1 \bullet T_{amb}^{(k)}}{UA + C1 + h \bullet A}$$

$$\text{where} \quad C1 = ACR \bullet \rho_r \bullet V_r \bullet Cp_r$$

After converged outlet water temperature and basement air temperature values are obtained, that is the relative error is less than 0.005, the unsteady state calculation begins.

Prediction of the transient response of the basement air temperature and the outlet water temperature is more complicated than the steady state response. The calculations of average floor surface temperature, rate of total energy input for the whole system, rate of backside heat loss to the soil and the rate of energy input to the enclosure are the same as under steady state conditions. However, an extra term, the rate of energy accumulation in the heating panel, expressed as

$$q_{accum}^{(k+1)} = \sum \rho_{ij} \bullet Vol_{ij} \bullet Cp_{ij} \bullet (T_{ij}^{(k+1)} - T_{ij}^{(k)}) \tag{4.19}$$

must be considered for the transient response calculation. The rate of heat accumulation in the panel is the rate of internal energy difference between the previous and current time. The relative error of the rate of total energy input for the complete system is the first step shown in Figure 4.6c. If the relative error is greater than 0.005, a new value of the current outlet water temperature is calculated according to

$$T_{wo}^{(k+1)} = T_{wi}^{(k+1)} - \frac{q_o^{(k+1)}}{\dot{m}_w \bullet Cp_w} \tag{4.20}$$

$$\text{where} \quad q_o^{(k+1)} = q_{up}^{(k+1)} + q_{loss}^{(k+1)} + q_{accum}^{(k+1)}$$

and the iterative calculation then returns to the step which imposes the boundary conditions. Iteration continues until the relative error is less than 0.005 indicating the current outlet water temperature is converged. Then the current basement air temperature can be updated. The calculation continues, for the next time interval, with step 2 of Figure 4.6b.

Chapter 5
Methods of Solution for the Simple Models

As mentioned previously in Chapter 4, two different types of model, designated as the simple and full models, were used to describe the hydronic floor heating system. Only the two kinds of the simple model, half-pipe and one-pipe model are considered in this chapter. Because of their nonrectangular domains, discretization into uniform grids cannot be used for the half-pipe and one-pipe models. The methods of discretization are described in this chapter. The chapter concludes with a presentation of the procedures used for solving the steady and unsteady state governing equations by the finite difference technique.

5.1 Half-Pipe Model

5.1.1 Discretization and Grid Generation for the Half-Pipe Model

Before the finite difference method can be employed, the domain must be discretized into grids. For a rectangular domain, uniform grids or nonuniform grids can be used, as shown in Figure 5.1. If the domain has a complex geometry, such grids cannot be used. In the half-pipe model, the domain as shown in Figure 5.2a is not rectangular in shape. Two different methods of discretization for use with a nonrectangular domain will now be described.

Grid generation involves the mapping of an irregular domain (x,y,z) into a rectangular domain (ξ,η,ζ) with discretization being performed in the rectangular domain.

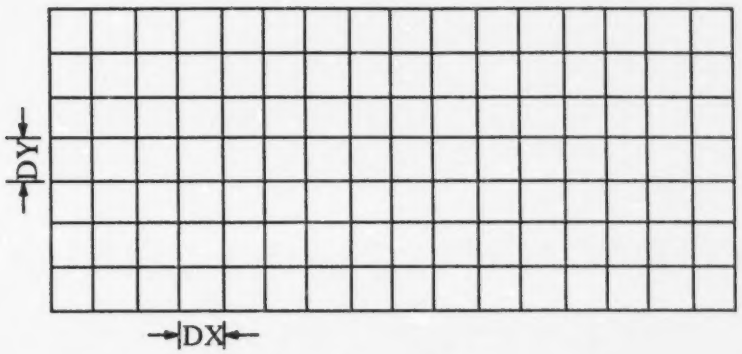

(a) Uniform Grids

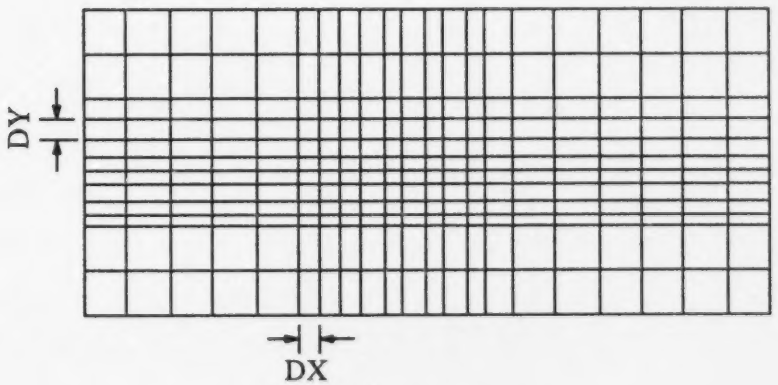

(b) Nonuniform Grids

Figure 5.1 Generated grids for a rectangular domain

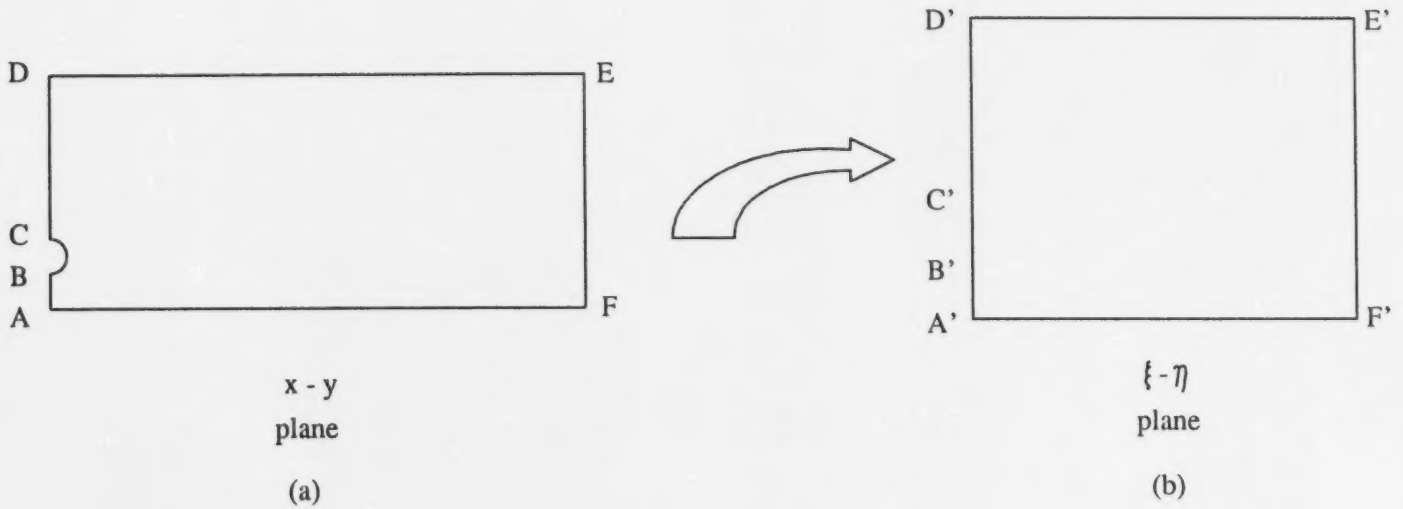

Figure 5.2 Half-pipe representation of the heating panel: Mapping of boundary values from (x , y) coordinates to a (ξ, η) coordinates

In this approach, the governing equations, originally functions of (x,y) are expressed in terms of (ξ,η) as independent variables as shown schematically in Figure 5.2b. Grid generation is then required in order to solve for the temperature distribution in the panel. The procedure employed to obtain the grids for the half-pipe representation is as follows

i) Fix grid points on all boundaries of the nonrectangular domain in Figure 5.2a. In this half-pipe simple model, 41 grid points were employed for the ABCD and EF boundaries with the other 41 grid points located on the AF and DE boundaries.

ii) The rectangular domain, as shown in Figure 5.2b, is discretized into 41 x 41 uniform grids.

iii) The boundaries AB, BC, CD, DE, EF and FA on plane (x,y) are then mapped into A'B', B'C', C'D', D'E', E'F' and F'A' on plane (ξ,η).

iv) The following partial differential equations, with P and Q values set to 0 for simplicity, are used to compute the interior grid point locations on plane (x,y).

$$\sigma\frac{\partial^2 x}{\partial\xi^2}-2\beta\frac{\partial^2 x}{\partial\xi\,\partial\eta}+\gamma\frac{\partial^2 x}{\partial\eta^2}+\delta\bullet(P\frac{\partial x}{\partial\xi}+Q\frac{\partial x}{\partial\eta})=0 \qquad (5.1)$$

$$\sigma\frac{\partial^2 y}{\partial\xi^2}-2\beta\frac{\partial^2 y}{\partial\xi\,\partial\eta}+\gamma\frac{\partial^2 y}{\partial\eta^2}+\delta\bullet(P\frac{\partial y}{\partial\xi}+Q\frac{\partial y}{\partial\eta})=0 \qquad (5.2)$$

where

$$\sigma = x_\eta^{\,2}+y_\eta^{\,2} \qquad \text{(i)}$$

$$\beta = x_\xi x_\eta + y_\xi y_\eta \qquad \text{(ii)}$$

$$\gamma = x_\xi^{\,2}+y_\xi^{\,2} \qquad \text{(iii)}$$

$$\delta = (x_\xi y_\eta + x_\eta y_\xi)^2 \qquad \text{(iv)}$$

With the Dirichlet boundary conditions from A' to F', the above partial differential equations (Fletcher, 1988) are solved on the rectangular domain by the finite difference method. The resulting grid points for the nonrectangular domain are shown in Figure 5.3. The generated grid points are nonorthogonal which means the trajectories of ξ_i and η_j are not perpendicular to each other at their intersection.

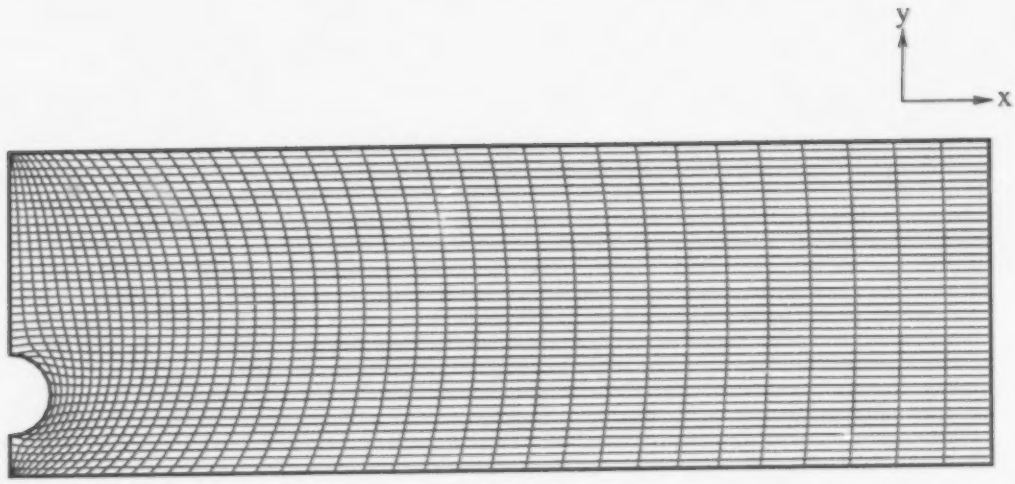

Figure 5.3 Mesh using grid generation

The other method employed to discretize the nonrectangular domain is to utilize nonuniform grids (Gerald and Weatley, 1970) with the intervals between the grid points allowed to be uneven. Consequently, for the curvature region, like BC in Figure 5.2a, the intervals between the grid points will be smaller than those in the straight section. The resulting grid points for the domain of the half-pipe model are shown in Figure 5.4.

5.1.2 Solution Procedure

In additional to the generation of interior grid points for the nonrectangular domain, equations for boundary conditions and the governing equation must be transformed. The boundary conditions in the (x,y) plane for the half-pipe model have been shown in section 4.2.1.2A of Chapter 4. The transformed boundary conditions, in the (ξ,η) co-ordinates corresponding to those in the (x,y) co-ordinates are

Subsystem 1: Heating Panel

The labels for the boundary conditions are shown in Figure 5.2b.

i) Boundary condition on A'B', C'D', E'F':

Figure 5.4 Mesh using nonuniform grids method

$$y_\eta \frac{\partial T}{\partial \xi} = y_\xi \frac{\partial T}{\partial \eta} \tag{5.3}$$

ii) Boundary condition on B'C': No change.

iii) Boundary condition on A'F':

$$x_\xi \frac{\partial T}{\partial \eta} = x_\eta \frac{\partial T}{\partial \xi} \tag{5.4}$$

iv) Boundary condition on D'E':

$$x_\xi \frac{\partial T}{\partial \eta} - x_\eta \frac{\partial T}{\partial \xi} + \frac{h}{k_{pl}} \bullet (x_\xi y_\eta - x_\eta y_\xi) T = \frac{h}{k_{pl}} \bullet (x_\xi y_\eta - x_\eta y_\xi) \bullet T_r \tag{5.5}$$

Subsystem 2: Enclosure

i) Boundary condition for the enclosure: No change.

The unsteady state governing equation is transformed to

$$\frac{\partial}{\partial \xi} \bullet \left(\frac{g_{22}}{g^{\frac{1}{2}}} \frac{\partial T}{\partial \xi} - \frac{g_{12}}{g^{\frac{1}{2}}} \frac{\partial T}{\partial \eta} \right) + \frac{\partial}{\partial \eta} \bullet \left(- \frac{g_{12}}{g^{\frac{1}{2}}} \frac{\partial T}{\partial \xi} + \frac{g_{11}}{g^{\frac{1}{2}}} \frac{\partial T}{\partial \eta} \right) = \frac{g^{\frac{1}{2}}}{\alpha_{pl}} \frac{\partial T}{\partial t} \tag{5.6}$$

where $g^{\frac{1}{2}} = x_\xi y_\eta - x_\eta y_\xi$

$$g_{11} = x_\xi^2 + y_\xi^2$$

$$g_{12} = x_\xi x_\eta + y_\xi y_\eta$$

$$g_{22} = x_\eta^2 + y_\eta^2$$

The steady state governing equation is obtained by setting the right hand side to zero.

No transformation of the boundary conditions and governing equation is necessary to apply the nonuniform grids method of solution as the governing equation with the boundary conditions is solved in the nonrectangular domain. However, the method of discretizing the second derivatives is different from the conventional central differencing scheme. The discretization of the boundary conditions follows the conventional forward and backward differencing schemes with the only difference in discretization from the conventional approach being that for the second derivatives. The unsteady state governing equation is

$$\frac{\partial^2 T}{\partial x^2} + \frac{\partial^2 T}{\partial y^2} = \frac{1}{\alpha_{pl}} \frac{\partial T}{\partial t} \tag{5.7}$$

With the steady state equation, obtained by setting the right hand side equal to zero.

The difference in the discretization is illustrated for the steady state governing equation

$$\frac{\partial^2 T}{\partial x^2} + \frac{\partial^2 T}{\partial y^2} = 0 \tag{5.8}$$

Discretization in the conventional manner for this equation yields

$$\frac{T_{i,j+1}^{(k)} - 2T_{ij}^{(k)} + T_{i,j-1}^{(k)}}{(DX)^2} + \frac{T_{i+1,j}^{(k)} - 2T_{ij}^{(k)} + T_{i-1,j}^{(k)}}{(DY)^2} = 0 \tag{5.9}$$

for the $\frac{\partial^2 T}{\partial x^2}$ and $\frac{\partial^2 T}{\partial y^2}$ terms respectively. For the nonuniform grids method, discretization of equation (5.8) gives

$$2\bullet\left(\frac{T_{i,j-1}^{(k)}-T_{ij}^{(k)}}{DXL\bullet(DXL+DXR)}+\frac{T_{i,j+1}^{(k)}-T_{ij}^{(k)}}{DXR\bullet(DXL+DXR)}\right)+2\bullet$$

$$\left(\frac{T_{i+1,j}^{(k)}-T_{ij}^{(k)}}{DYU\bullet(DYD+DYU)}+\frac{T_{i-1,j}^{(k)}-T_{ij}^{(k)}}{DYD\bullet(DYD+DYU)}\right)=0 \qquad (5.10)$$

Where the first two terms approximate $\frac{\partial^2 T}{\partial x^2}$, and the last two terms $\frac{\partial^2 T}{\partial y^2}$. The positions of the variables in equation (5.10) are shown in Figure 5.5.

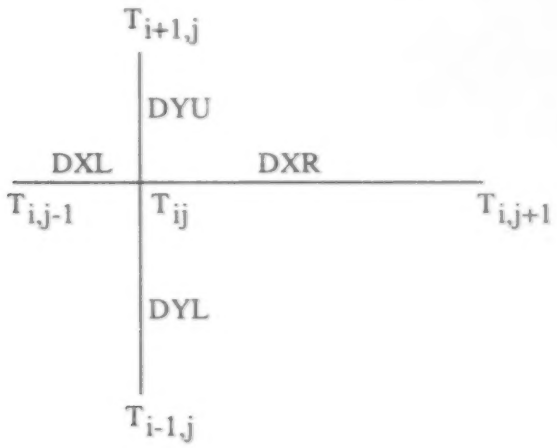

Figure 5.5 Notation for nonuniform grids

5.1.3 Comparison of Results

As shown in the previous section, two methods of solution, grid generation and the use of nonuniform grids are used to solve for the temperature distribution in the top layer of the heating panel in the simple model. The finite difference numerical technique is used as a tool to discretize the equations for these two methods of solutions.

The results from using these two methods of solutions presented in Figures 5.6 and 5.7, show the steady state temperature profiles when the average water temperature of 50°C is, taken as the temperature at the tubing-gypsum interface. As can be observed,

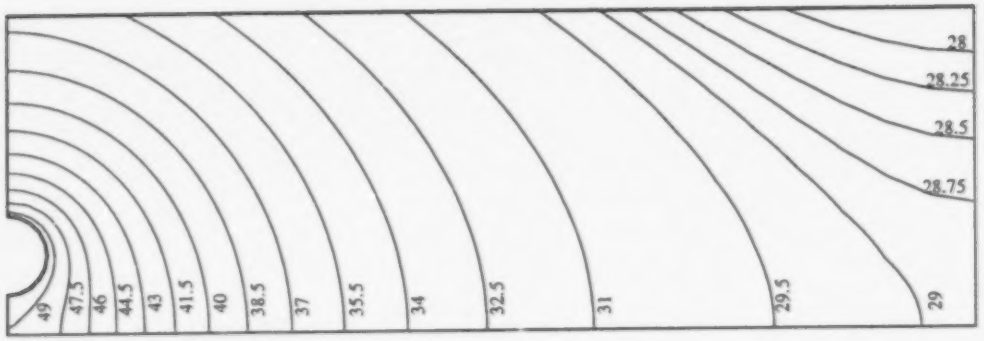

Figure 5.6 Temperature distribution for the simple model using grid generation

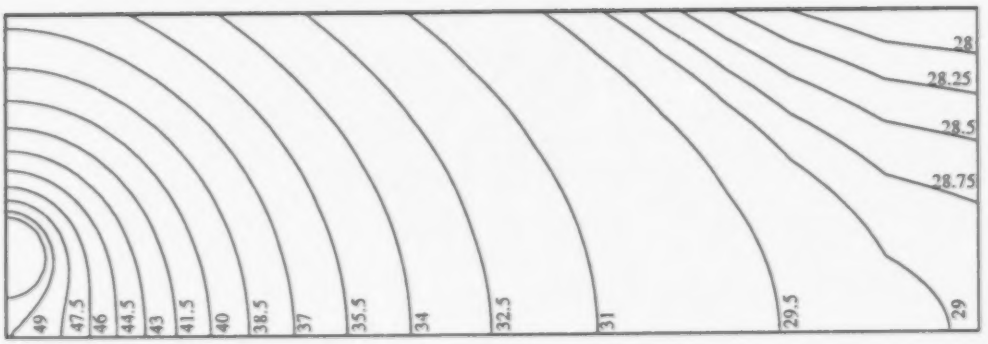

Figure 5.7 Temperature distribution for the simple model using nonuniform grids

there is virtually no difference in the calculated temperature distribution in the heating panel using the grid generation and nonuniform grids solution techniques. Close analysis of the calculated profiles reveals that the temperatures solved by grid generation are slightly higher than those solved by using nonuniform grids.

The dynamic response of the room air temperature and floor surface temperature as a result of a step change of the average water temperature from 50°C to 60°C are displayed in Figures 5.8 and 5.9. The initial steady state room air temperature and average floor surface temperature using the grid generation technique are approximately 0.5°C higher than the values calculated using the nonuniform grids method, and as can be seen, the final steady state values show the same pattern.

5.1.4 Evaluation of the Choices of Methods of Solution for Full Model

Two methods of discretization of the nonrectangular domain have been introduced in the last section. In the grid generation method, the finite difference technique is used to solve the two partial differential equations for the generated grids. On the other hand, no equations need to be solved for the generated grids using the nonuniform grids method as the sizes of the grids are chosen by trial and error. A poor (or incorrect) choice of the sizes of the grids makes the solutions quite different, as will be shown in the Chapter 6 for full model. The governing equations in these two methods are different with the transformed governing equation for the grid generation solution technique being much more complicated than the original governing equation used for the nonuniform grids technique.

Since the difference between the computed profiles from these two methods is very small, the choice of the method of solution for subsequent calculations will be governed by the considerations of computation time and memory space. Since both programs have been utilized on an IBM RISC system/6000, it is possible to provide an

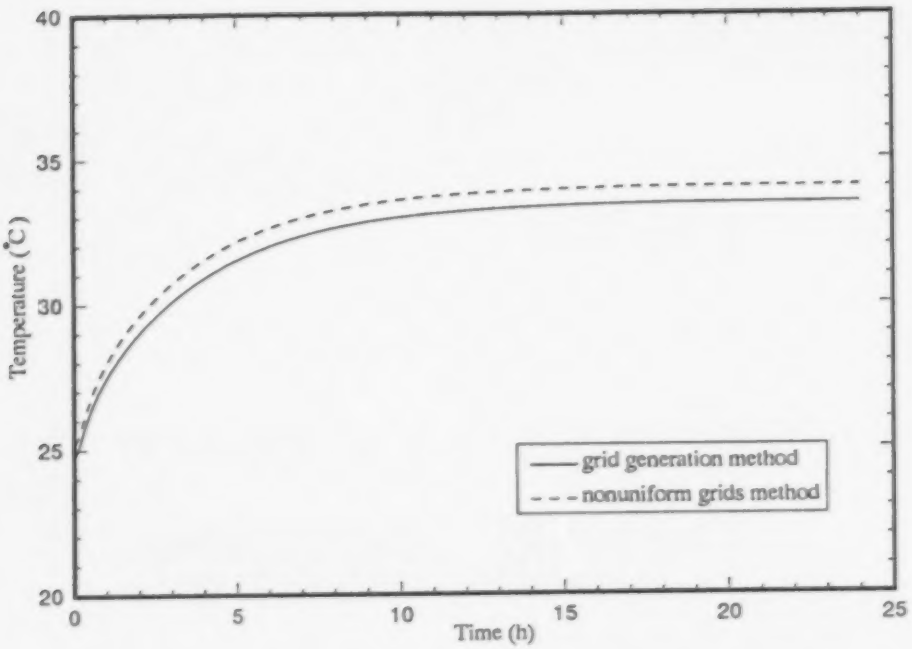

Figure 5.8 The response of room air temperature for a step change in average water temperature from 50°C to 60°C

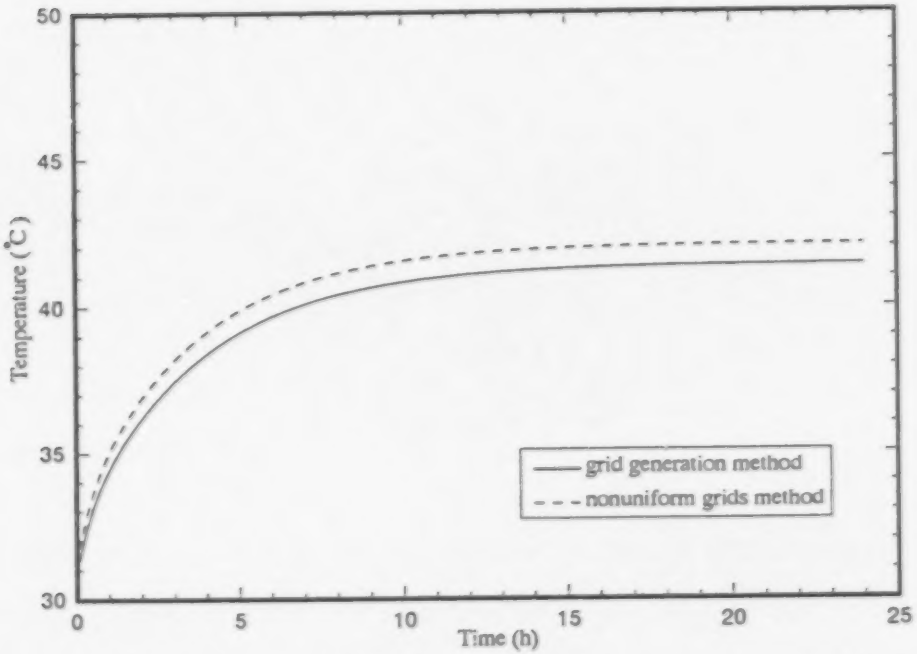

Figure 5.9 The response of floor surface temperature for a step change in average water temperature from 50°C to 60°C

objective comparison of the computation time and memory space. For a transient response calculation of 24 hours duration, 8.5 minutes of computation time is required for the grid generation solution while only 3.5 minutes for the nonuniform grids method. In terms of memory usage, the grid generation approach requires more memory than does the nonuniform grids method. The number of grids (C x D) in the domain required for grid generation is 41 x 41 and the number required for nonuniform grids is 31 x 38. After discretization of the governing equation in either method, the equation is of the form $\underline{\underline{A}}\,\underline{T} = \underline{u}$, with the following A matrix structure:

$$\begin{bmatrix}
a_{1,1} & a_{1,2} & a_{1,3} & 0 & \cdots & 0 & a_{1,D+1} & 0 & \cdots & 0 & a_{1,2D+1} & 0 & \cdots & 0 \\
a_{2,1} & a_{2,2} & a_{2,3} & a_{2,4} & 0 & \cdots & 0 & a_{2,D+2} & 0 & \cdots & 0 & a_{2,2D+2} & \ddots & \vdots \\
a_{3,1} & a_{3,2} & a_{3,3} & a_{3,4} & a_{3,5} & 0 & \cdots & 0 & a_{3,D+3} & 0 & \cdots & 0 & \ddots & 0 \\
0 & \ddots & \ddots & \ddots & \ddots & \ddots & 0 & \cdots & 0 & \ddots & 0 & \cdots & 0 & a_{(C-2)D,CD} \\
\vdots & 0 & \ddots & \ddots & \ddots & \ddots & \ddots & 0 & \cdots & 0 & \ddots & 0 & \cdots & 0 \\
0 & \ddots & 0 & \ddots & \ddots & \ddots & \ddots & \ddots & 0 & \cdots & 0 & \ddots & 0 & \vdots \\
a_{D+1,1} & 0 & \ddots & 0 & \ddots & \ddots & \ddots & \ddots & \ddots & 0 & \cdots & 0 & \ddots & 0 \\
0 & a_{D+2,2} & 0 & \ddots & 0 & \ddots & \ddots & \ddots & \ddots & \ddots & 0 & \cdots & 0 & a_{(C-1)D,CD} \\
\vdots & 0 & a_{D+3,3} & 0 & \ddots & 0 & \ddots & \ddots & \ddots & \ddots & \ddots & 0 & \cdots & 0 \\
0 & \ddots & 0 & \ddots & 0 & \ddots & 0 & \ddots & \ddots & \ddots & \ddots & \ddots & 0 & \vdots \\
a_{2D+1,1} & 0 & \ddots & 0 & \ddots & 0 & \ddots & 0 & \ddots & \ddots & \ddots & \ddots & \ddots & 0 \\
0 & a_{2D+2,2} & 0 & \ddots & 0 & \ddots & 0 & \ddots & 0 & \ddots & \ddots & \ddots & \ddots & a_{CD-2,CD} \\
\vdots & 0 & \ddots & 0 & \ddots & 0 & \ddots & 0 & \ddots & 0 & \ddots & \ddots & \ddots & a_{CD-1,CD} \\
0 & \cdots & 0 & a_{CD,(C-2)D} & 0 & \cdots & 0 & a_{CD,(C-1)D} & 0 & \ddots & 0 & a_{CD,CD-2} & a_{CD,CD-1} & a_{CD,CD}
\end{bmatrix}$$

(5.11)

The system of equations $\underline{\underline{A}}\,\underline{T} = \underline{u}$ is solved using the LINPACK software (Dongarra et al, 1984). Since the $\underline{\underline{A}}$ matrix is a nine banded nonsymmetric matrix, the LINPACK software uses an $\underline{\underline{F}}$ matrix to store all the elements within the big band. In the grid generation technique, the size of the $\underline{\underline{F}}$ matrix is 247 x 1681. Each element in the $\underline{\underline{F}}$ matrix is a double precision number of 8 bytes in size with the result that the whole $\underline{\underline{F}}$ matrix occupies 3.32 MB memory. In the nonuniform grids method, the size of the $\underline{\underline{F}}$ matrix is 187 x 1178 which occupies only 1.76 MB memory so the size of memory

required for the grid generation method is almost double the size of memory for the nonuniform grids method. In additional, extra memory spaces are required for the grid generation method to store the position of every grid point. Since the nonuniform grids method saves computation time and memory, this method will be used to solve the full model which involves more than twenty times the number of grid points used for the half-pipe simple model.

5.2 One-Pipe Model

The one-pipe model is the extension of the half-pipe model for the analysis of heat flow in the heating panel with one embedded hole. The domain of the one-pipe model has been shown in Figure 4.4. Based on the results for the half-pipe model, the responses have been calculated using the nonuniform grids methods. The nonuniform grids method discretized the one-pipe domain as shown in Figure 5.10.

The calculated steady state profiles in the heating panel, for the one embedded hole model are shown in Figure 5.11. As can be observed, the shape and trends of the profiles for the one-pipe model are similar to those calculated using the half-pipe model. The predicted dynamic response of room air temperature and floor surface temperature due to a step change of the average water temperature from 50°C to 60°C using the nonuniform grids method for the one-pipe model are shown in Figure 5.12 and 5.13. Also shown in these figures are the previously calculated responses obtained using the half-pipe model. The results show that the predicted room air temperature and floor surface temperature using the half-pipe model are about 0.1°C higher than those obtained from the one-pipe model. The computation time for predicting the dynamic response for a 24 hour period was 7 minutes, double the time for the response calculated using the half-pipe model.

5.3 Conclusion

The simulated steady state temperature profiles and the transient response results

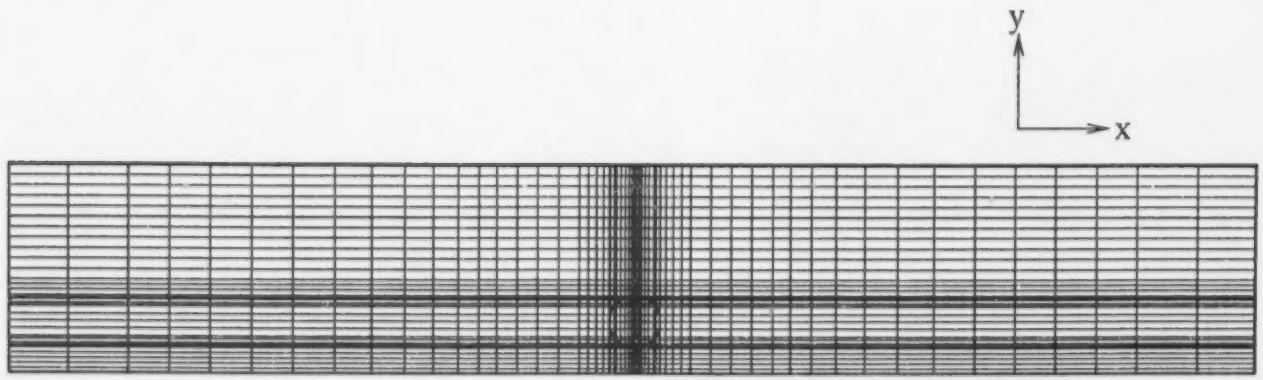

Figure 5.10 Mesh using nonuniform grids for one-pipe model

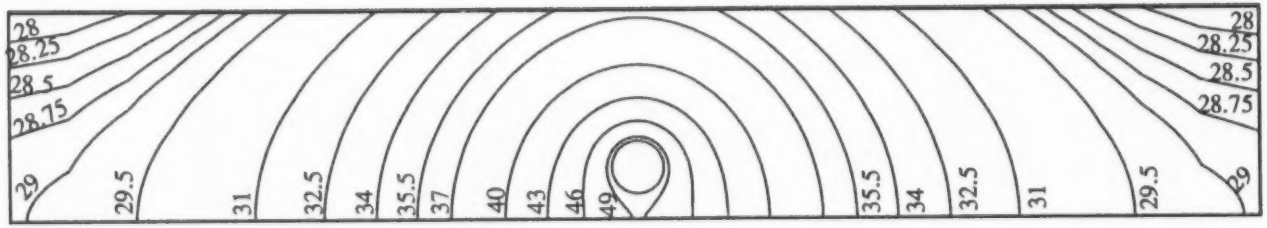

Figure 5.11 Temperature distribution for one-pipe model

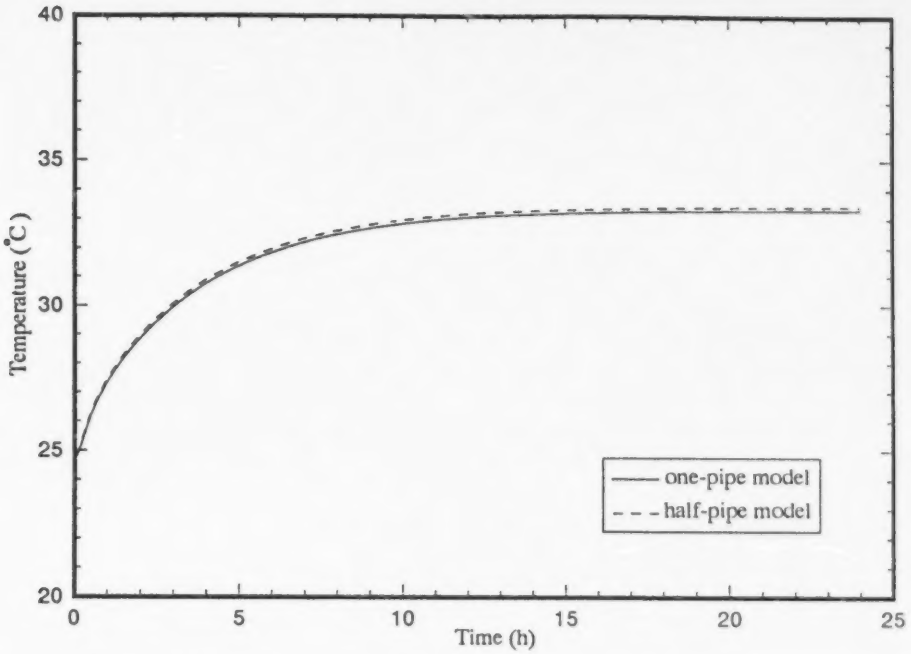

Figure 5.12 The response of room air temperature for a step change in average water temperature from 50 °C to 60 °C

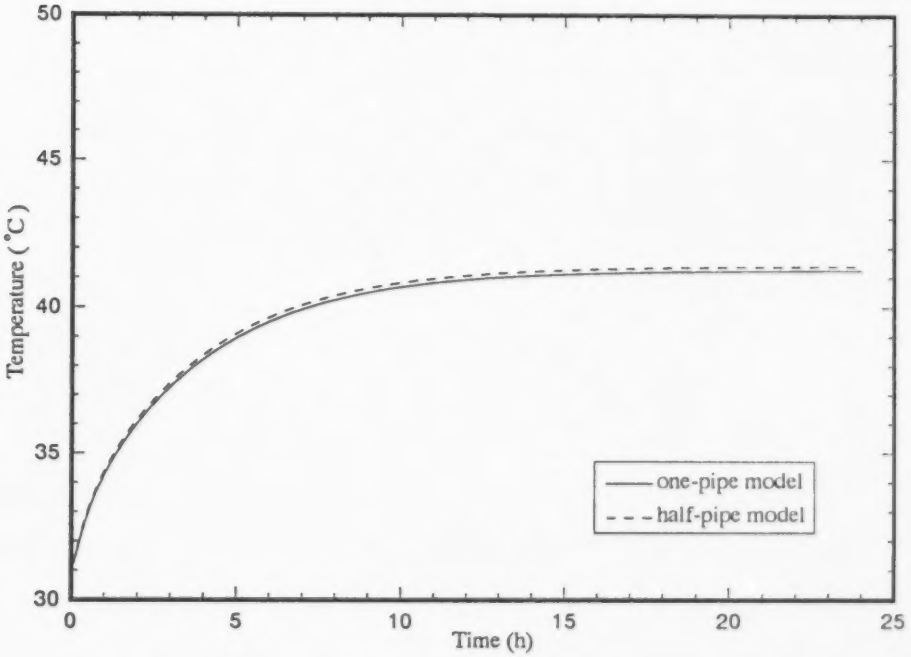

Figure 5.13 The response of floor surface temperature for a step change in average water temperature from 50 °C to 60 °C

obtained using the grid generation and the nonuniform grids methods of solution for the half-pipe simple model were found to be similar. Since it is not an easy task to discretize a domain which has complex geometry using grid generation, and when the performance of the two methods are compared in terms of the amount of memory space and computation time, it was decided to use the nonuniform grids method to solve the one-pipe simple model. As the predicted values computed from the half-pipe and one-pipe simple model are almost the same, it was decided that all computations for the full model presented in the next chapter would be performed using the nonuniform grids method of solution.

Chapter 6
Methods of Solution for the Full Model

Two different methods of solution for the simple models have been discussed in the last chapter. On the basis of those results it was concluded that the nonuniform grids method would be the most suitable method for solving the full model rather than the grid generation method. In this chapter, the details of using the nonuniform grids method with finite difference scheme to determine the steady state and dynamic response of the system using the full model are discussed as well an alternate method of solution, the finite element approach. The results from applying these two different numerical techniques will be compared in the next chapter.

6.1 Finite Difference Method with Nonuniform Grids

6.1.1 Discretization

Just as for the half-pipe or one-pipe simple models, the temperature distribution isotherms in the composite panel for the full model are determined by solving the governing equations numerically. The nonrectangular domain of the composite panel has been shown in Figure 4.2. The domain must be discretized before any numerical method is employed. The domain for the full model is divided into ten sections with a hole located in each section with each section of the same dimensions and each hole at the same location in each section. The choice of the number of grids has an important effect on the temperatures in the composite panel, room air temperature and water temperature. The effect of the number of grids on panel surface temperature, temperature at the interface of

the insulation and concrete, temperature at the interface of the gypsum cement and insulation, bottom surface temperature, outlet water temperature and room air temperature is shown in Table 6.1.

Table 6.1
The effect of the number of grids in one section on computed temperature

Grid Size x-dir y-dir	T_{surf}(°C)	T_{in2} (°C)	T_{in1} (°C)	T_{bot} (°C)	T_r (°C)	T_{wo} (°C)
49 x 38	30.378	33.112	21.237	20.507	26.760	40.830
59 x 38	30.065	32.676	21.161	20.442	26.494	40.879
63 x 38	29.968	32.541	21.138	20.422	26.412	40.895
65 x 38	29.924	32.479	21.128	20.413	26.375	40.902
69 x 38	29.846	32.344	21.100	20.390	26.309	40.915
71 x 38	29.807	32.290	21.091	20.381	26.275	40.921
69 x 30	29.893	32.383	21.119	20.407	26.349	40.907
69 x 29	29.893	32.383	21.119	20.407	26.347	40.907
69 x 28	**29.893**	**32.384**	**21.118**	**20.407**	**26.347**	**40.907**
69 x 27	29.955	32.437	21.143	20.430	26.401	40.896

As can be seen in Table 6.1, an increase in the number of grid points in the x-direction (x-dir) from 59 to 69, decreases the T_r value by approximately 0.2°C which is a significant difference. If the numbers of grid points in the x-direction is increased from 65 to 71, the T_{surf} value decreases by 0.12°C and the T_r value decreases by 0.1°C. The total heat input to the system is 2534.3 W and 2522.2 W for grids of 65 x 38 and 71 x 38 respectively. As can be observed, for a difference of 0.1°C in the T_r value the total heat input increases by 12 W so the most suitable choice of grid size is taken as 69 x 38 which has a total heat

input of 2525.8 W. For the y-direction (y-dir), decreasing the number of grids by 10 reduces the number of grid points in the matrix from 681 x 38 (25878) to 681 x 28 which results in 19068 total grid points. Furthermore, the difference in the value of T_r between using 69 x 28 and 69 x 38 grids is only 0.04°C so a suitable choice for the number of grids for each section is 69 x 28, and the total number of grids required for the whole domain is 681 x 28. The resulting mesh for one section of the whole domain is shown in Figure 6.1. The locations of the two interfaces are shown in the figure and as can be seen, grid points are imposed at the two interfaces and that very coarse grids appear in the concrete layer. The coarse grid in the concrete results because the difference in temperature between the top surface and bottom surface of concrete is only 1°C. For the insulation and gypsum cement layers, fine grids are required since the temperature variations in these two layers is quite large, typically 20°C.

6.1.2 Governing Equations and Boundary Conditions

In the full model, the form of the governing equation is similar to the one in the simple model. However, instead of one governing equation used in the simple model, in the full model, a governing equation is required for each layer of the composite panel. The three equations are

gypsum cement

$$\frac{\partial^2 T}{\partial x^2}+\frac{\partial^2 T}{\partial y^2}=\frac{1}{\alpha_{p1}}\frac{\partial T}{\partial t} \tag{6.1}$$

insulation

$$\frac{\partial^2 T}{\partial x^2}+\frac{\partial^2 T}{\partial y^2}=\frac{1}{\alpha_{p2}}\frac{\partial T}{\partial t} \tag{6.2}$$

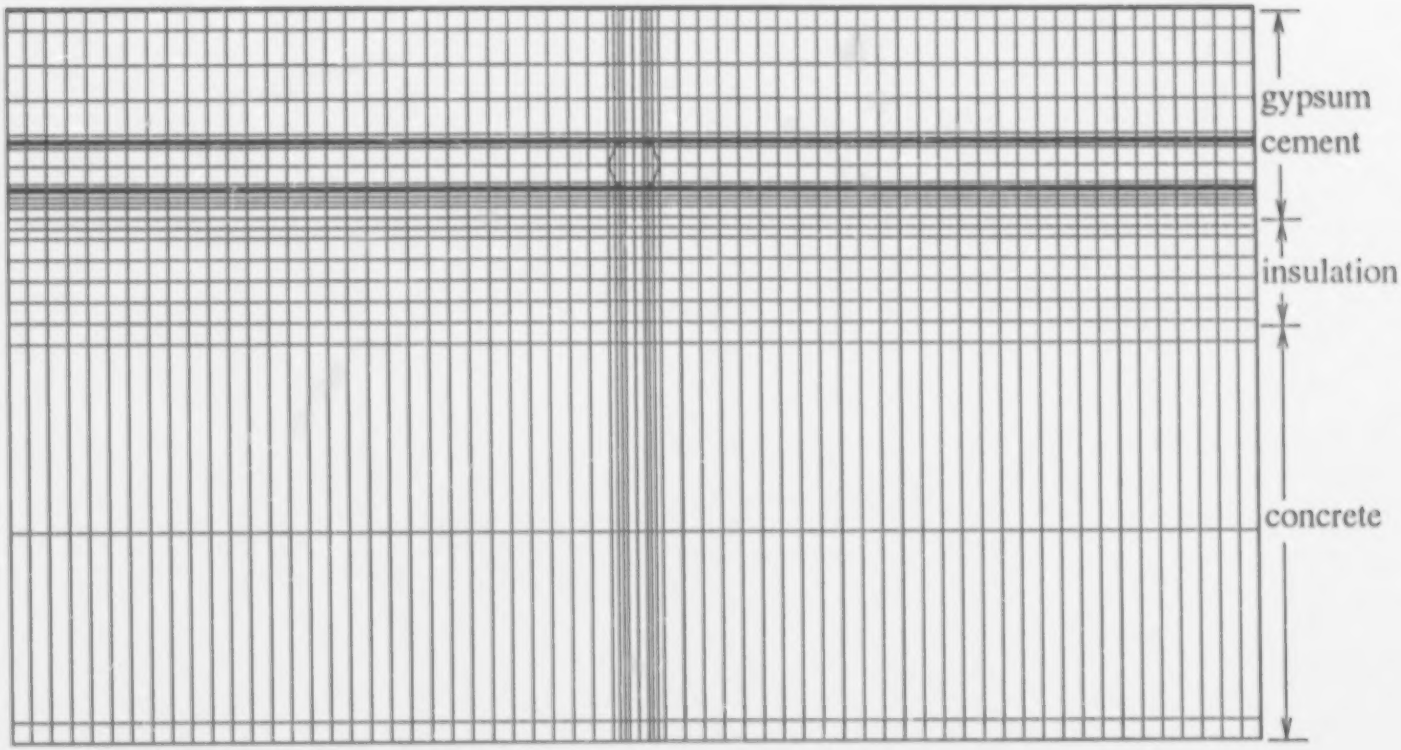

Figure 6.1 Grid mesh for one section of the domain of the full model

concrete

$$\frac{\partial^2 T}{\partial x^2}+\frac{\partial^2 T}{\partial y^2}=\frac{1}{\alpha_{p3}}\frac{\partial T}{\partial t} \qquad (6.3)$$

Under steady state conditions, the terms on the right hand side in the above equations are zero. The system dynamic response is obtained by solving these unsteady state governing equations using the implicit method Crank-Nicholson. There is no difference in the simulated dynamic temperature responses between DT of 1 minute versus 2 minutes. However, when the value of DT was increased to 4 minutes, the responses were quite different so a DT value of 2 minutes the same time interval as for the frequency of data collection was employed. The Crank-Nicholson method is applied using the following discretization of the governing equation

$$-T_1 \bullet T_{i,j-1}^{(k+1)} - T_2 \bullet T_{i-1,j}^{(k+1)} - (T_3 - \frac{1}{\alpha}) \bullet T_{i,j}^{(k+1)} - T_4 \bullet T_{i+1,j}^{(k+1)} - T_5 \bullet T_{i,j+1}^{(k+1)} =$$

$$T_1 \bullet T_{i,j-1}^{(k)} + T_2 \bullet T_{i-1,j}^{(k)} + (T_3 + \frac{1}{\alpha}) \bullet T_{ij}^{(k)} + T_4 \bullet T_{i+1,j}^{(k)} + T_5 \bullet T_{i,j+1}^{(k)} \qquad (6.4)$$

where

$$T_1 = \frac{2}{DXL \bullet (DXL + DXR)}$$

$$T_2 = \frac{2}{DYD \bullet (DYD + DYU)}$$

$$T_3 = -2((\frac{1}{DXL + DXR}) \bullet (\frac{1}{DXL} + \frac{1}{DXR}) + (\frac{1}{DYU + DYL}) \bullet (\frac{1}{DYL} + \frac{1}{DYU}))$$

$$T_4 = \frac{2}{DYU \bullet (DYL + DYU)}$$

$$T_5 = \frac{2}{DXR \bullet (DXL + DXR)}$$

The boundary conditions AD, DE, EH and AH, shown in Figure 4.2, are treated as discussed in Chapter 4. The manner in which the boundary conditions BG and CF are handled is as follows.

Boundary condition BG

At the interface between the concrete and the insulation, the heat flow must be balanced in the X-direction and Y-direction as shown in Figure 6.2.

For simplicity, the direction of heat flow from the element is positive. The symbols A1, A2 and A3 represent areas per unit length.

The rate of heat flow from $T_{ij}^{(k+1)}$ to $T_{i,j-1}^{(k+1)}$ (q_1) is

$$\left(\frac{k_{p2}A_1 + k_{p3}A_2}{L1}\right)\bullet\left(T_{i,j}^{(k+1)} - T_{i,j-1}^{(k+1)}\right) \qquad (6.5)$$

where $$A_1 = \frac{L4}{2}$$

$$A_2 = \frac{L3}{2}$$

The rate of heat flow from $T_{ij}^{(k+1)}$ to $T_{i,j+1}^{(k+1)}$ (q_2) is

$$\left(\frac{k_{p2}A_1 + k_{p3}A_2}{L2}\right)\bullet\left(T_{ij}^{(k+1)} - T_{i,j+1}^{(k+1)}\right) \qquad (6.6)$$

where $$A_1 = \frac{L4}{2}$$

$$A_2 = \frac{L3}{2}$$

The rate of heat flow from $T_{ij}^{(k+1)}$ to $T_{i-1,j}^{(k+1)}$ (q_3) is

$$(k_{p2})(A_3)\bullet\left(\frac{T_{ij}^{(k+1)} - T_{i-1,j}^{(k+1)}}{L3}\right) \qquad (6.7)$$

where $$A_3 = \frac{L2}{2} + \frac{L1}{2}$$

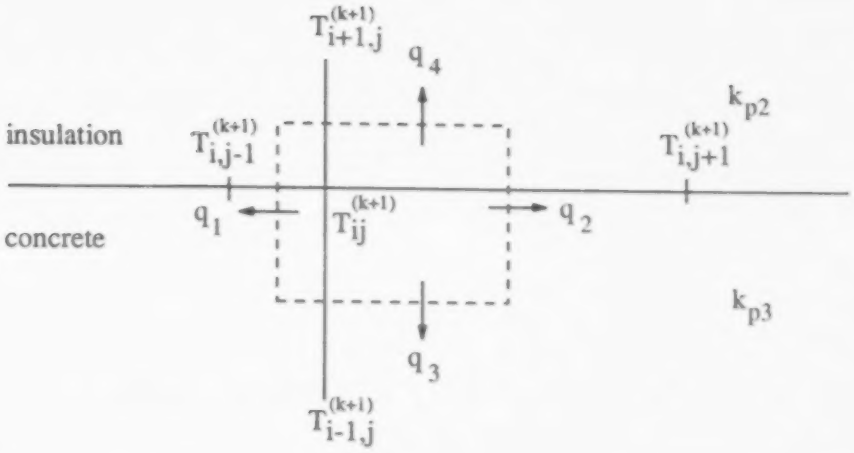

Figure 6.2 Heat flow at the interface of concrete and insulation layers

The rate of heat flow from $T^{(k+1)}_{ij}$ to $T^{(k+1)}_{i+1,j}$ (q_4) is

$$(k_{p3})(A_3)\bullet\left(\frac{T^{(k+1)}_{ij}-T^{(k+1)}_{i+1,j}}{L4}\right) \qquad (6.8)$$

where $$A_3=\frac{L2}{2}+\frac{L1}{2}$$

The heat balance equation at this interface for each element is

$$q_1+q_2+q_3+q_4=\frac{(m_{p2})_{ij}(Cp_2)_{ij}+(m_{p3})_{ij}(Cp_3)_{ij}}{DT}\bullet[T^{(k+1)}_{ij}-T^{(k)}_{ij}] \qquad (6.9)$$

For steady state condition, the term on the right hand side equals zero.

Boundary condition CF

The equations used to represent the interface of the insulation and gypsum cement layers are the same as those for the interface of the insulation and concrete layers except that the physical properties are of the gypsum cement and insulation.

Combining the boundary conditions and the governing equations, a set of simultaneous equations can be expressed in the form of $\underline{A'}\,\underline{T} = \underline{U'}$. The structure of the $\underline{A'}$ matrix depends on the form of discretization used for the first derivative.

The derivative $\frac{\partial T}{\partial x}$ is discretized using

Forward differencing scheme

$$\frac{\partial T}{\partial x} = \frac{3T_{i,j} - 4T_{i,j-1} + T_{i,j-2}}{2DX} \tag{6.10}$$

Backward differencing scheme

$$\frac{\partial T}{\partial x} = \frac{-T_{i,j+2} + 4T_{i,j+1} - 3T_{i,j}}{2DX} \tag{6.11}$$

The discretization $\frac{\partial T}{\partial y}$ is similar to $\frac{\partial T}{\partial x}$ except that x is replaced by y in these expressions and the truncation error is $O(DX^2)$ or $O(DY^2)$, and the resulting structure of the $\underline{A}'$ matrix is an unsymmetric (nine band) matrix as shown in equation (5.11). If discretization of the $\frac{\partial T}{\partial x}$ and $\frac{\partial T}{\partial y}$ derivatives is performed by using the simple first order schemes of forward differencing

$$\frac{\partial T}{\partial x} = \frac{T_{i,j+1} - T_{i,j}}{DX} \tag{6.12}$$

and backward differencing

$$\frac{\partial T}{\partial x} = \frac{T_{i,j} - T_{i,j-1}}{DX} \tag{6.13}$$

The discretization of $\frac{\partial T}{\partial y}$ is similar to $\frac{\partial T}{\partial x}$ except that x is replaced by y. With the above discretization, the truncation error is O(DX) or O(DY) and the structure of $\underline{A}'$ matrix becomes an unsymmetric seven band matrix of the form

$$
\begin{bmatrix}
a_{1,1} & a_{1,2} & a_{1,3} & 0 & \cdots & 0 & a_{1,D+1} & 0 & \cdots & 0 \\
a_{2,1} & a_{2,2} & a_{2,3} & a_{2,4} & 0 & \cdots & 0 & a_{2,D+2} & \ddots & \vdots \\
a_{3,1} & a_{3,2} & a_{3,3} & a_{3,4} & a_{3,5} & 0 & \cdots & \ddots & \ddots & 0 \\
0 & \ddots & \ddots & \ddots & \ddots & \ddots & \ddots & \cdots & \ddots & a_{(C-1)D,CD} \\
\vdots & 0 & \ddots & \ddots & \ddots & \ddots & \ddots & \ddots & \cdots & 0 \\
0 & \ddots & \ddots & \ddots & \ddots & \ddots & \ddots & \ddots & 0 & \vdots \\
a_{D+1,1} & 0 & \ddots & \ddots & \ddots & \ddots & \ddots & \ddots & \ddots & 0 \\
0 & a_{D+2,2} & \ddots & \ddots & \ddots & \ddots & \ddots & \ddots & \ddots & a_{CD-2,CD} \\
\vdots & \ddots & \ddots & 0 & \ddots & \ddots & \ddots & \ddots & \ddots & a_{CD-1,CD} \\
0 & \cdots & 0 & a_{CD,(C-1)D} & 0 & \cdots & 0 & a_{CD,CD-2} & a_{CD,CD-1} & a_{CD,CD}
\end{bmatrix}
\qquad (6.14)
$$

For the full model, the total number of grids (C x D) is 681 x 28. The LINPACK software transfers the full $\underline{A}'$ matrix to matrix $\underline{F}'$ which stores the elements only within the bands. The size of the $\underline{F}'$ matrix is 85 x 19068 if the $\underline{A}'$ matrix is a seven band matrix but the size of $\underline{F}'$ matrix will become 169 x 19068 if the $\underline{A}'$ matrix is a nine band matrix. The computation time and memory used by the nine band matrix are almost twice those required when the seven band matrix is employed. The difference in the results between using the two forward and backward differencing schemes with the truncation error of O(DX) and O(DY) and both schemes with the truncation error of $O(DX^2)$ and $O(DY^2)$ is within 0.1°C. It is important to put fine grids at all boundaries so that the errors of O(DX) and O(DY) can be reduced. The complete set of 19068 simultaneous linear equations is solved by the LINPACK software which uses Gaussian elimination with partial pivoting to compute the LU factorization of the $\underline{F}'$ matrix to solve the system $\underline{A}'\ \underline{T} = \underline{U}'$.

6.2 Finite Element Approach

In this section the other numerical solution procedure, the finite element method, used to solve the partial differential equations is discussed. The finite element method of solution involves rewriting the partial differential equations into piecewise application of a

weak variational form which multiplies the governing equation with an appropriate test function (v) and then integrates the product over the element domain Ω^e. The governing equation

$$\alpha \nabla^2 T = \frac{\partial T}{\partial t} \tag{6.15}$$

rewritten in weak variational form (Reddy, 1984) including the boundary conditions can be stated as

$$\int_\Omega \alpha \ \nabla v \ \nabla T \, d\Omega - \oint_\Gamma v \alpha \ \bar{n} \frac{\partial T}{\partial \bar{n}} \, d\Gamma + \int_\Omega v \frac{\partial T}{\partial t} \, d\Omega = 0 \tag{6.16}$$

In this expression, the first term is the left hand side of the governing equation, the second term represents the boundary conditions along the arc length of the domain and the third term the time-varying term.

In the Galerkin method (Reddy, 1984), the test function is identical to the interpolation function. Since it is difficult to select a single interpolation function over the entire domain, the continuous domain has to be discretized into elements, which can be triangular or quadrilateral or a combination of both shapes. Each element is described by a set of piecewise polynomial interpolation functions which are defined only for the element. For the system under study, the domain is divided into triangular elements by using the Super2d™ software (Anon, 1992) to generate a nonuniform mesh consisting of 6842 elements with approximately nine triangular elements around each pipe. The mesh for each section is not the same, as can be seen from the meshes for the ten sections shown in Figures 6.3a to 6.3e. The two dashed lines shown in each of the sections show the locations of the two interfaces. Unlike the finite difference method which imposes grid points at each of the interfaces, it can be observed that the sides of the elements are not imposed at the interfaces.

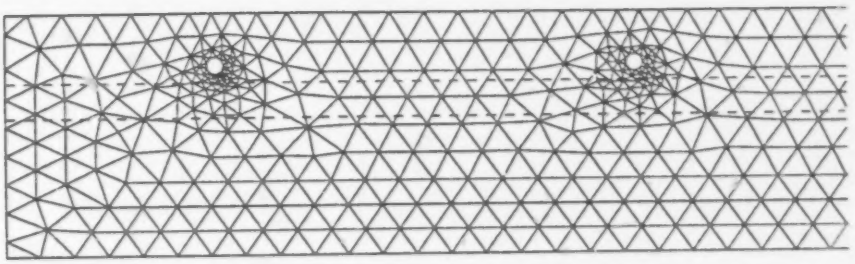

(a) tubes 1 and 2

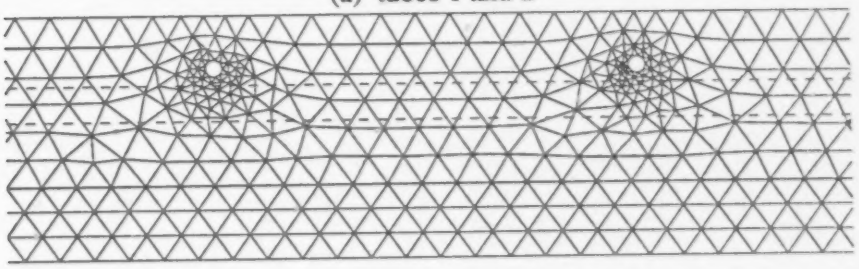

(b) tubes 3 and 4

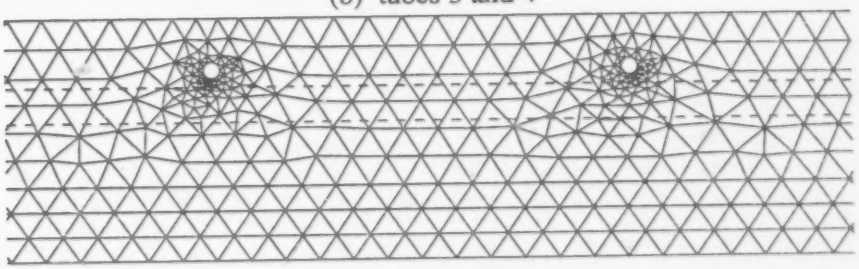

(c) tubes 5 and 6

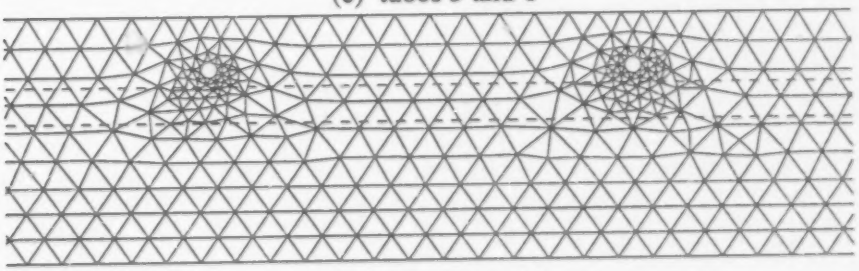

(d) tubes 7 and 8

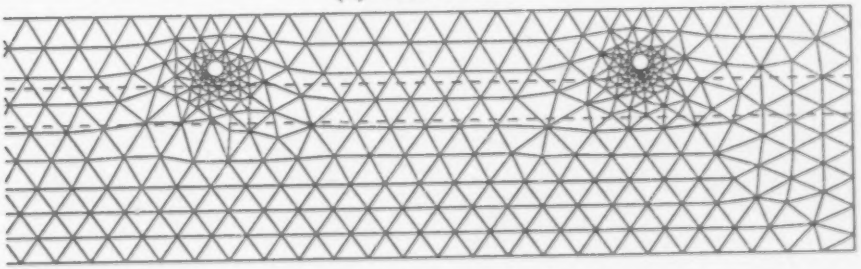

(e) tubes 9 and 10

Figure 6.3 Mesh sections for the finite element method

The application of the Galerkin finite element method over an element is

$$\int_{\Omega^e} \alpha \nabla \psi \, \nabla T \, d\Omega^e - \oint_{\Gamma^e} \psi \, q_n \, d\Gamma + \int_{\Omega^e} \psi \frac{\partial T}{\partial t} \, d\Omega^e = 0 \qquad (6.17)$$

where $$q_n = \bar{n} \alpha \frac{\partial T}{\partial \bar{n}}$$

The approximate solution for equation (6.17), over an element, is

$$T(x,y) = \sum_{i=i}^{n} \psi_i T(x_i, y_i) \qquad (6.18)$$

In this work, n is taken to be equal to 6 so there are six nodes associated with each triangular element with the first three nodes on the vertices of the triangle and the other three nodes located at the midpoint of each side of the triangle. The ψ_i are quadratic Lagrangian interpolation functions. The numerical formulation for the computation is established through the following steps. The first step involves substitution of equation (6.18) into (6.17) to give

$$\sum_{i=1}^{n} \int_{\Omega^e} \alpha \, \nabla \psi_j \, \nabla \psi_i \, T_i \, d\Omega^e - \oint_{\Gamma^e} \psi_j \, q_n \, d\Gamma + \int_{\Omega^e} \psi_j \, \psi_i \frac{\partial T_i}{\partial t} \, d\Omega^e = 0 \qquad (6.19)$$

$$j = 1, 2, \cdots n$$

For the first time step, the term $\frac{\partial T_i}{\partial t}$ is discretized by the Euler scheme (because $T_i^{(k-1)}$ is not available when k = 1) using the expression

$$\frac{\partial T}{\partial t} = \frac{T_i^{(k+1)} - T_i^{(k)}}{DT} \qquad (6.20)$$

but after the first time step, the discretization is based on the pure implicit method, Gear scheme (Fortin et al., 1985), that is

$$\frac{\partial T_i}{\partial t} = \frac{3T_i^{(k+1)} - 4T_i^{(k)} + T_i^{(k-1)}}{2DT} \qquad (6.21)$$

The time step, DT is taken as 2 minutes, the same as used for the finite difference method. Substitution of equations (6.20) and (6.21) into (6.19) respectively yields

$$\sum_{i=1}^{n}\int_{\Omega^e}\alpha\,\nabla\psi_j\,\nabla\psi_i\,T_i^{(k)}\,d\Omega^e-\oint_{\Gamma^e}\psi_j\,q_n^{(k)}\,d\Gamma^e+\sum_{i=1}^{n}\int_{\Omega^e}\psi_j\,\psi_i\left(\frac{T_i^{(k+1)}-T_i^{(k)}}{DT}\right)d\Omega^e=0 \quad (6.22)$$

for the Euler discretization and

$$\sum_{i=1}^{n}\int_{\Omega^e}\alpha\,\nabla\psi_j\,\nabla\psi_i\,T_i^{(k)}\,d\Omega^e-\oint_{\Gamma^e}\psi_j\,q_n^{(k)}\,d\Gamma^e+\sum_{i=1}^{n}\int_{\Omega^e}\psi_j\,\psi_i\left(\frac{3T_i^{(k+1)}-4T_i^{(k)}+T_i^{(k-1)}}{2DT}\right)d\Omega^e=0 \quad (6.23)$$

for the implicit Gear discretization

The solution procedure, will be illustrated by considering equation (6.23). Moving the unknowns to the left hand side and the known terms to the right side yields

$$\sum_{i=1}^{n}\frac{3}{2DT}\int_{\Omega^e}\psi_j\,\psi_i\,T_i^{(k+1)}d\Omega^e=\sum_{i=1}^{n}\left(\oint_{\Gamma_e}\psi_j\,q_n^{(k)}\,d\Gamma^e-\int_{\Omega^e}\nabla\psi_j\,\nabla\psi_i\,T_i^{(k)}\,d\Omega^e\right.$$

$$\left.+\int_{\Omega^e}\frac{4\psi_j\,\psi_i\,T_i^{(k)}-\psi_j\,\psi_i\,T_i^{(k-1)}}{2DT}\,d\Omega^e\right) \quad (6.24)$$

$$j=1,2,\cdots n$$

which can be rewritten as

$$\sum_{i=1}^{n}K_{ij}^{(e)}\,T_i^{(k+1)(e)}=\sum_{i=1}^{n}F_{ij}^{(e)} \quad (6.25)$$

where $$K_{ij}^{(e)}=\frac{3}{2DT}\int_{\Omega^e}\psi_j\,\psi_i\,d\Omega^e$$

and

$$F_{ij}^{(e)}=\oint_{\Gamma^e}\psi_j\,q_n^{(k)}\,d\Gamma-\int_{\Omega^e}\alpha\,\nabla\psi_j\,\nabla\psi_i\,T_i^{(k)}\,d\Omega^e+\int_{\Omega^e}\frac{4\psi_j\,\psi_i\,T_i^{(k)}-\psi_j\,\psi_i\,T_i^{(k-1)}}{2DT}d\Omega^e \quad (6.26)$$

$$j=1,2,\cdots n$$

In this work, the size of the $\underline{K}^{(e)}$ matrix is 6 X 6 and the matrix is symmetric, i.e. $K_{ij}^{(e)}=K_{ij}^{(e)}$. The boundary conditions are imposed on the first term of $F_{ij}^{(e)}$ and the integrands calculated by using the 6-point Gaussian quadrature method. Finally, the finite

element equations for all elements are assembled together to form a "global" matrix $\underline{\underline{K}}$ matrix and "global" vector $\underline{F}$, that is

$$\underline{\underline{K}}\,\underline{T} = \underline{F} \tag{6.27}$$

with the temperatures calculated by LU factorization for the mesh points of the domain.

In this study, the Poly2d™ (Anon, 1992) software was employed to solve for the temperatures for this unsteady state two-dimensional formulation of the heating panel. In order to solve for the desired temperatures of this system, some modifications to the Poly2d™ software were introduced by Dr. Hayes of the Department of Chemical Engineering, University of Alberta who holds the license for the Poly2d™ software. The necessary modifications to the package were

i) To allow for convective heat transfer to the room and conductive heat flow to the soil, the option of utilizing Cauchy boundary conditions was added.

ii) To provide for different thermal conductivities, densities and heat capacities in each layer, the code was modified to handle different thermal properties for each layer of the panel.

iii) Iteration algorithms were incorporated in order to establish the room air temperature and outlet water temperature values as explained in Section 4.3.

iv) The linear triangular elements were modified into quadratic triangular elements.

Chapter 7
Comparison of Experimental and Simulation Results

In the last three chapters, the characteristics of the two simple models and of the full model, boundary conditions and different numerical methods of solution for each model have been presented. Since no computation of outlet water temperature and no consideration of heat loss to the soil were considered in the simple models, the full model was developed to represent the actual system. In this chapter, the finite element and the nonuniform grids with finite difference approach are used to solve for the steady and unsteady state temperatures. The simulated results using these two numerical techniques will be compared. A comparison of the simulated results with the experimental data will be presented with respect to the steady state temperature profiles and dynamic temperature responses for an abrupt change in inlet water temperature. In addition, the sensitivity of system responses to changes in parameters and physical property values will be illustrated with the simulated results.

7.1 Experimental Procedure

All the experimental tests have been performed on the heating system installed in the basement of the experimental house. Since there are two large windows located in the south wall on the main floor of the experimental house, two separate transient response tests were performed in order to determine the effect of solar radiation entering the upper

zone on the room air temperature of the lower zone. One test was performed with the insulating shutters open, and the other with the shutters closed. Both tests were conducted under the same operating conditions. At the beginning of the experiment, the inlet water temperature was maintained constant at 45°C and when the basement air temperature reached steady state, the temperature of the inlet water temperature was abruptly changed to 55°C. This temperature remained fixed for about 24 hours so that the basement air temperature had enough time to reach the new steady state. All the initial steady state operating conditions for the tests and the parameter values used for simulation of the system dynamic response are summarized in Table 7.1.

Table 7.1
Initial steady state conditions and parameter values for simulation

Variable / Parameter		First Test (shutters open)	Second Test (shutters closed)
$*T_{wi}$	(°C)	44.9	45.7
$*T_{wo}$	(°C)	41.0	41.5
$*T_r$	(°C)	25.8	28.4
$*T_{surf}$	(°C)	28.52	30.3
$*T_{amb}$	(°C)	9.7	9.3
$*\dot{m}$	(kg/s)	0.149	0.152
*ACR	(1/hr)	0.2	0.2
$*T_{s1}$	(°C)	12.75	13.72
$*T_{s2}$	(°C)	6.84	15.5
q_{ceil}	(W)	45.92	43.93
h	($W/m^2°C$)	15.45	24.26
UA	($W/°C$)	92.92	151.58
k_{s1}	(W/m°C)	0.5145	0.4903

Note: The initial steady state conditions are denoted by an asterisk.

As can be observed from Table 7.1, the values of the h and UA parameters established from the steady state conditions exhibited a large difference even though the operating conditions were similar except for the shutter position. In the second test, the h and UA parameter values increased by 57 percent and 63.13 percent respectively from

their original values of 15.45 W/m²°C and 92.92 W/°C. The increase in the values of h and UA by a large percentage in the second test is caused by an increase of basement air temperature, ambient temperature, the soil temperature located north of the house, the water flow rate and the difference of the inlet and outlet water temperatures in the second test. Even a small increase of 0.5°C in the difference between the inlet and outlet water temperature will elevate the panel surface temperature and basement air temperature and rate of total energy input for the complete system which in turn will increase the value of h by more than 10 percent. This increase will also affect the value of UA. In the later section, the effects of the change in the UA and h values and the physical property values on the dynamic temperature responses will be presented.

7.2 Predicted and Experimental Steady State Temperature Profiles and Dynamic Responses Temperature

7.2.1 First Test : Shutters Open

Predicted steady state temperature profiles and dynamic temperature responses using the full model have been computed by using both the finite element and finite difference numerical methods. A comparison of these two kinds of predicted results obtained using the two different numerical techniques is presented in Figures 7.1 to 7.8. Also, the predicted results are compared with the experimental data shown in these figures.

The steady state temperature profiles at the initial operating conditions, when T_{wi} equals 45°C, are shown in Figures 7.1 and 7.2 as computed by the finite difference method and finite element method respectively. As can be observed, the temperature contours calculated by the finite difference method are smoother than those obtained using the finite element method. The temperatures computed by the finite difference method were also about 1°C higher than those established using the finite element method.

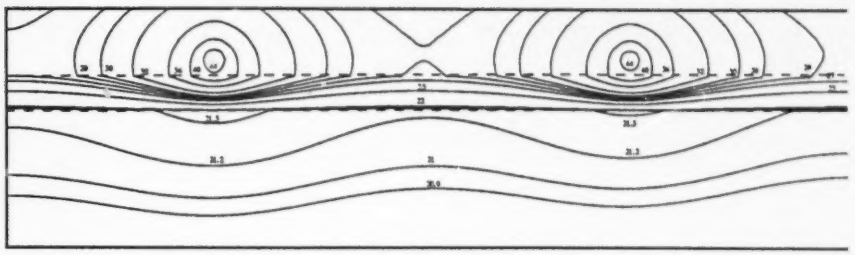

(a) tubes 1 and 2

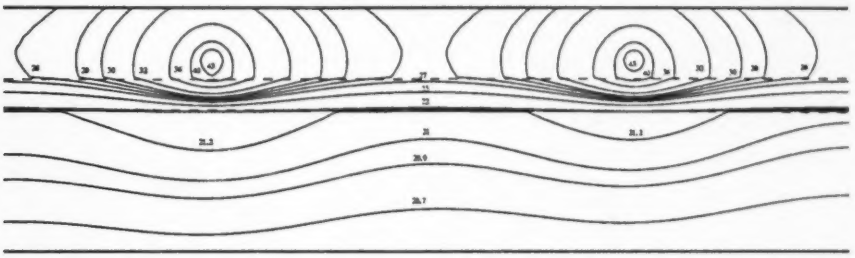

(b) tubes 3 and 4

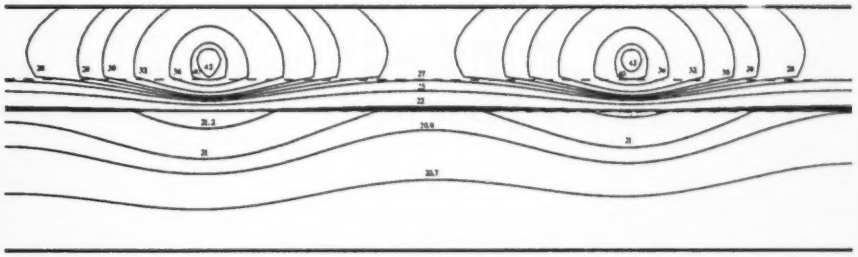

(c) tubes 5 and 6

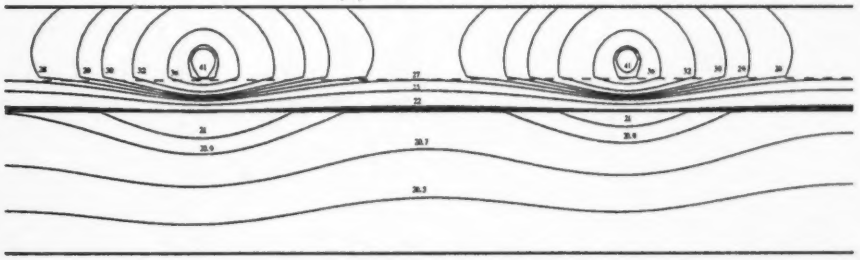

(d) tubes 7 and 8

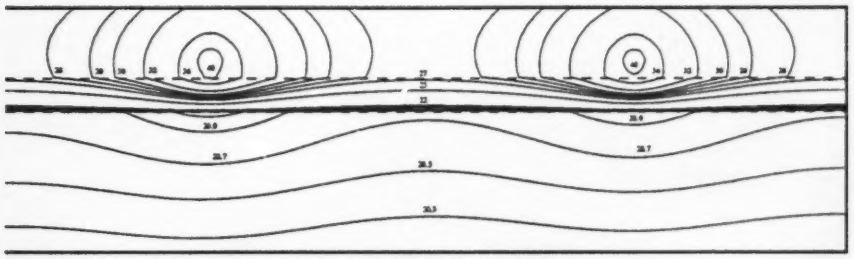

(e) tubes 9 and 10

Figure 7.1 Temperature profiles in the heating panel computed by the finite difference method

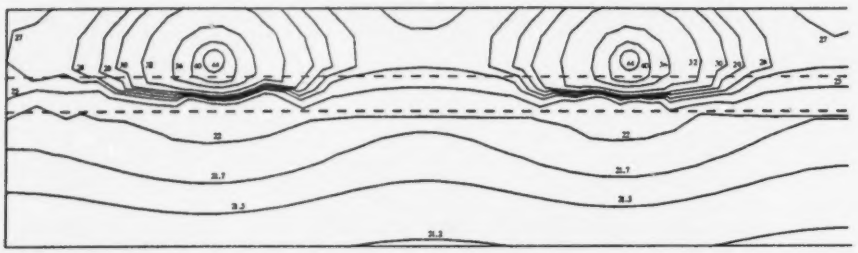

(a) tubes 1 and 2

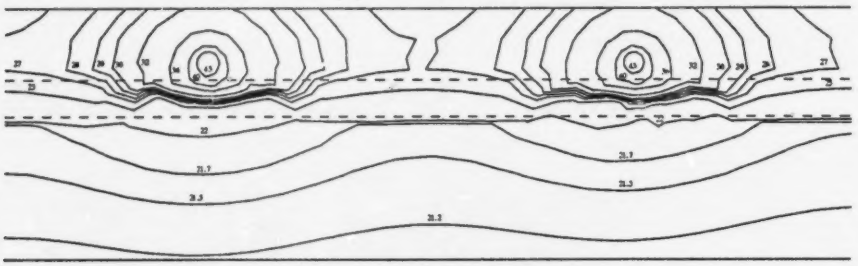

(b) tubes 3 and 4

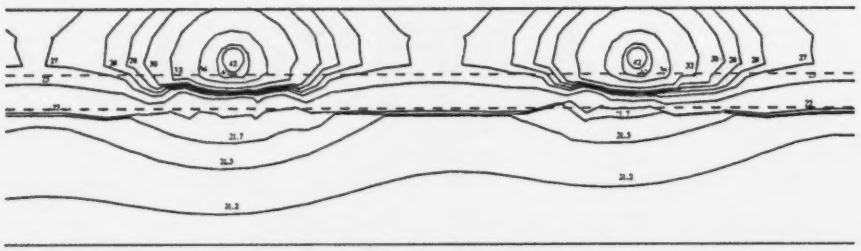

(c) tubes 5 and 6

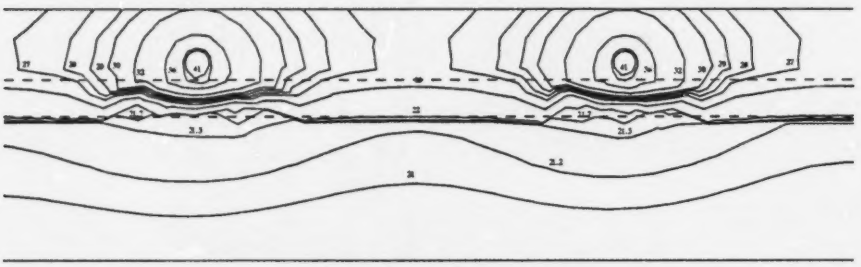

(d) tubes 7 and 8

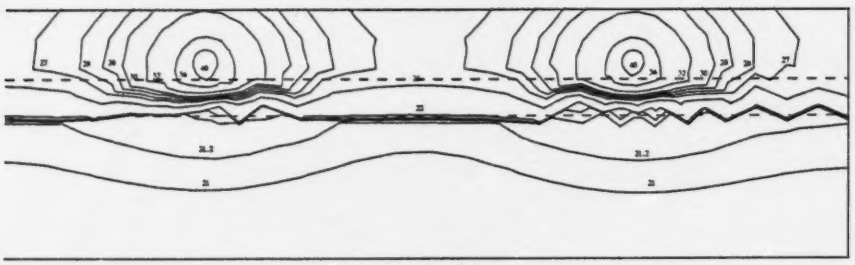

(e) tubes 9 and 10

Figure 7.2 Temperature profiles in the heating panel computed by the finite element method

Figures 7.3a to 7.3d show the computed temperature profiles at the different surfaces and interfaces of the composite panel. The experimental values of the panel surface temperature, also plotted in Figure 7.3a, were measured at 5 cm intervals. Temperatures were measured from the south wall, 1.5m left of the east wall, to the centre of the basement. All the temperature profiles show peak values, which are located directly above the tubing with the minimum values located somewhere in between the tubing. The first peak occurs at the location of the first tube and the last peak at the location of the tenth tube as represented by holes in the model. As can be seen, the pattern of the experimental data is similar to the simulated results but the maximum temperatures are not as pronounced. As can be observed in Figures 7.3a and 7.3b, the trends and shapes of the temperature profiles calculated using the two different numerical techniques agree with each other. The finite difference method predicts temperature values that are about 1°C higher than calculated by the finite element method. In contrast to this difference, the temperature profiles at the interface of the insulation and concrete, and the bottom surface temperature of the composite panel shown in Figures 7.3c and 7.3d, the temperatures computed from the finite element method are higher than those from finite difference method by about 0.75°C. The shape and trend of the profiles for both methods are identical except for the temperature at the interface of the insulation and the concrete computed from finite element method. There is no apparent explanation for the nature of the calculated profile.

Figures 7.4a to 7.4d show the calculated steady state temperature profiles for an inlet water temperature of 55°C and the basement air temperature at steady state. The temperature profiles are similar to those predicted when the inlet water temperature was 45°C as shown in Figures 7.3a to 7.3d. The only difference between the computed temperature shown in these two sets of figures results from the 10°C higher inlet water temperature. For the panel surface temperature, the simulated results at the peak locations in Figure 7.4a are higher than those in Figure 7.3a by a magnitude of about 6.4°C to 6.8°C

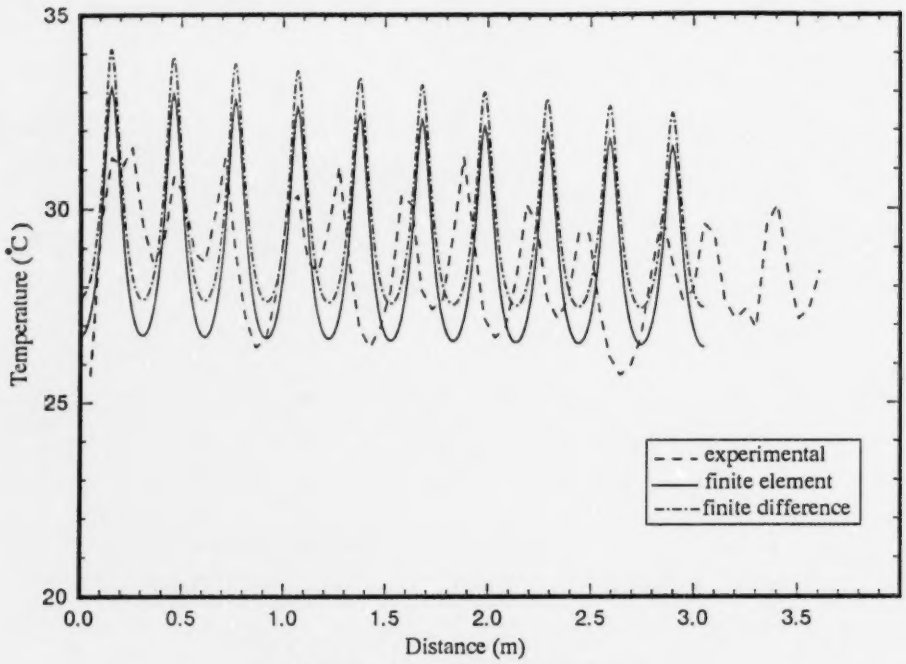

(a) Panel top surface temperature

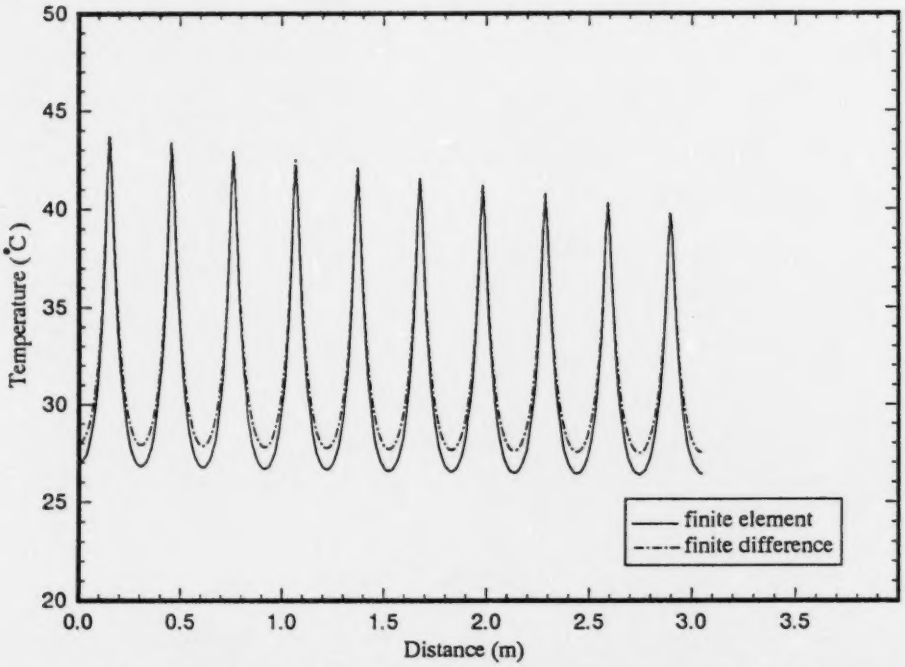

(b) Temperature at the interface of the gypsum cement and insulation

Figure 7.3 Initial steady state temperature profiles for an inlet water temperature of 45°C (first test)

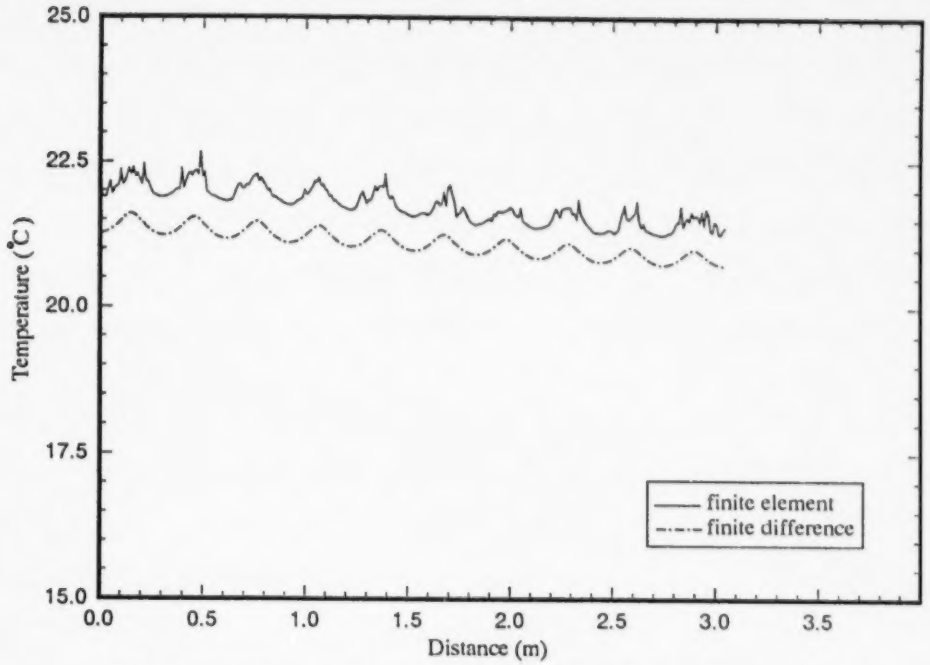

(c) Temperature at the interface of the insulation and concrete

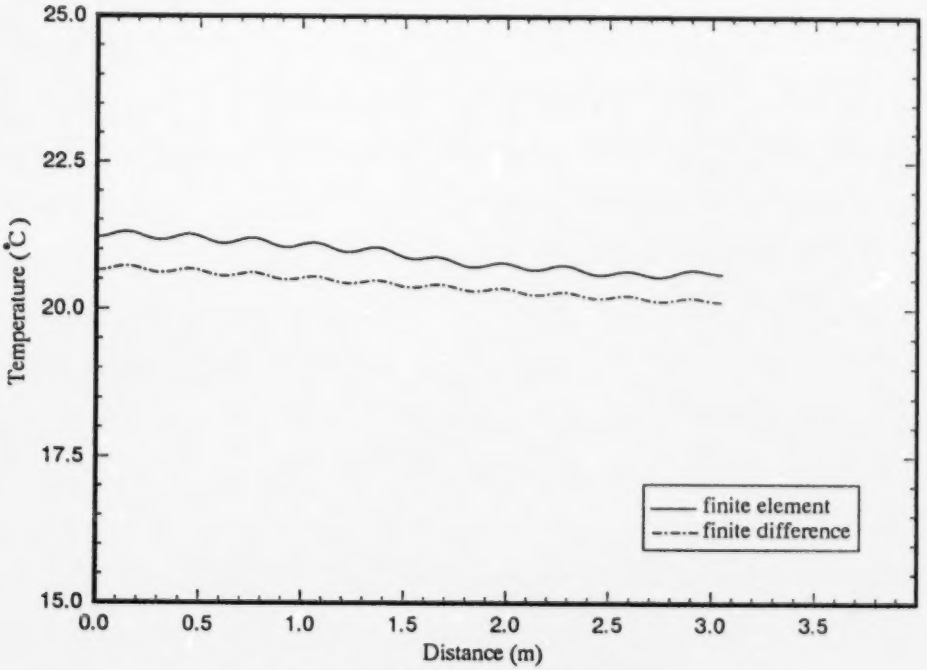

(d) Panel bottom surface temperature

Figure 7.3 Initial steady state temperature profiles for an inlet water temperature of 45°C (first test)

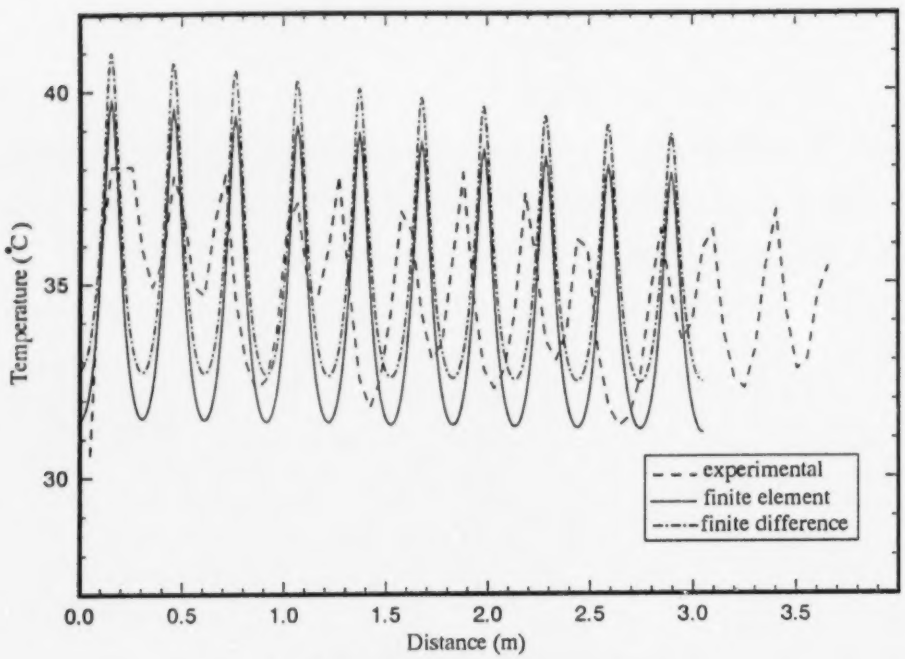

(a) Panel top surface temperature

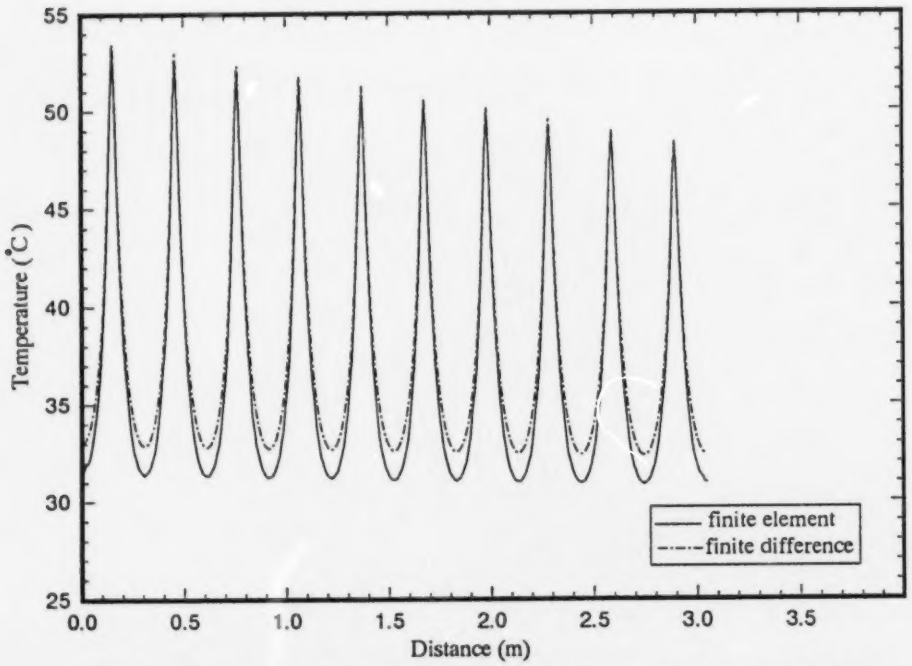

(b) Temperature at the interface of the gypsum cement and insulation

Figure 7.4 Final steadv state temperature profiles for an inlet water temperature of 55°C (first test)

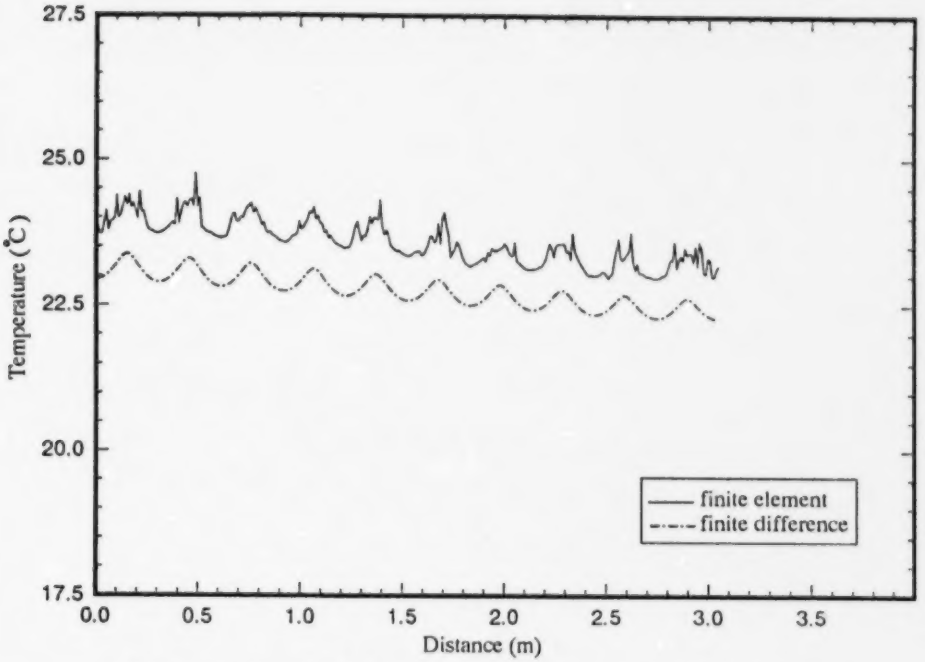

(c) Temperature at the interface of the insulation and concrete

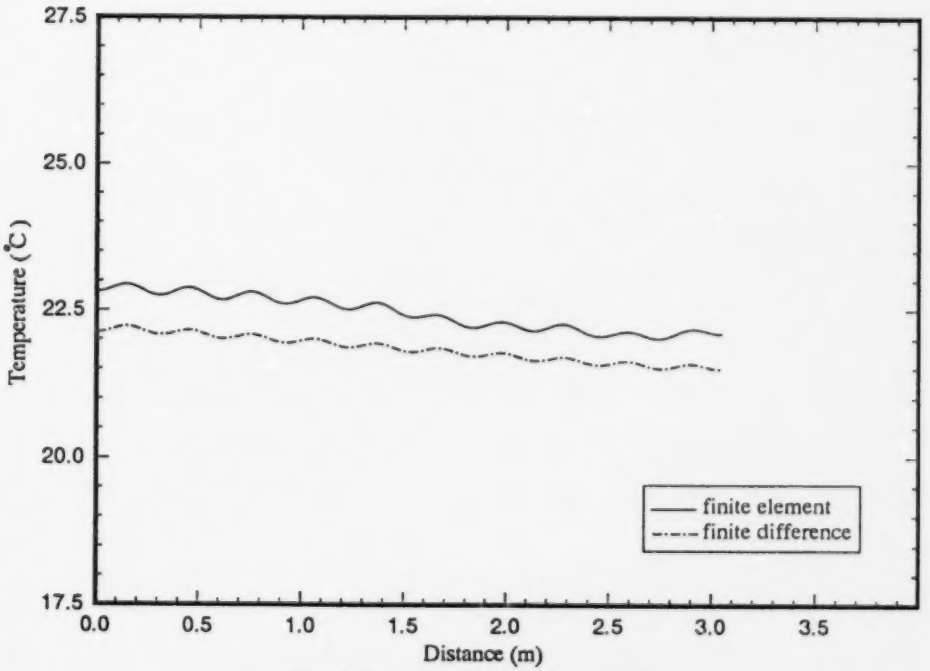

(d) Panel bottom surface temperature

Figure 7.4 Final steady state temperature profiles for an inlet water temperature of 55°C (first test)

with the peaks closer to the first tube higher than those near to the tenth tube. The increase in temperature of most of the minimum values is about 5°C. The experimental results at the peak locations are approximately 7°C higher due to the 10°C increase in inlet water temperature while the difference of the minimum temperatures is approximately 5.5° C to 6.5°C. The largest differences occur close to the location of the first hole. The minima of the temperature profiles at the interface of the insulation and the concrete range from 1.5°C to 1.75°C higher for the 55°C water temperature and at the peak locations, the difference is about 1.6°C. The predicted bottom surface temperatures (maximum and minimum values) are about 1.6°C higher for the inlet water temperature set at 55°C.

Of more interest than the steady state temperature profiles are the dynamic response of the basement air temperature, panel surface temperature, bottom surface temperature and zone outlet water temperature in response to a change in the inlet water temperature from 45°C to 55°C. The experimental and simulated transient temperature responses are shown in Figure 7.5a to 7.5d. The trends of the simulated basement air temperatures, shown in Figure 7.5a, are similar but the finite difference approach values are about 1.0°C higher than those calculated using the finite element method. The simulated temperatures are shown to be higher in magnitude than the experimental data for most of the transient. Comparing the two simulated results, the predictions from the finite element method show close agreement with the experimental results at steady state, but the finite difference method predictions do not. It should also be noted that the experimental response is slower than either of the simulated responses.

For the panel surface temperature shown in Figure 7.5b, both the simulated responses and the experimental data are very similar to those of basement air temperature both in magnitude and trend. Also, just as the finite difference method predicted higher basement air temperatures than observed or calculated using the finite element method, a similar pattern is evident for the panel surface temperature. However, the computed bottom surface temperature response solved by the finite element method is about 0.5°C

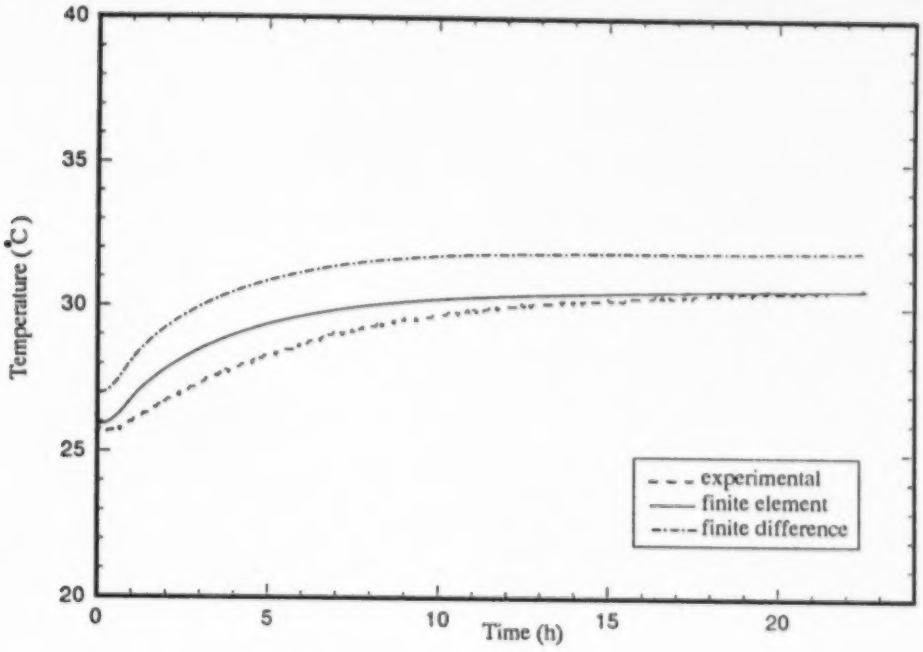

(a) Basement air temperature

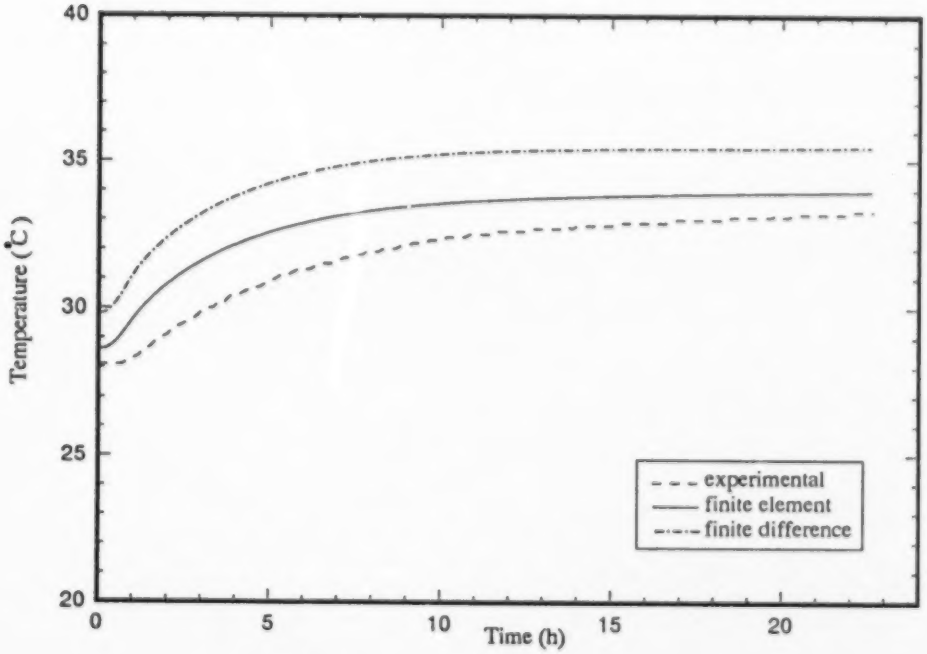

(b) Panel top surface temperature

Figure 7.5 Temperature dynamic responses for a step change in inlet water temperature from 45°C to 55°C (first test)

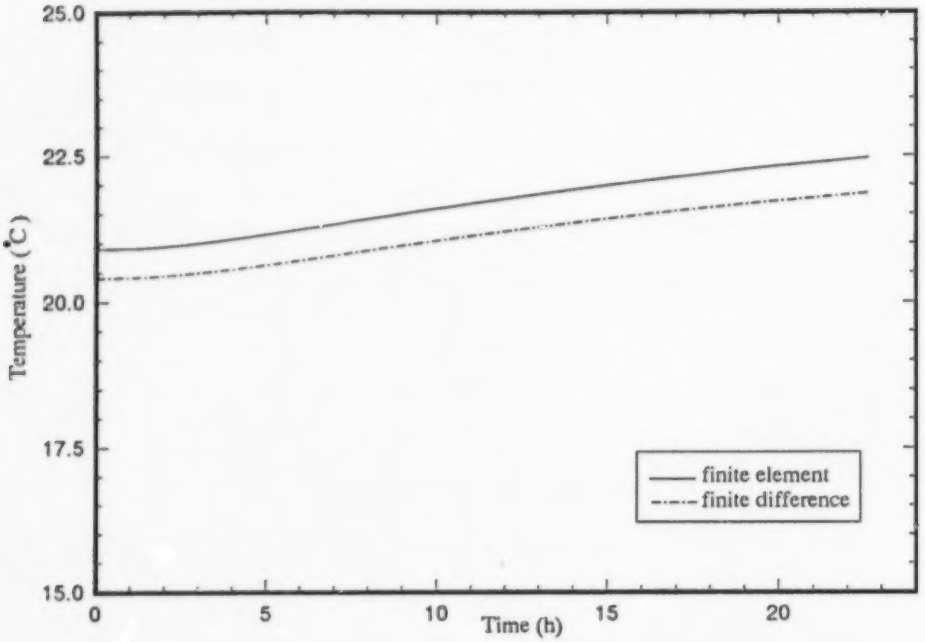

(c) Panel bottom surface temperature

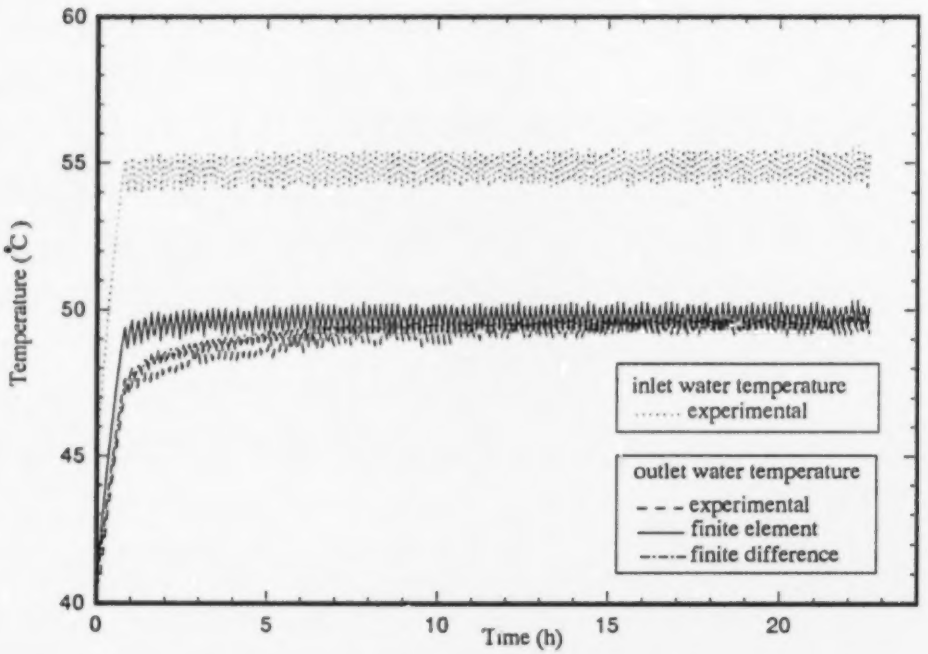

(d) Outlet water temperature

Figure 7.5 Temperature dynamic responses for a step change in inlet water temperature from 45℃ to 55℃ (first test)

higher than that obtained by finite difference method. In Figure 7.5d, the experimental and calculated responses of outlet water temperature to the step change of inlet water temperature from 45°C to 55°C. The finite difference predictions follow quite closely the experimental response while the finite element method predicted temperature rises slightly faster resulting in temperatures that are about 2°C higher for the first hour with the difference decreasing at longer times.

7.2.2 Second Test : Shutters Closed

The operating procedure for the second test are the same as those used for the first test, except that the upper zone shutters of the experimental house were closed. The initial steady state temperature profiles at the surfaces and interfaces calculated using the values in Table 7.1 are presented in Figures 7.6a to 7.6d. The trends of the simulated profiles in Figure 7.6 are similar to those displayed in Figure 7.3 but the magnitudes of the temperatures are higher than those in Figure 7.3 even though the operating conditions are similar in both tests. The maximum panel surface temperatures in Figure 7.6 are almost identical to those in Figure 7.3 but the minimum temperatures are approximately 0.3°C higher. For comparison of the predicted profiles for the two interface temperatures and the bottom surface temperature shown in Figures 7.6 b, 7.6c and 7.6d with those in Figures 7.3b, 7.3c and 7.3d reveals values that are about 1°C higher. The results in Figures 7.7a to 7.7d show that the change in the temperature profiles after the step change of the inlet water temperature to 55°C agrees with the change observed between the predicted values in Figures 7.3 and 7.4.

The experimental and predicted dynamic response of basement air temperature, panel surface temperature, bottom surface temperature and outlet water temperature to the 10°C abrupt increase in inlet water temperature are presented in Figure 7.8. The predicted responses in Figures 7.8a to 7.8c are similar and only the response of the outlet water temperature, plotted in Figure 7.8d, differing during the initial phase of the transient

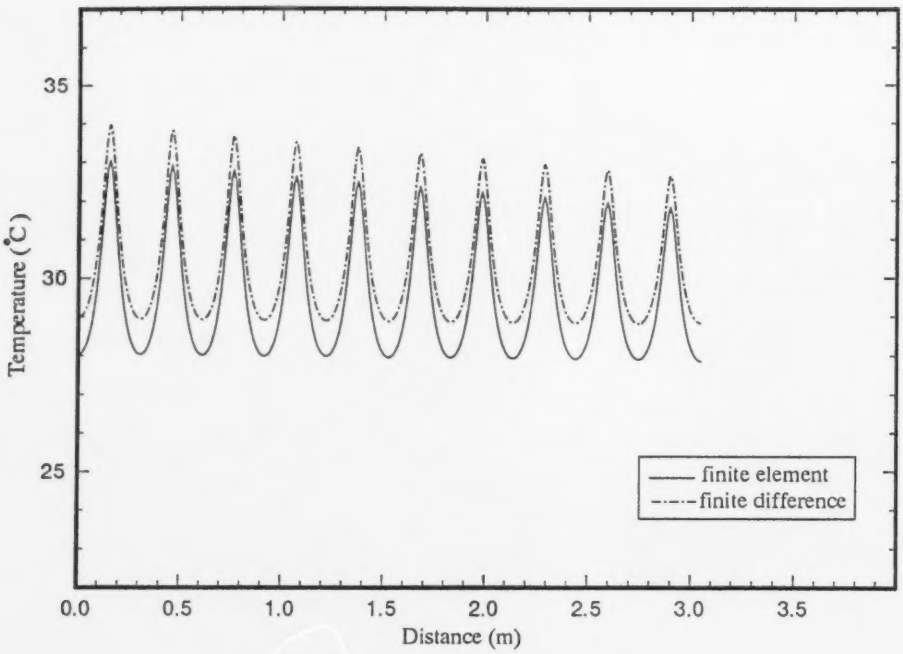

(a) Panel top surface temperature

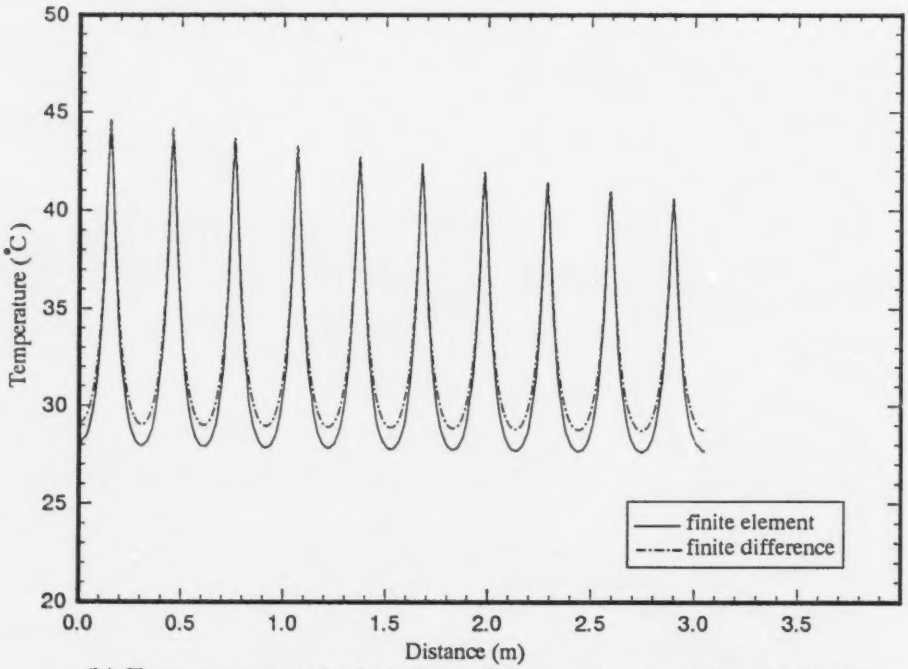

(b) Temperature at the interface of the gypsum cement and insulation

Figure 7.6 Initial steady state temperature profiles for an inlet water temperature of 45°C (second test)

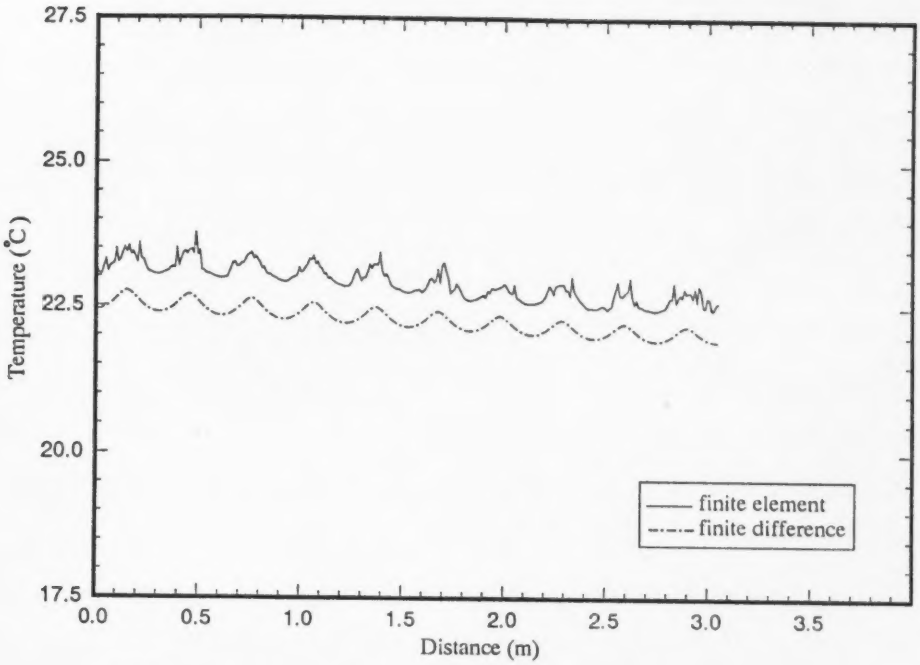

(c) Temperature at the interface of the insulation and concrete

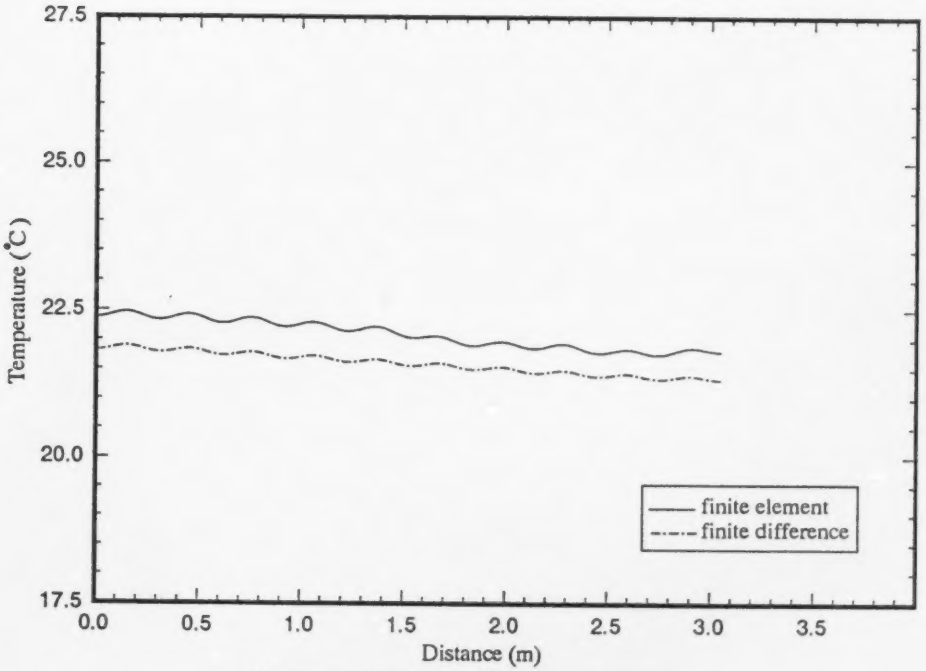

(d) Panel bottom surface temperature

Figure 7.6 Initial steady state temperature profiles for an inlet water temperature of 45°C (second test)

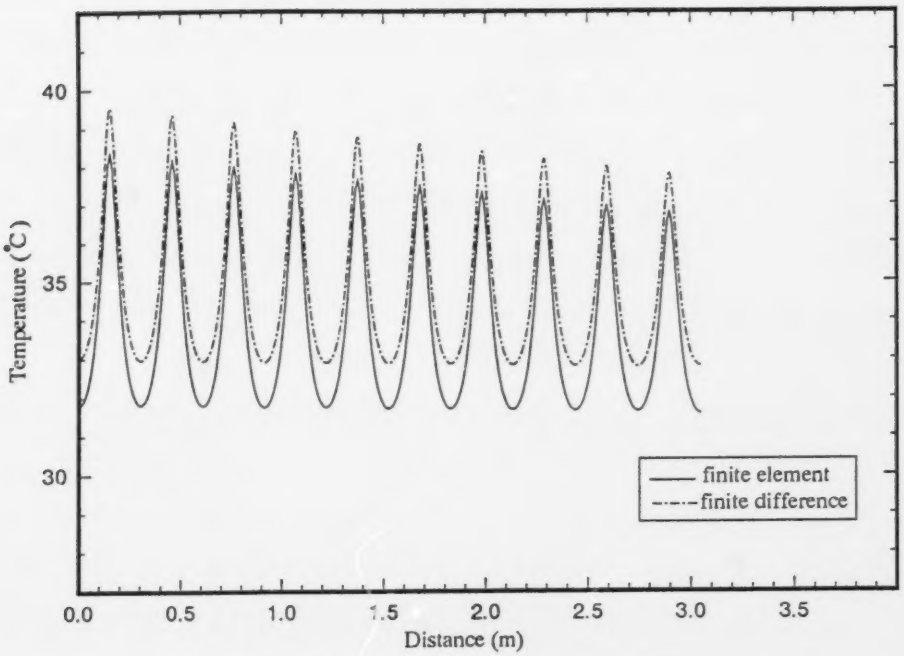

(a) Panel top surface temperature

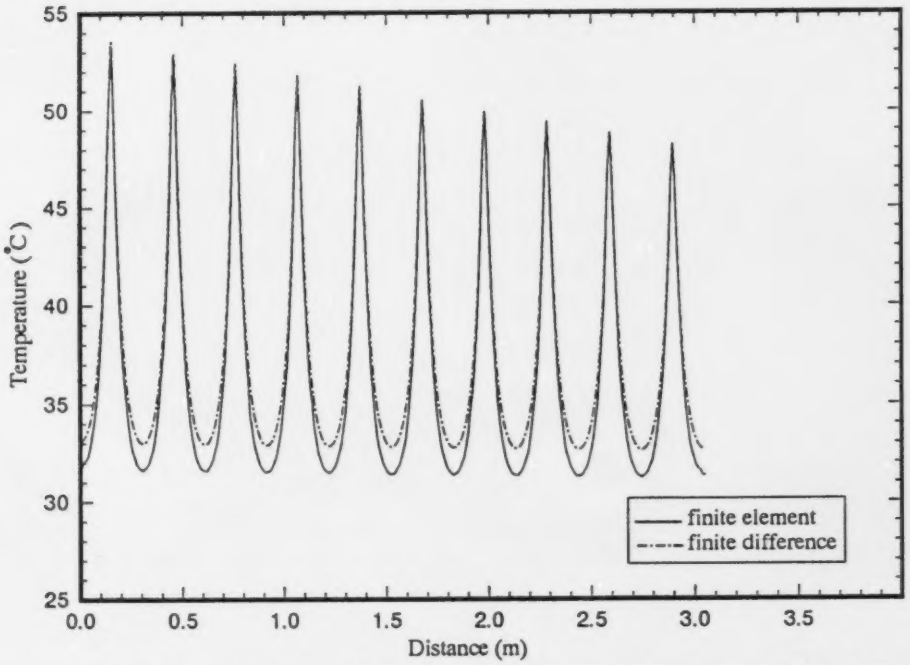

(b) Temperature at the interface of the gypsum cement and insulation

Figure 7.7 Final steady state temperature profiles for an inlet water temperature of 55°C (second test)

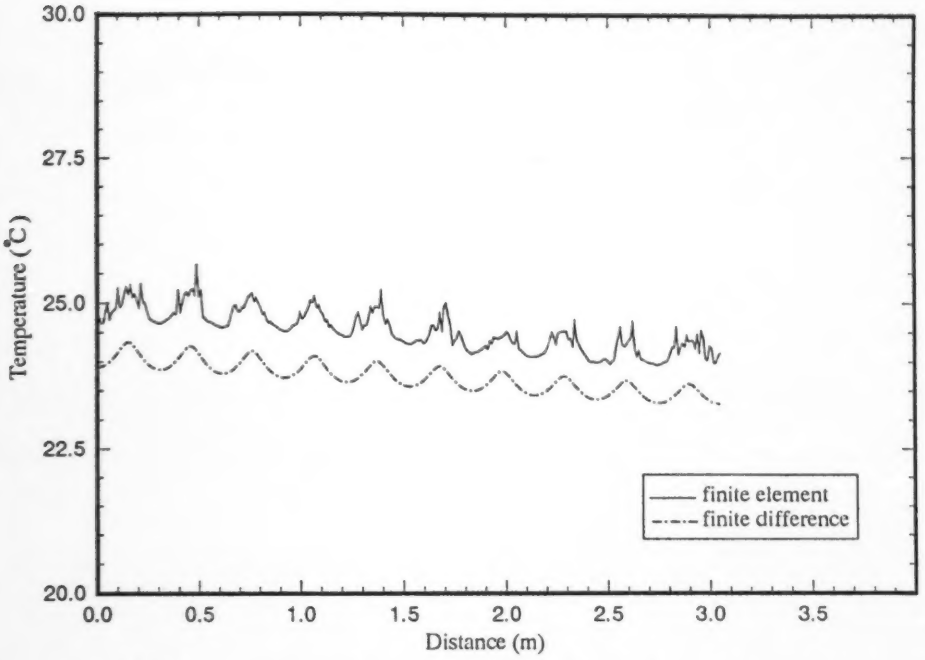

(c) Temperature at the interface of the insulation and concrete

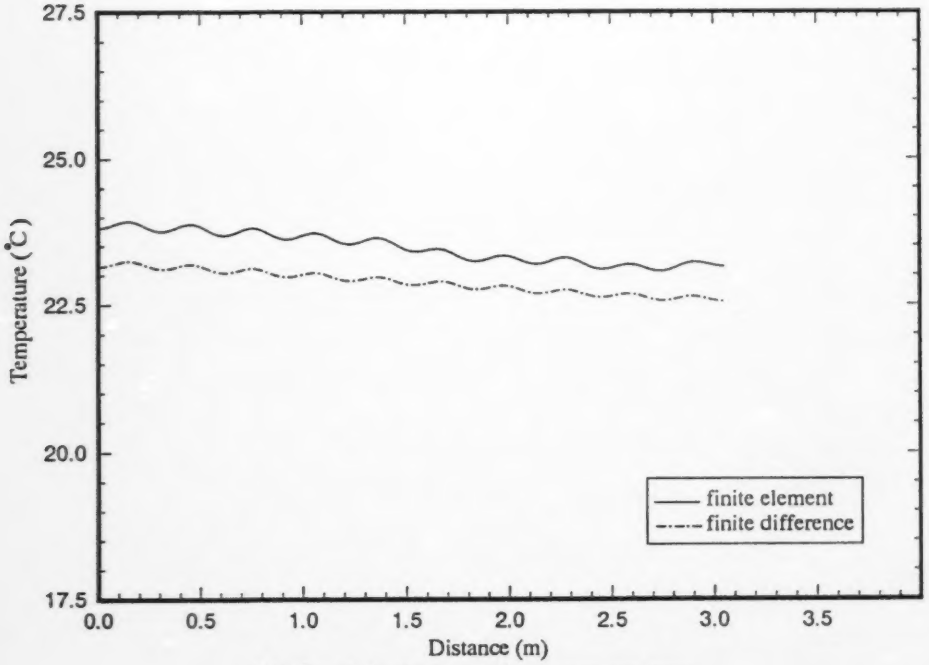

(d) Panel bottom surface temperature

Figure 7.7 Final steady state temperature profiles for an inlet water temperature of 55°C (second test)

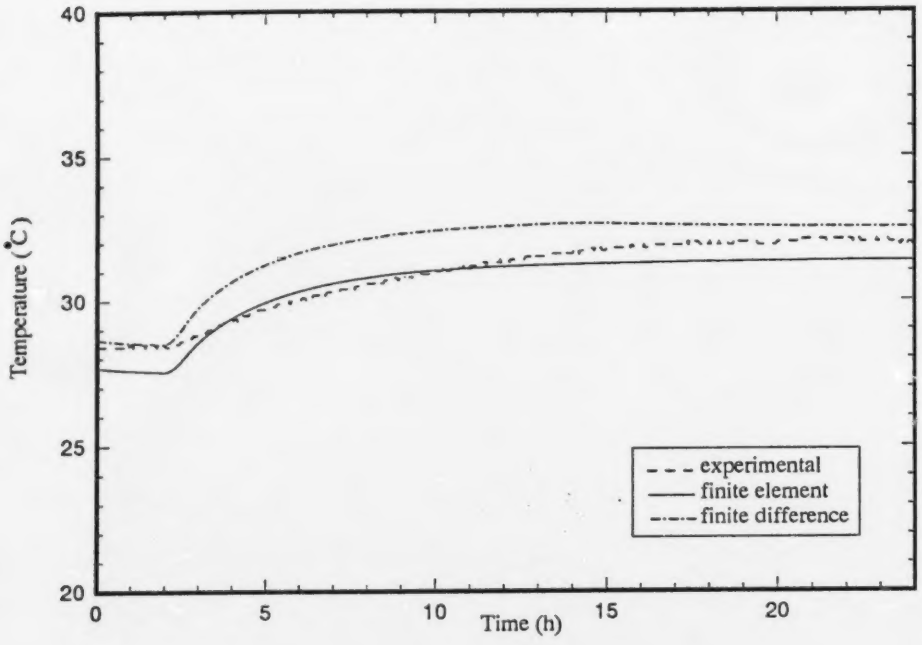

(a) Basement air temperature

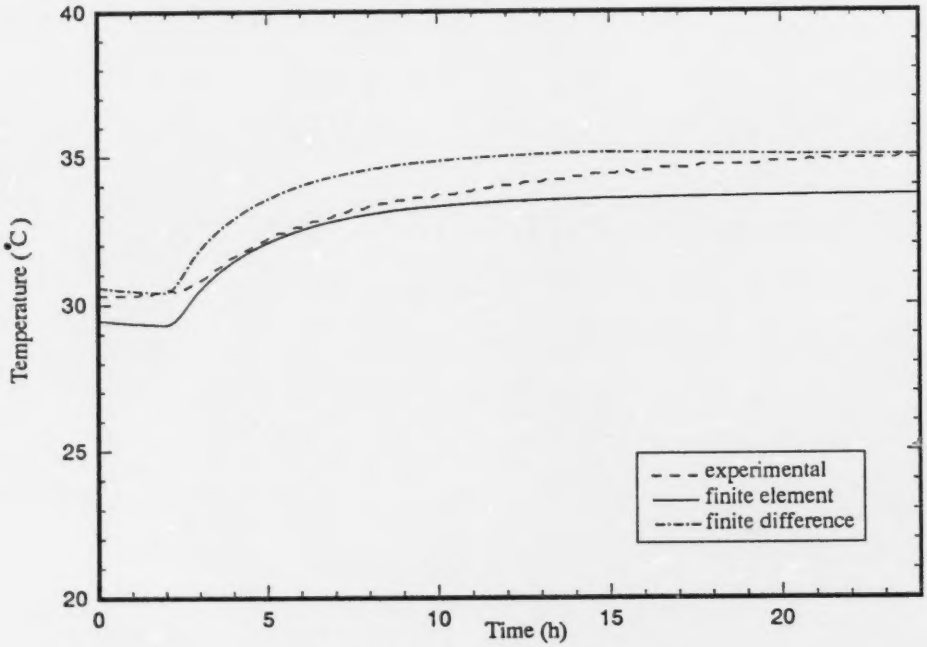

(b) Panel top surface temperature

Figure 7.8 Temperature dynamic responses for a step change in inlet water temperature from 45℃ to 55℃ (second test)

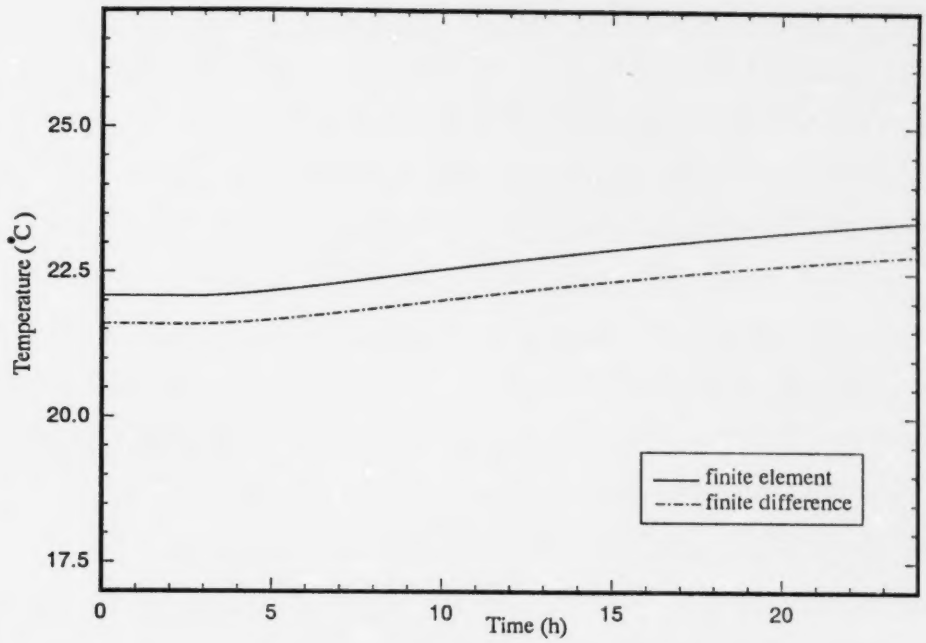

(c) Panel bottom surface temperature

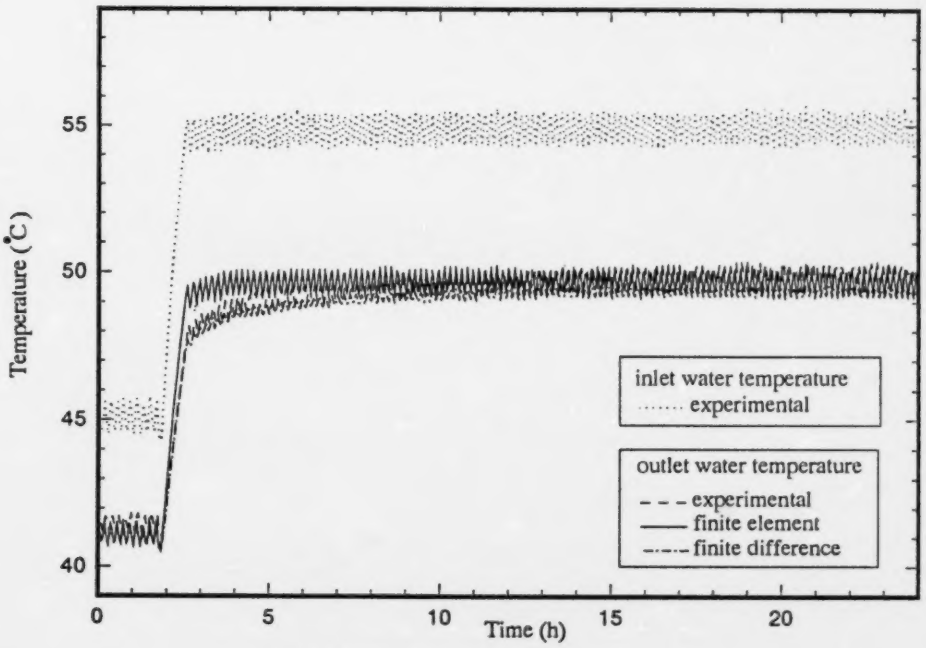

(d) Outlet water temperature

Figure 7.8 Temperature dynamic responses for a step change in inlet water temperature from 45℃ to 55℃ (second test)

response with the biggest difference being only 1.5°C. Comparison of the experimental and the simulated responses for basement air temperature and panel surface temperature show that both the finite element and finite difference predictions are satisfactory. The final steady state basement air temperature and panel surface temperature calculated using the finite difference method are closer to the experimental data than the values obtained with the finite element method.

7.3 Discussion

As shown by the results in Figures 7.1 and 7.2 the initial steady state temperature profile in the panel is seen to be smoother, and more natural, using the finite difference method than for the finite element method. However, the actual profiles calculated using the finite element method were also smooth but appear choppy because of limitations of the graphic software Tecplot used for plotting the calculated temperature profiles. The temperature profiles using the finite difference method differ slightly from those calculated using the finite element method. The difference in the method of discretization along the two interfaces used by the two numerical techniques may lead to this difference. In the finite difference method, grid points are imposed at the interfaces, but in the finite element method, the mesh is not imposed at the interfaces, as was shown in Figures 6.1 and 6.3 respectively. Furthermore the method used to establish the equation to solve for temperature distribution at the interfaces in the finite element method is different from the finite difference method. In the finite difference method, the heat balances in the x and y directions are made on each node which is treated as an element (cf Section 6.1.2). On the other hand, in the finite element method the interfaces are located within the elements. Yet the governing equations are still imposed on those elements.

The experimental panel surface temperature was found to be lower than the predicted values as shown in Figures 7.3a and 7.4a. This is likely due to the fact that in the experimental house, the tubing is not installed at the depth in the gypsum cement

specified in the model. If the tubing is located lower than 0.635 cm from the bottom as specified in the model, the panel surface temperature will be lower than predicted. Also if the layer of gypsum cement is thicker than the 5 cm specified in the model, this will also result in the experimental values being lower than the calculated values. Furthermore, the fact that the experimental maximum and minimum panel surface temperatures do not correspond with the predicted extreme values would imply that the spacing of the tubing is not exactly 0.3 m as specified in the model.

The difference between the simulated dynamic responses of basement air temperature and panel surface temperature, as shown in Figures 7.5a and 7.5b, for the two methods of solution for the first six hours of the response is slightly less than 1°C which is the difference between the calculated initial steady state temperature. As described in Section 7.2.1, the difference in the predicted responses of outlet water temperature to the step change of inlet water temperature from 45°C to 55°C using the finite difference method and finite element method was approximately 2°C for the first hour. After the first six hours, the difference between these two calculated responses was reduced to a minimum of about 1°C and remained the same in the remaining time of the test. Since the difference in magnitude between these two calculated responses of the outlet water temperature did not remain unchanged for the first six hours, it leads to the shapes of the two calculated dynamic temperature curves slightly different for the same period of time, as can be seen from the dynamic behaviour of the basement air temperature and panel surface temperature in Figures 7.5a and 7.5b.

In order to establish the effect of solar radiation energy gain in the upper zone on the basement air temperature, two sets of 24 hour test data were collected, one with the shutters open, the other with them closed. The results are shown in Figures 7.9a and 7.9b. During the test with the shutters open, the upper zone air temperature increased from 20°C to about 24.5°C due to an increase in solar radiation and outdoor air temperature from 0840 to 1840 hours as shown in Figure 7.9. With the shutters closed, the upper zone

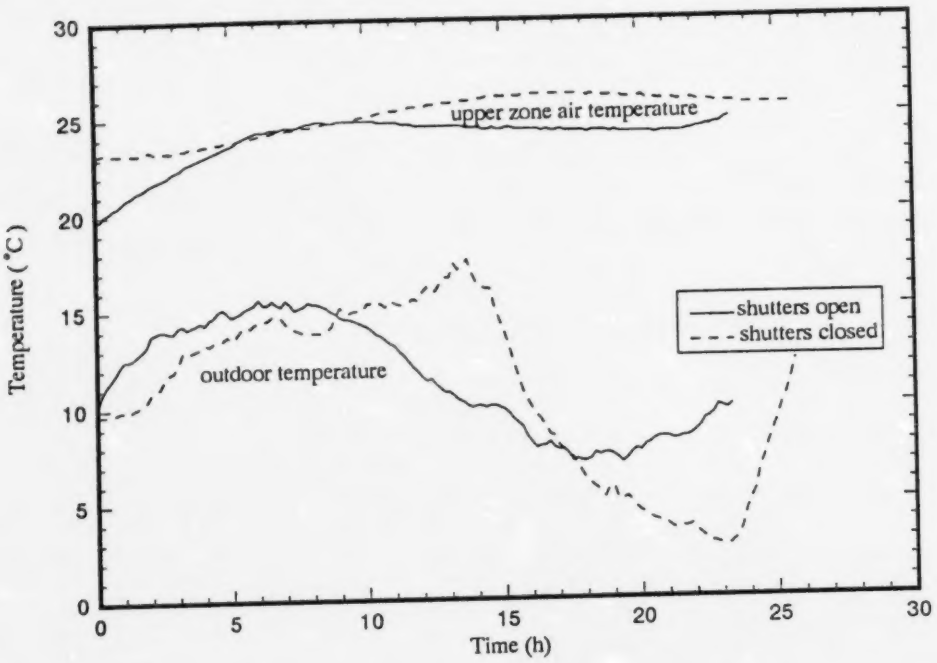

(a) Upper zone air and outdoor temperatures

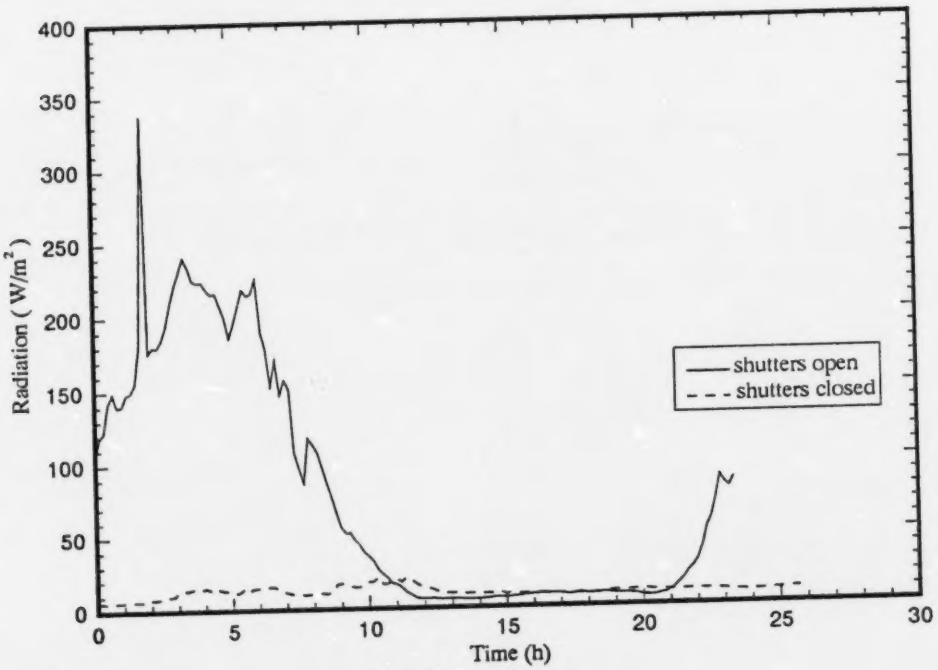

(b) Solar radiation

Figure 7.9 Solar radiation, upper zone air and outdoor temperatures versus time

air temperature changed from 23.5°C to 26°C from 0720 to 2000 hours due to the increase in outdoor air temperature. The measured solar radiation gain in the upper zone is shown in Figure 7.9b. For the solar gain with the shutters open, the solar radiation caused the upper zone air temperature as shown in Figure 7.9a to increase by 3°C. This small increase did not affect the basement air temperature very much. Further evidence is given by the calculated values of q_{ceil} given in Table 7.1 which shows only a negligible difference of 2 W which can be neglected.

7.4 Effect of Model Parameters

The sensitivity of the dynamic temperature responses of basement air temperature, panel surface temperature and outlet water temperature were examined by changes in individual parameter values. All predicted responses calculated using the finite element method of solution, using the initial steady state temperature of the first test (cf Figures 7.5a, 7.5b, 7.5d).

Seven of the ten simulation tests were performed to determine the sensitivity of the response to a change in physical properties of the gypsum cement, insulation, concrete and the soil under the composite panel. For example, the heat capacity of the gypsum cement is reported as 988.03 J/kg at 29.4°C yet temperature profiles in Figures 7.1 and 7.2 show that the temperature distribution in the gypsum cement layer 27°C to 45°C so the effect of different heat capacities is studied. The thermal conductivity of the insulation will obviously vary with temperature and since the temperature in the insulation layer varies from 20°C to 40°C, the effect of different values on the responses is investigated. Also, since the soil thermal conductivity may vary from 0.1 to 1 W/m°C, as it is particularly affected by moisture content, the effect of values other than the approximate value, computed from experimental data that was used for the previous simulations is studied.

The calculated h value, established from the experimental data, is not considered accurate because of measurement errors. As discussed in the previous section, a

measurement error of 0.5°C in the inlet or outlet water temperature leading to a change in the water temperature difference (between inlet and outlet) by 0.5°C will cause a change in the calculated h value of approximately 13 percent. The UA value, which is computed from the experimental data and h value, will also be increased or decreased by this error. Hence, the effect of different UA and h values on the response of the basement air temperature, panel surface temperature and outlet water temperature was examined by two further simulations. The last simulation conducted to illustrate the sensitivity of the predicted dynamic temperature responses to the different values of q_{ceil} which is computed from the experimental data and the approximate value of k_{ceil} parameter.

Test 1 : Increase in the heat capacity and density of the insulation and concrete

The dynamic response of the basement air temperature, panel surface temperature and outlet water temperature, were calculated for values of the heat capacity and density of both the insulation and concrete layers 20 and 40 percent higher than the values of the heat capacity of 1214 J/kg°C and the density of 35.24 kg/m^3 for the insulation and the values of 921 J/kg°C and 2242.51 kg/m^3 for the concrete used in the previous simulations. As can be seen from the predicted response plotted in Figure 7.10, the dynamics are not affected by a change in these parameter values.

Test 2 : Increase in the heat capacity and density of the gypsum cement

The predicted temperature responses displayed in Figure 7.11 were obtained using gypsum cement density and heat capacities of 1601.83 kg/m^3 and 988.03 J/kg°C (base case) and values 20 and 40 percent higher. As can be observed, the basement air temperature and panel surface temperature responses approach the experimental results if the density and capacity are increased by 40 percent. The results in Figure 7.11 show that the transient response of outlet water temperature is not influenced by an increase in gypsum cement density and heat capacity.

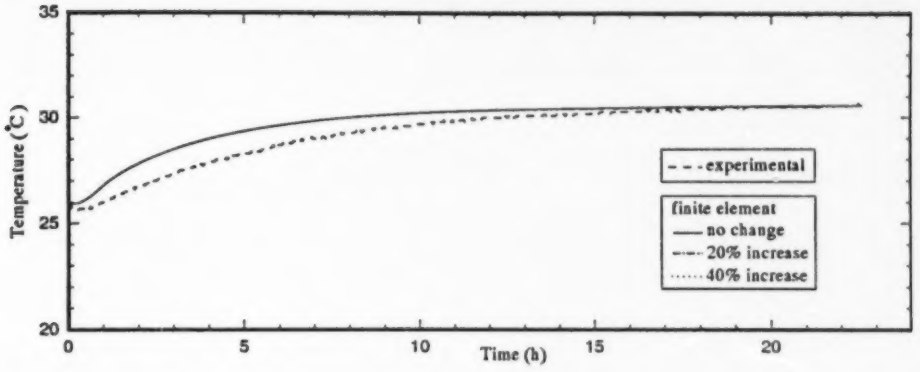

(a) Basement air temperature

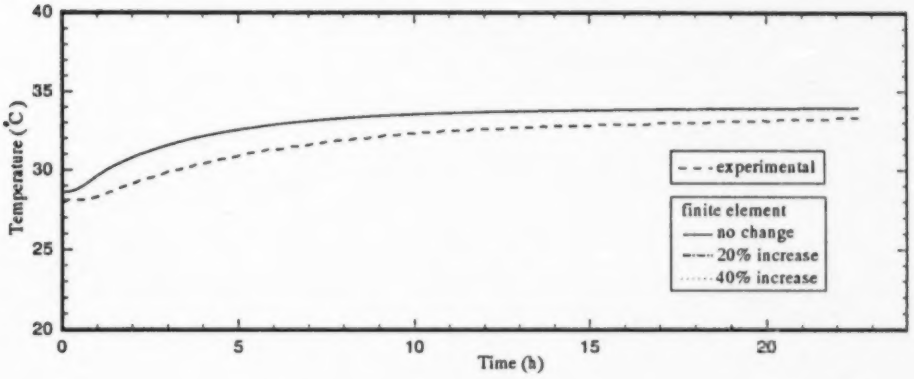

(b) Panel top surface temperature

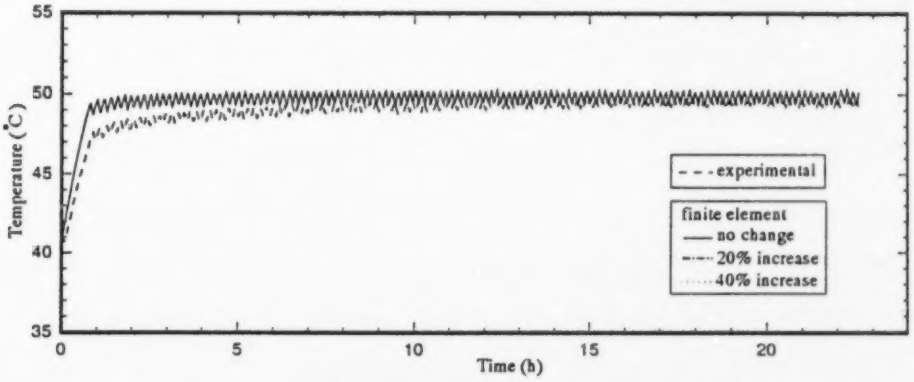

(c) Outlet water temperature

Figure 7.10 Response of system temperatures to a change in the densities and heat capacities of the insulaton and concrete

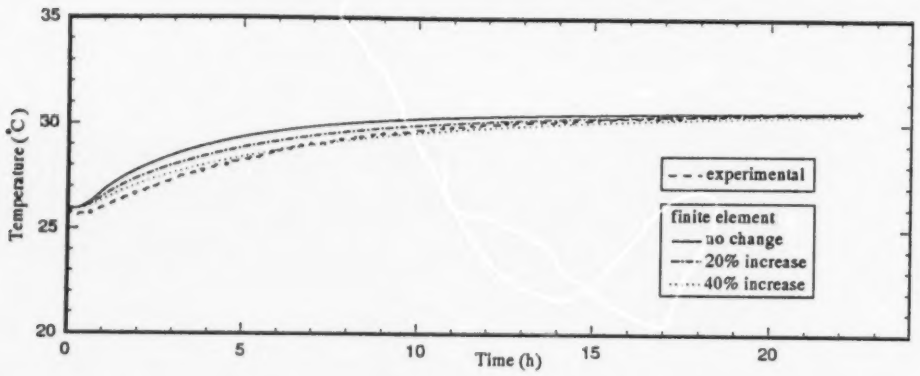

(a) Basement air temperature

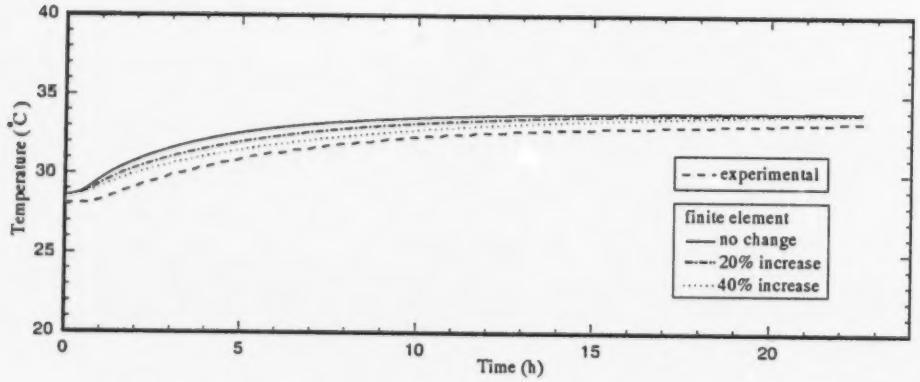

(b) Panel top surface temperature

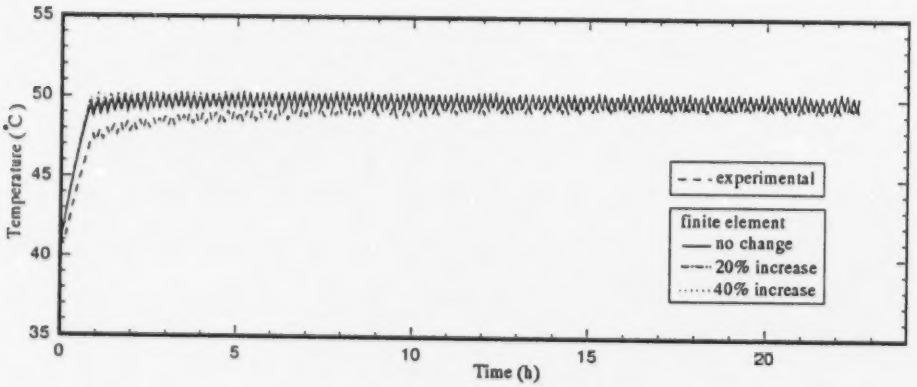

(c) Outlet water temperature

Figure 7.11 Response of system temperatures to a change in the density and heat capacity of the gypsum cement

Test 3 : Increase in the heat capacity and density of all three materials

The temperature transient responses in Figure 7.12 result when the density and heat capacity of all three materials in composite panel are increased. Comparison of these results with those in Figure 7.11 show that the calculated dynamic behavior is the same. This is because only the change in heat capacity and density of the insulation and the concrete do not affect the response as demonstrated by the results in Figure 7.10.

Test 4 : Increase in the thermal conductivity of the concrete

As shown in Figure 7.13, the response of basement air temperature, panel surface temperature and outlet water temperature remain unchanged even if the thermal conductivity of concrete is increased by 20 percent from the value of 1.731 W/m°C used for the previous simulations.

Test 5 : Decrease in the thermal conductivity of the insulation

As demonstrated in Figure 7.14, an increase in the thermal conductivity of the insulation by even 20 percent results in an insignificant change to the dynamic response of basement air temperature and panel surface temperature. The transient response of outlet water temperature was not affected by the change in thermal conductivity of the insulation.

Test 6 : Increase and decrease in the thermal conductivity of the gypsum cement

A 10 percent increase or decrease in the thermal conductivity of the gypsum cement caused a corresponding increase or decrease of 0.7°C in the basement air temperature and about a 1°C increase or decrease in panel surface temperature, as can be seen by the computed responses in Figures 7.15a and 7.15b. The change in thermal conductivity did not affect the response of outlet water temperature as shown by the response plotted in Figure 7.15c.

Test 7 : Increase and decrease in the thermal conductivity of the soil

An increase or decrease in the thermal conductivity of the soil up to 20 percent had no significant effect on the response of the system temperatures as shown by the results

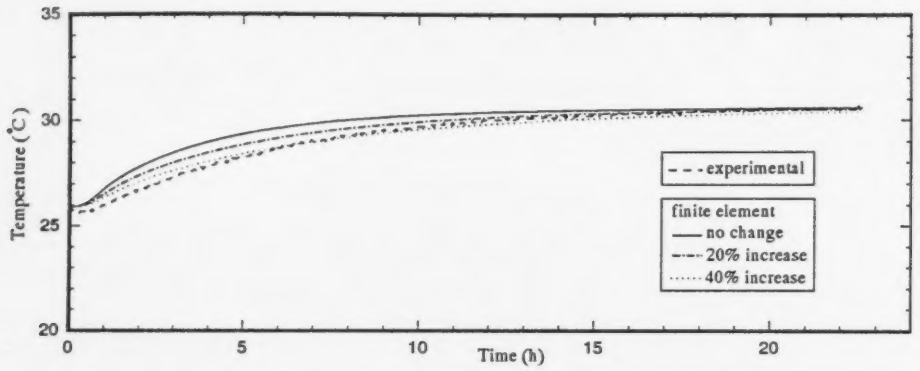

(a) Basement air temperature

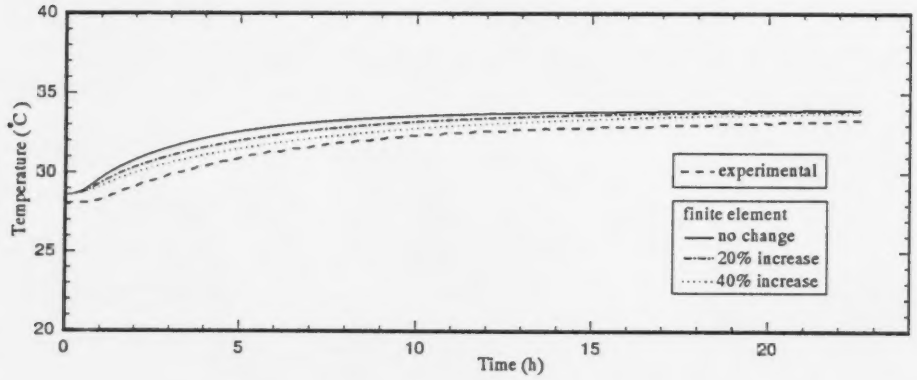

(b) Panel top surface temperature

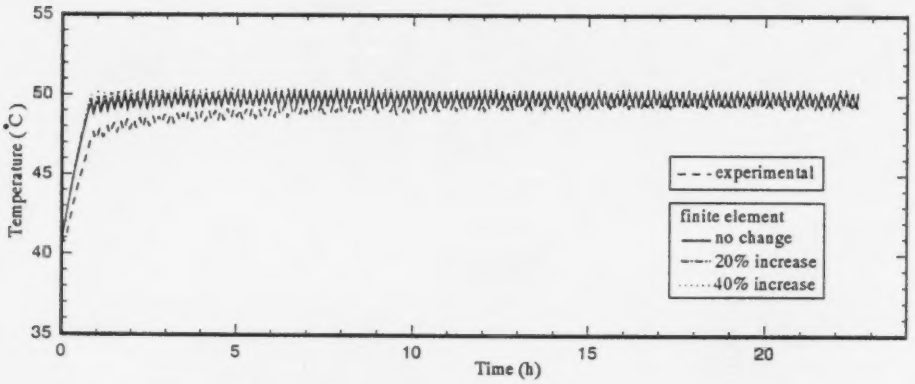

(c) Outlet water temperature

Figure 7.12 Response of system temperatures to a change in the densities and heat capacities of the gypsum cement, insulaton and concrete

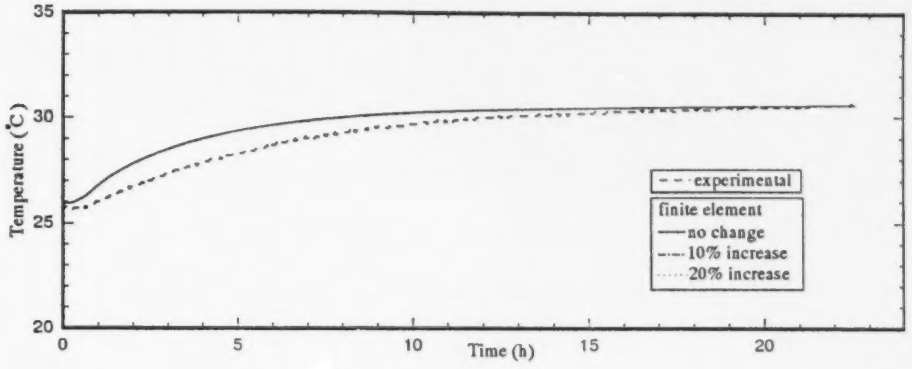

(a) Basement air temperature

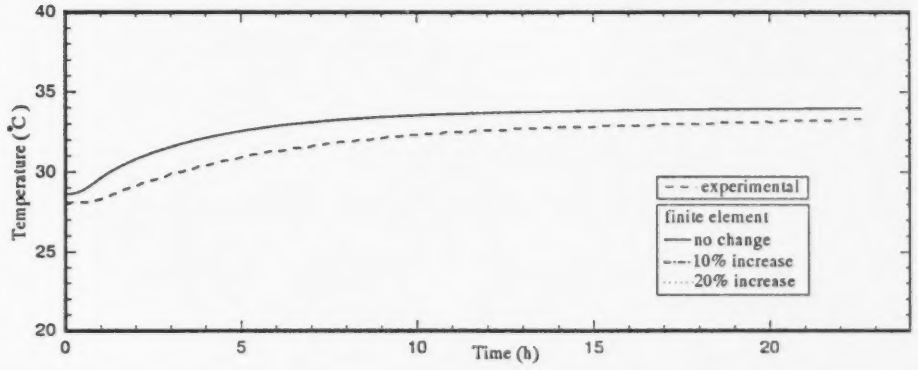

(b) Panel top surface temperature

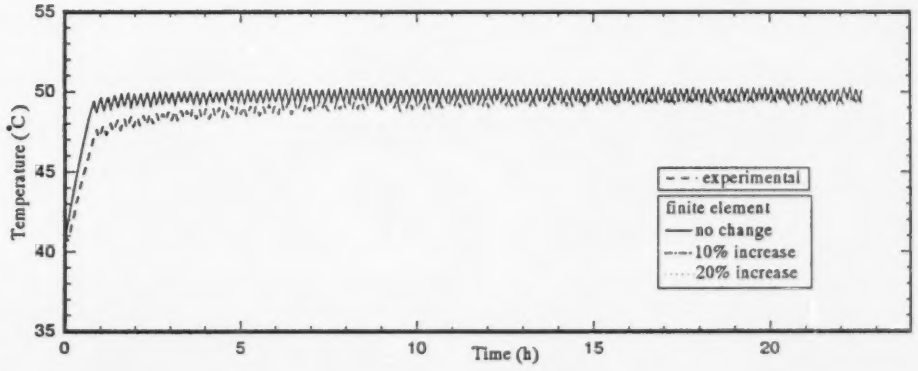

(c) Outlet water temperature

Figure 7.13 Response of system temperatures to a change in the thermal conductivity of the concrete

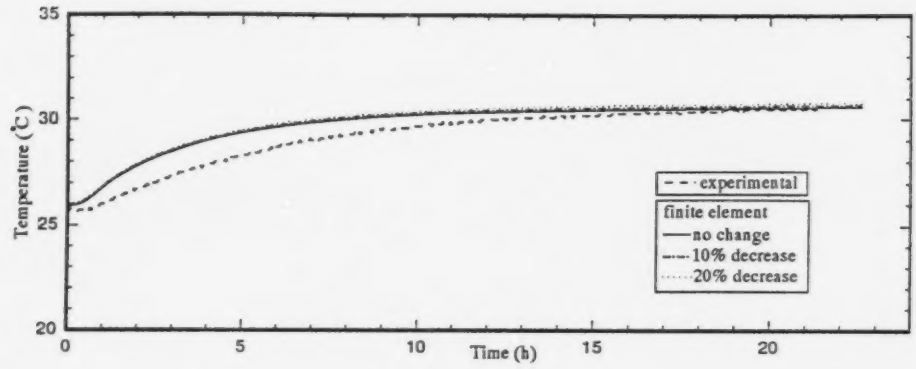

(a) Basement air temperature

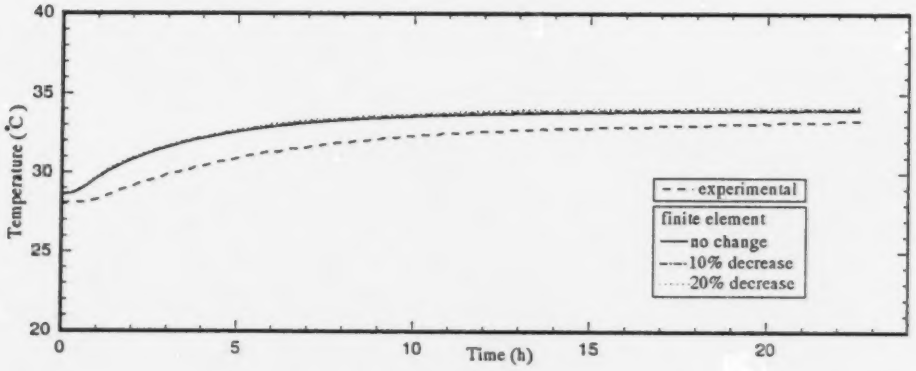

(b) Panel top surface temperature

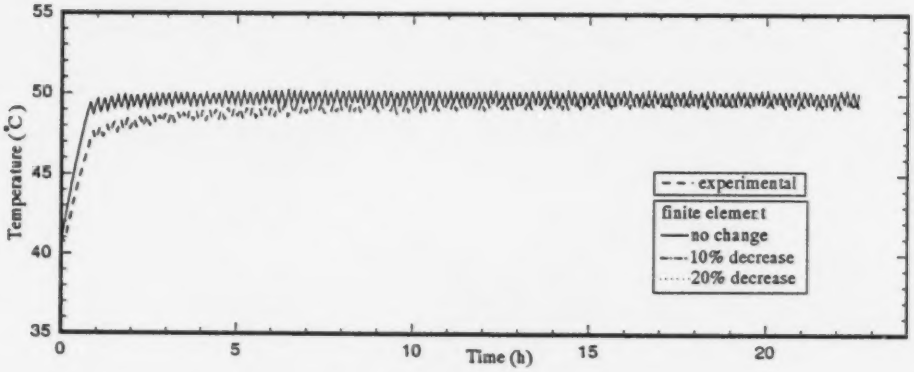

(c) Outlet water temperature

Figure 7.14 Response of system temperatures to a change in the thermal conductivity of the insulation

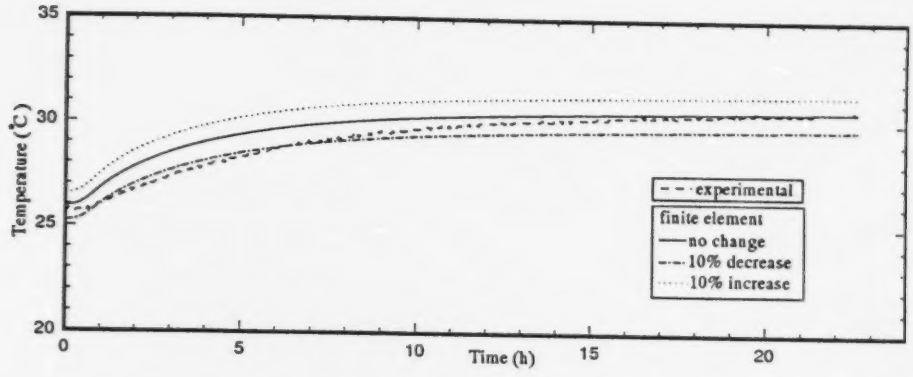

(a) Basement air temperature

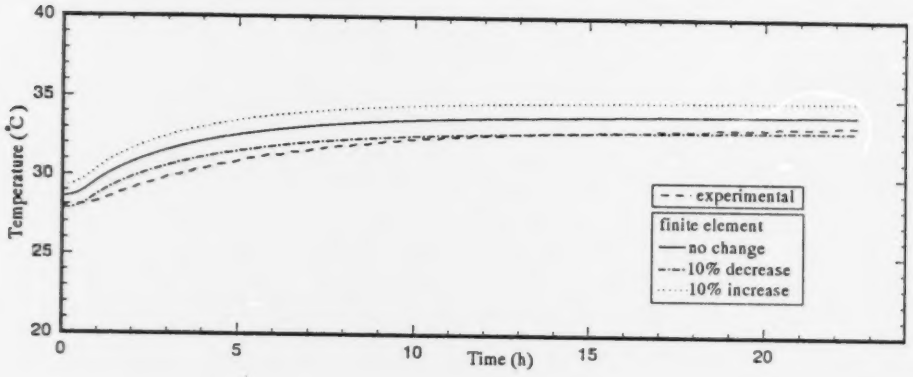

(b) Panel top surface temperature

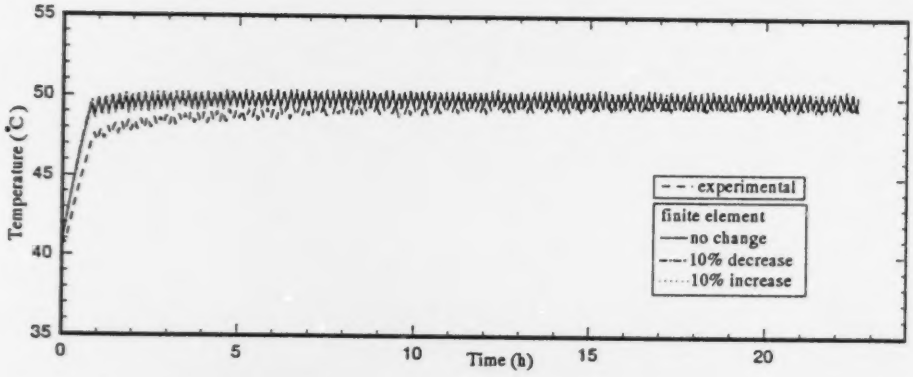

(c) Outlet water temperature

Figure 7.15 Response of system temperatures to a change in the thermal conductivity of the gypsum cement

plotted in Figure 7.16. Analysis of the calculated values shows that even for a 20 percent change in the conductivity from 0.515 W/m°C, a difference of 0.2°C in basement air temperature and panel surface temperature resulted. The change in thermal conductivity did not influence the dynamic behaviour of the outlet water temperature.

Test 8 : Increase and decrease in the UA parameter value

As mentioned at the beginning of this section, the difference in the UA value between the first and second test, did affect the dynamic response of basement air temperature and panel surface temperature. As shown by the transient responses of the temperatures plotted in Figure 7.17a, 10 percent increase or decrease in the UA value caused a 1°C increase or decrease in the basement air temperature and for a 20 percent change, the basement air temperature changed by 2°C. As can be observed, and would be expected, the change in the UA value has the same effect (magnitude) on the panel surface temperature as for the basement air temperature. The change in the UA value did not affect the outlet water temperature.

Test 9 : Increase or decrease in the combined convective and radiative heat transfer coefficient

An increase or decrease in the h value of even up to 10 percent was not found to affect the basement air temperature by more than 0.3°C. The dynamic response of the system temperatures for 5 and 10 percent changes in the h value of 15.45 W/m²°C is displayed in Figure 7.18.

Test 10 : Heat loss/gain to/from the upper zone

The effect of a change in the heat loss/gain through the ceiling, q_{ceil} is shown by the system temperature responses plotted in Figure 7.19. As can be seen, changes of up to 30 percent do not influence the dynamic behaviour of the basement air temperature, panel surface temperature or outlet water temperature. This is as would be expected because the magnitude of q_{ceil} is negligible when compared with the amount of heat loss to the surrounding soil and the backside heat loss.

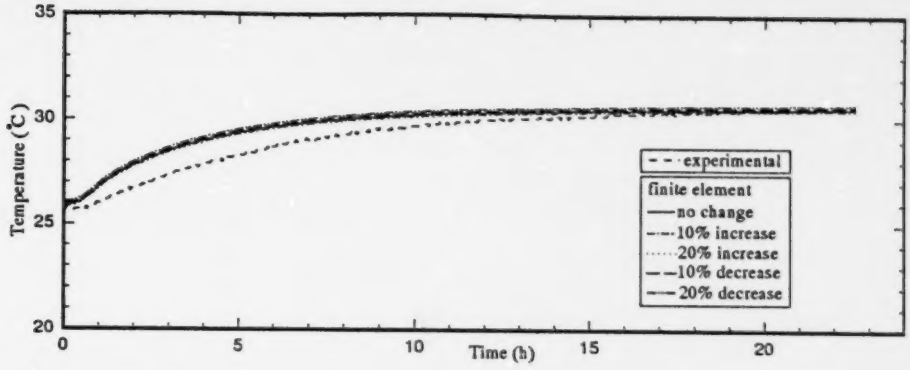

(a) Basement air temperature

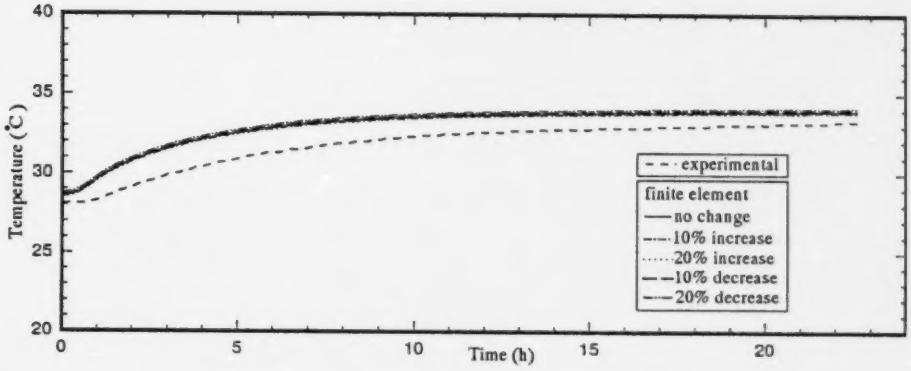

(b) Panel top surface temperature

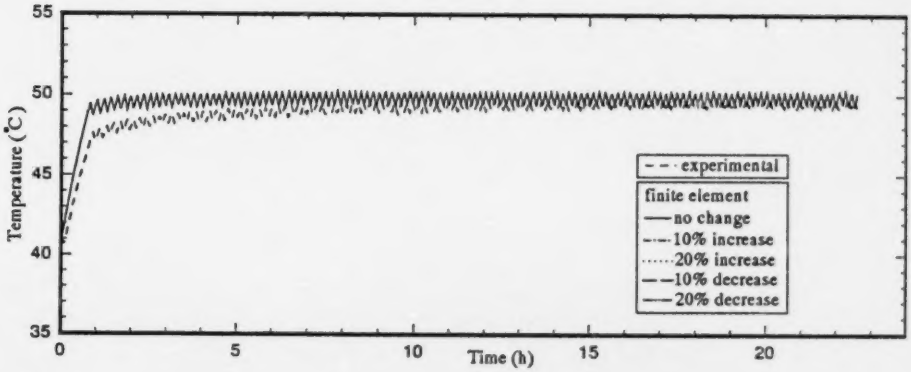

(c) Outlet water temperature

Figure 7.16 Response of system temperatures to a change in the thermal conductivity of the soil located under the concrete

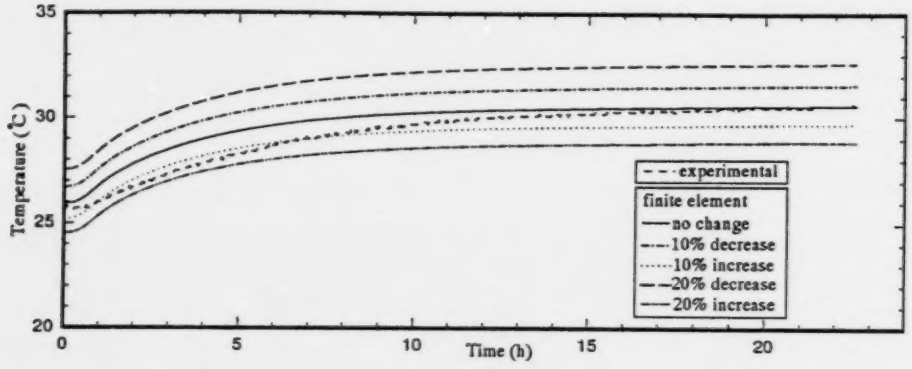

(a) Basement air temperature

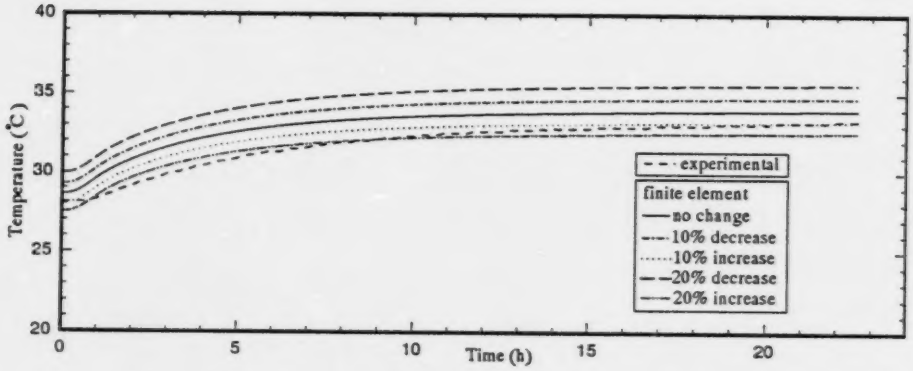

(b) Panel top surface temperature

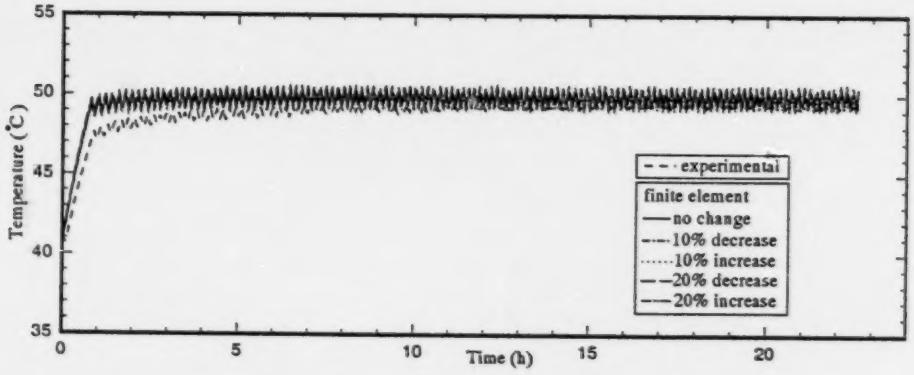

(c) Outlet water temperature

Figure 7.17 Response of system temperatures to a change in the overall heat transfer coefficient

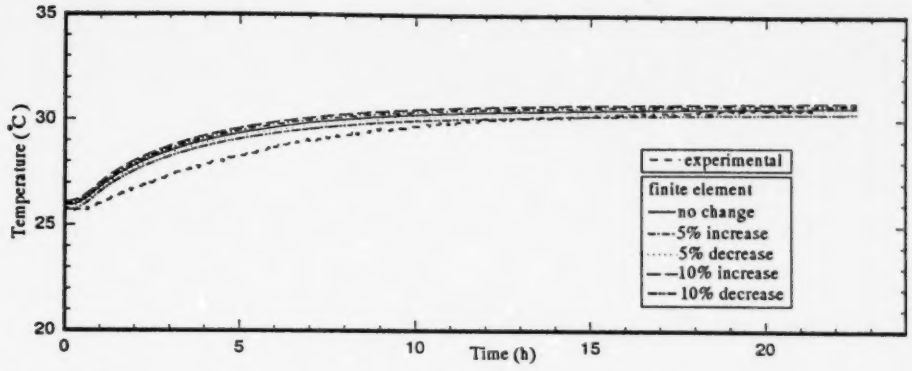

(a) Basement air temperature

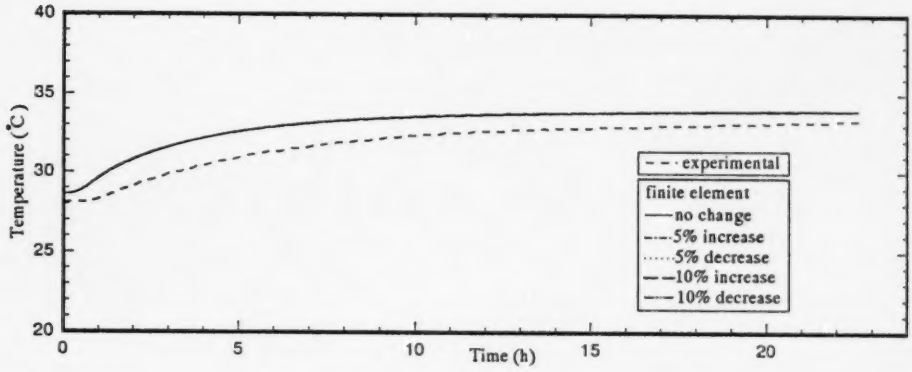

(b) Panel top surface temperature

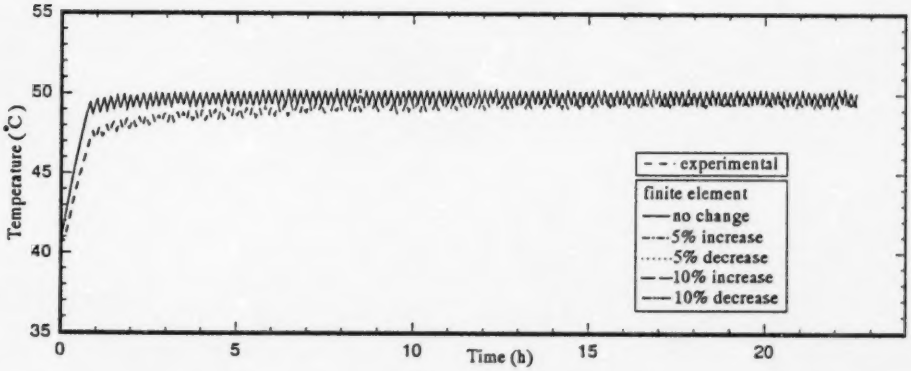

(c) Outlet water temperature

Figure 7.18 Response of system temperatures to a change in the combined convective and radiative heat transfer coefficient

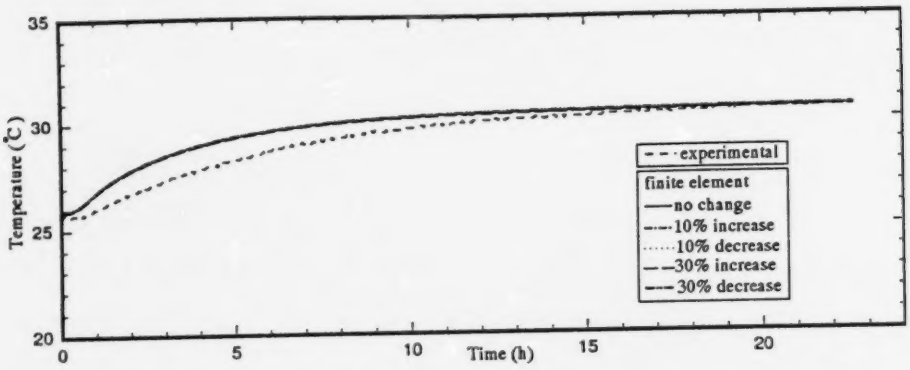

(a) Basement air temperature

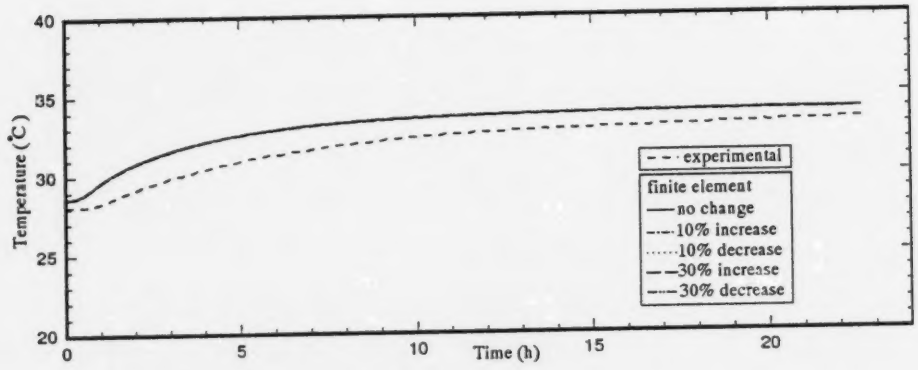

(b) Panel top surface temperature

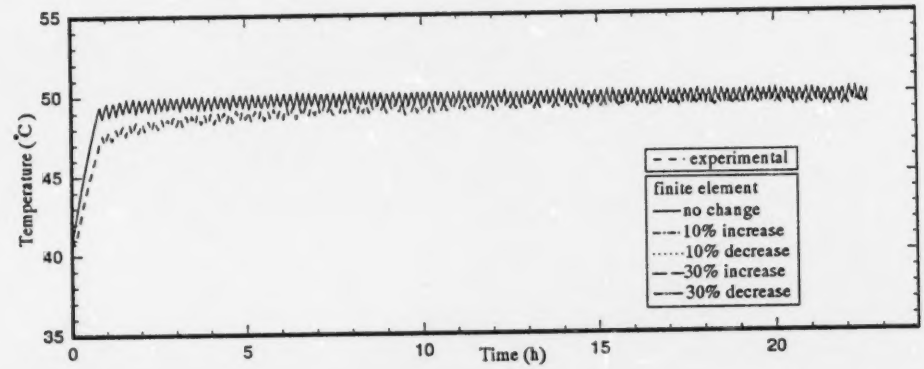

(c) Outlet water temperature

Figure 7.19 System temperature dynamic responses for changes in heat loss or gain to the upper zone

7.5 Conclusions

On the basis of the experimental and simulation results presented in this chapter, it can be concluded that

1. The effect of the solar radiation energy input to the upper zone does not affect the basement air temperature.

2. The computation time for the finite element approach is one-half the time required for the finite difference simulation.

3. The difference of about 1°C in the surface temperature profiles between the finite difference and finite element methods is considered to be due to different methods for location, grid points at the interfaces. The trends of the temperature profile calculated using the two methods are similar.

4. The small difference between the simulated dynamic response of the basement air temperature and the experimental response can be attributed to the magnitude of the parameter values as demonstrated by the series of sensitivity simulations. A 40 percent increase in the heat capacity and density of the gypsum cement will shift the predicted dynamic response to agree with the experimental results as shown in Figure 7.11.

5. An increase or decrease of 10 percent in the UA value causes a significant change of 1°C increase or decrease in the basement temperature and up to 20 percent increase or decrease causes 2°C change in the basement temperature. On the other hand, an increase or decrease in the h value of up to 10 percent, the basement air temperature changes by less than 0.3°C.

6. An increase or decrease of up to 40 percent in the physical properties of the insulation and concrete layers have no significant effect on the dynamic response of basement air temperature and panel surface temperature.

7. The assumption of the heat loss q_{ceil} as a constant is justified as even an increase of 30 percent does not affect the predicted transient response of basement air temperature, panel surface temperature or outlet water temperature.

Chapter 8
Experimental Testing of Two Control Laws

In the previous two chapters, simple half-pipe and one-pipe models were developed as well as the full model. The full model can be employed to study the dynamic behavior of the system temperatures of one of the hydronic floor heating systems installed in the experimental house as shown in Chapter 7. Recently, MacCluer (1989) has proposed a flux modulation control strategy that is suggested to provide superior control to conventional temperature modulation systems. In this chapter, experimental results from applying algorithms that implement on-off and proportional control for control of basement air temperature of the experimental house are presented. These strategies were selected because of their simplicity and their similarity to the type of strategy proposed by MacCluer.

8.1 Experimental Equipment

The schematic control signal diagram of the equipment used for control of basement air temperature in the experimental house is shown in Figure 8.1. As can be seen, following the terminology introduced in Chapter 4, the hydronic heating model is equivalent to subsystem 1 and the room model to subsystem 2. The other block, the boiler and tank model, represents the electric boiler and hot water tank, shown in Figure 3.6. The electric power source is simply the power supply to the electric boiler. Two controllers, the water temperature and room temperature controller are used in this

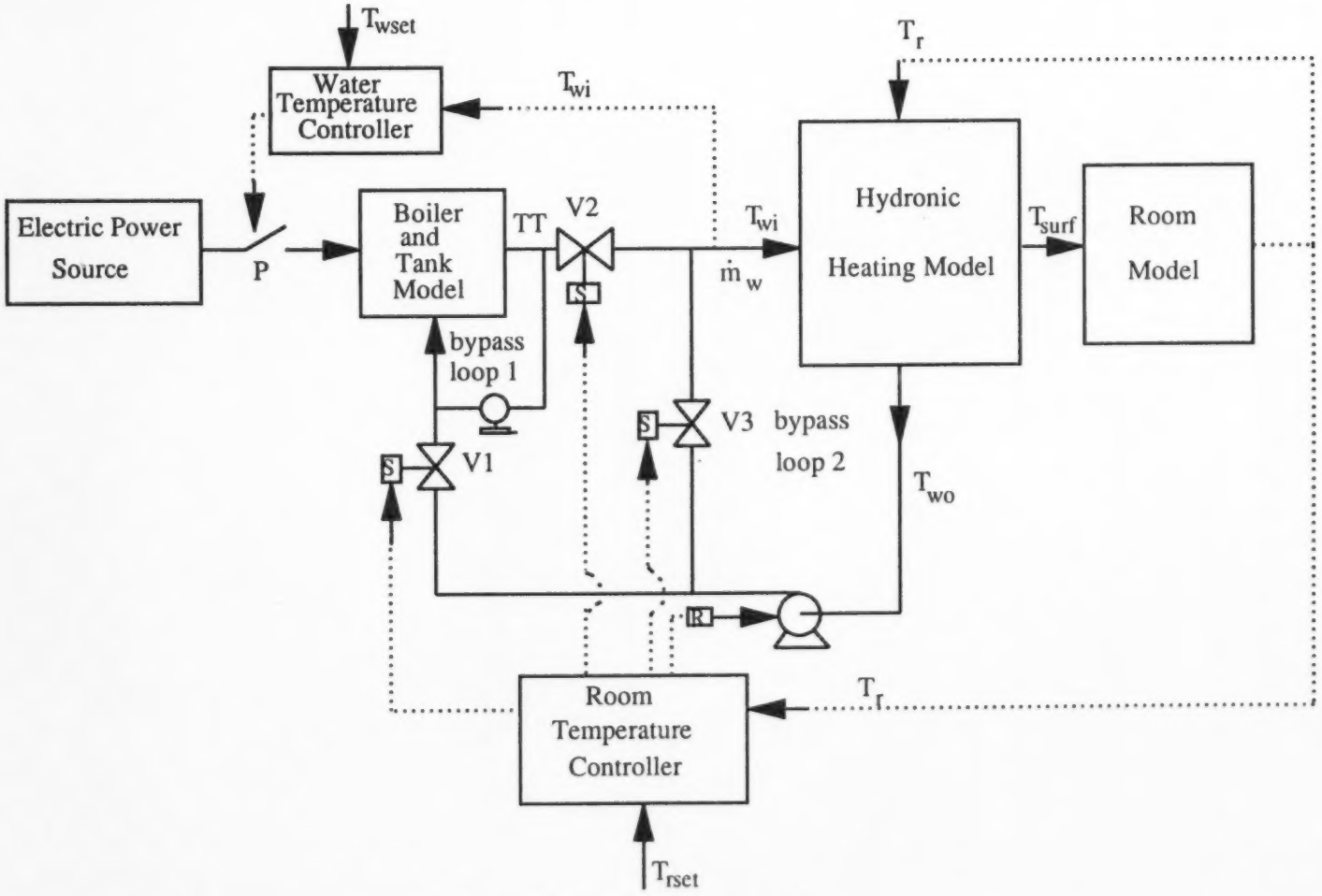

Figure 8.1 Control Signal Diagram

system. The water temperature controller is used to maintain the inlet water temperature at the specified water temperature setpoint, T_{wset} and the room temperature controller, the main controller, is used to maintain the basement air temperature at the desired value (setpoint). The control strategies for these two controllers are written in quickbasic and implemented using the IBM XT microcomputer. The functional details of these two controllers are described in the next two sections.

8.1.1 Water Temperature Controller

The control algorithm for the water temperature controller was originally developed to control boiler outlet temperature, TT. However, in order to maintain a constant inlet water temperature to the hydronic heating system, TT is replaced by T_{wi} as the controlled variable. The control algorithm employs a simple on-off control law. If the water temperature, T_{wi} becomes 0.5°C lower than $T_{wset,}$ the controller will send a signal to the relay to apply power to the boiler. If T_{wi} remains greater then T_{wset}, power is not applied to the boiler. It should be noted that V4, a hand valve is always about half-open to provide water circulation in bypass loop 1.

8.1.2 Room Temperature Controller

The two inputs to the room temperature controller are the measurement of basement air temperature, T_r and the desired basement air temperature, T_{rset} (setpoint). The form of the control algorithm depends on the type of control law, e.g. on-off, proportional, etc. that is to be employed. The controller generates four output signals of which three are signals to electric valves, V1, V2 and V3. The fourth signal, R, to the pump, may be used to turn the pump on or off but in this study the pump is operated continuously.

On-off control

If T_r is smaller than T_{rset} by more than 0.5°C, the controller will cause valves V1 and V2 to be open and valve V3 to be closed, so that water is circulating only in the main loop. The other action of the controller will close valves V1 and V2 and open valve V3 if T_r is smaller than T_{rset} by less than 0.5°C. This causes the water to circulate only in bypass loop 2. The control law can be stated as

$(T_{rset} - T_r) \geq 0.5$: V1 = open, V2 = open, V3= closed, R = power on

$(T_{rset} - T_r) < 0.5$: V1 = closed, V2 = closed, V3= open, R = power on

Proportional Control

The proportional control law governs the amount of time during a cycle that there is water flow to the heating panel with an objective of maintaining the value of T_r equal to T_{rset}. In this work, a typical operation of six cycles per hour is employed so the length of each cycle is ten minutes. The action of the control law must adjust the time during each cycle of ten minutes that there is flow of water to the heating panel. This time, relative to the cycle time, known as the "percentage on-time". The "percentage on-time", P is related to room air temperature, as defined in Figure 8.2. The maximum value of T_{rset} is $T_H$while T_L is the minimum value of T_{rset} with the "percentage on-time" relative to room air temperature expressed as

$$\text{Slope} = \frac{1}{(T_L - T_H)} \tag{8.1}$$

The "percentage on-time", P_{set} when the room air temperature is at the setpoint is considered as

$$P_{set} = \text{Slope} \bullet (T_{rset} - T_H) \tag{8.2}$$

The control law can be stated as

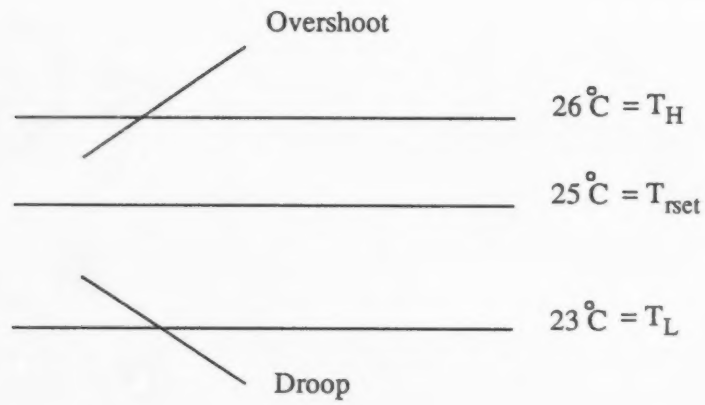

(a) Maximum, minimum and set point temperatures

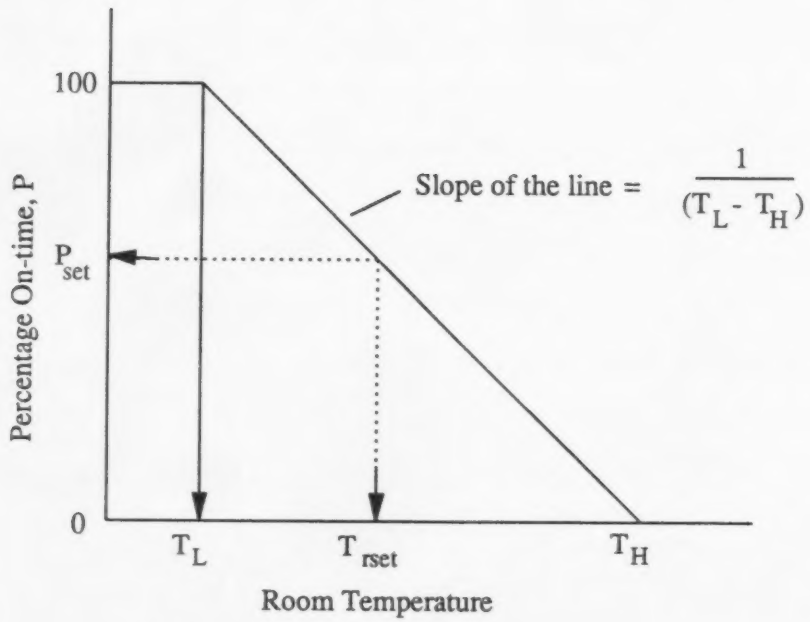

(b) Definition of "Percentage On-time"

Figure 8.2 Proportional action controller

```
If ( T_r > T_H ) then
        P = 0
Elseif ( T_r < T_L ) then
        P = 100
Else
        If T_r = T_rset then
                P = P_set
        Endif
        If (  ( T_r > T_rset ) and ( T_r < T_H )  ) then
                P = P_set - Slope • ( T_rset - T_r )
        Else
                P = P_set + Slope • ( T_r - T_rset )
        Endif
Endif
```

The amount of "on-time" in one cycle is defined as:

$$\text{On-time} = (P) \bullet (\text{cycle length}) / 100$$

Once the value of on-time has been computed, the controller will send the control signals to the devices according to the following:

For example:

If P = 0%, then the on-time will be zero minutes, that is V1 = closed, V2 = closed and V3 = open for the entire ten minutes cycle.

If P = 100%, then the on-time will be 10 minutes, that is V1 = open, V2 = open and V3 = closed for the entire ten minutes cycle.

If P = 70%, then the on-time will be seven minutes. It means that V1 and V2 will be open and V3 closed for seven minutes, and then V1 and V2 will be closed and V3 open for the remaining three minutes.

8.2 Results

8.2.1 On-Off Control

For a setpoint change of basement air temperature from 25.0°C to 30.0°C, on-off control is used to bring the basement air temperature to the new setpoint. From the experimental results displayed in Figure 8.3a, it can be seen that it takes about 30 hours

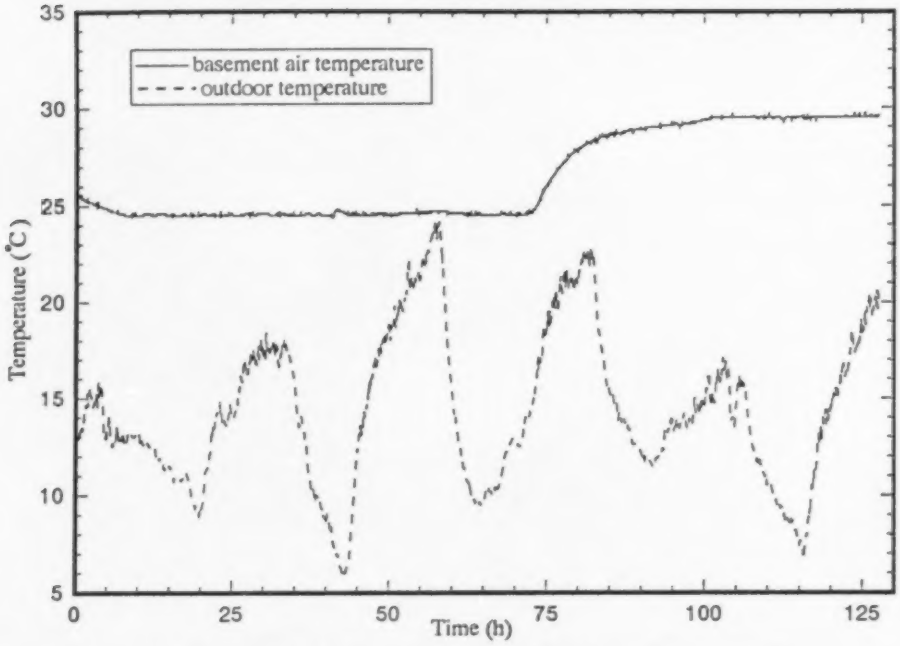

(a) Basement air temperature and outdoor temperature

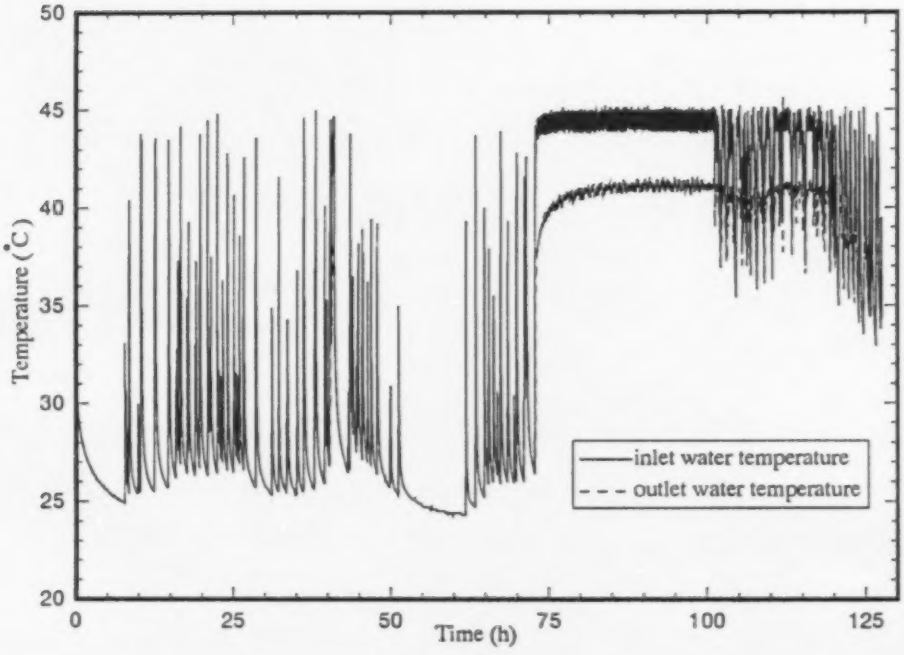

(b) Heat panel inlet and outlet water temperatures

Figure 8.3 Control performance using an on-off control law for a step change in setpoint from 25℃ to 30℃

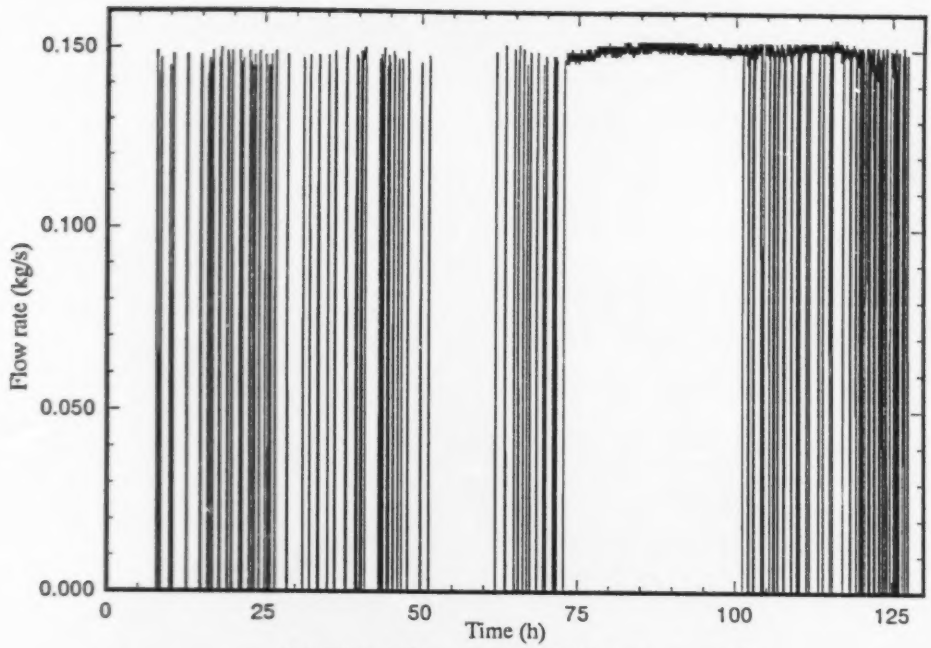

(c) Water flow rate to the heating panel

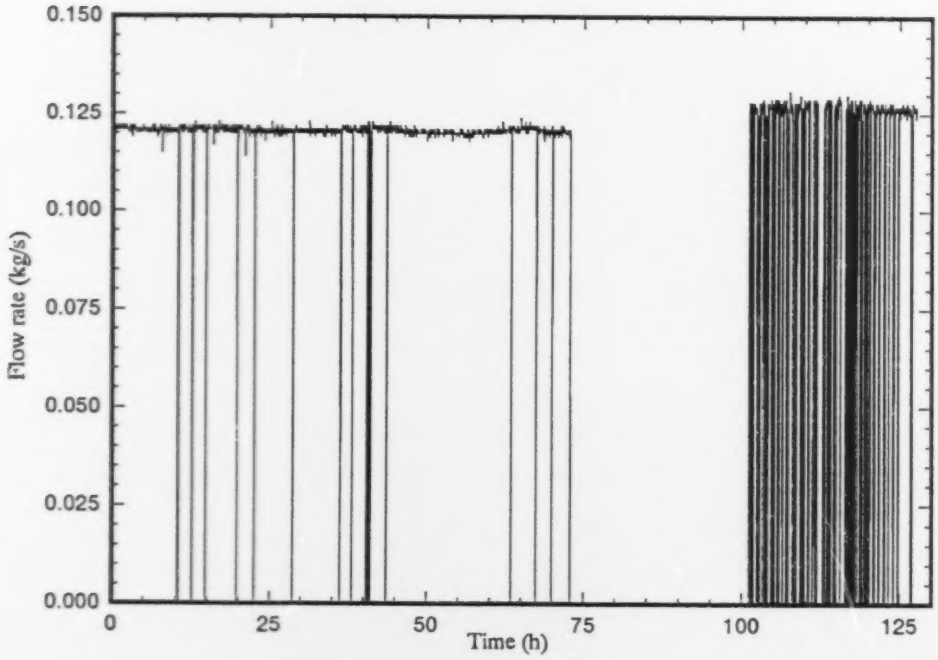

(d) Water flow rate in bypass loop 2

Figure 8.3 Control performance using an on-off control law for a step change in setpoint from 25℃ to 30℃

for the air temperature to increase to 29.5°C. As can be observed, the basement air temperature has never reached the new setpoint value of 30°C, that is the controller exhibits 0.5°C undershoot. This undershoot is characteristic of this on-off control algorithm because the allowable temperature has been set to 0.5 below the setpoint. During the heat-up period which is between time = 72.5 and 102.5 hours, water is circulated through the circuit so that the basement air temperature can reach the new steady state with the fastest rate. In Figure 8.3c, it can be seen that the inlet and outlet water temperatures exhibit significant changes, after 100 hours when the air temperature is within -0.5°C of the new setpoint of T_{rset} = 30°C. This is because the inlet and outlet water temperatures decrease when bypass loop 2 is operative (valves V1 and V2 closed) and increase when the water is being supplied from the boiler, that is valves V1 and V2 open with V3 closed.

8.2.2 Proportional Control

The test of proportional action involved starting with the basement air temperature at 21.5°C and increasing the setpoint to 25°C. As can be observed from the results displayed in Figure 8.4, the basement air temperature not only reaches 25°C but has an overshoot of 0.5°C which occurs 8 hours from the time the setpoint was increased. Since with proportional action there will be alternating water flow from the boiler and just through the bypass loop this pattern should be exhibited in Figures 8.4d and 8.4e. However, the results do not show this operation because of the two minute sampling time of the IBM XT computer. This occurs because if valve V3 closes and valves V1 and V2 open within the sample interval, this will not be logged until the next sample instant. It is interesting to note the low water temperatures of 30 - 35 °C in Figure 8.4c after about 25 hours of operation. This occurs because only a low "percentage on-time", (the time required for water flow from the boiler) is adequate to maintain the basement air temperature at the desired temperature.

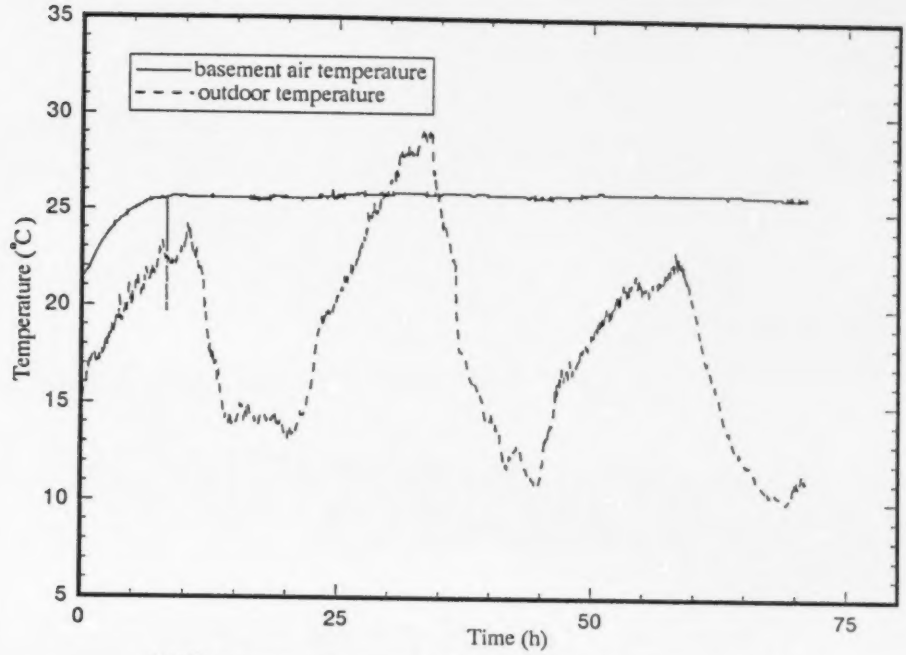

(a) Basement air temperature and outdoor temperature

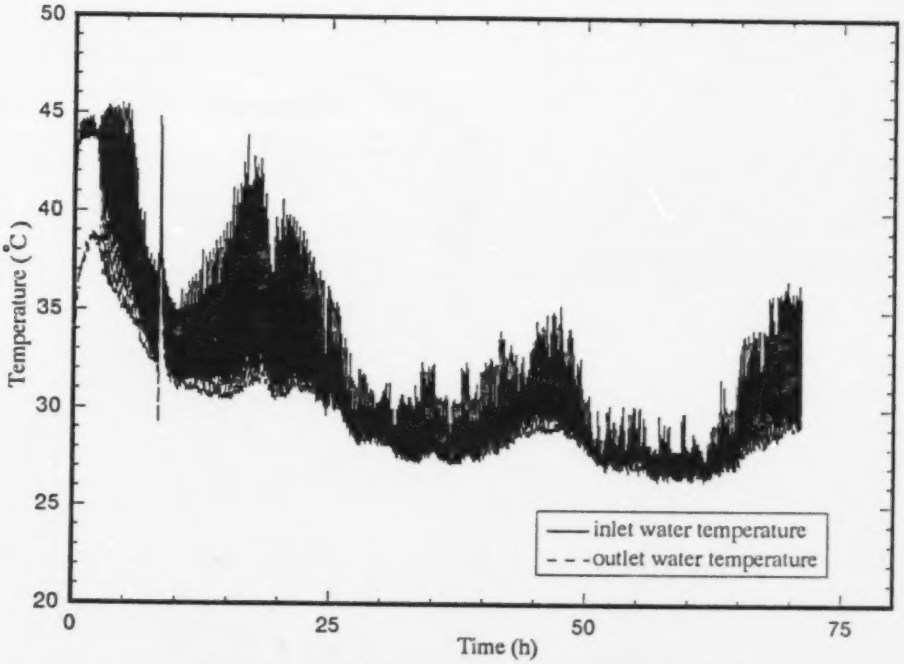

(b) Heat panel inlet and outlet water temperatures

Figure 8.4 Control performance using a proportional control law for a step change in setpoint from 21℃ to 25℃

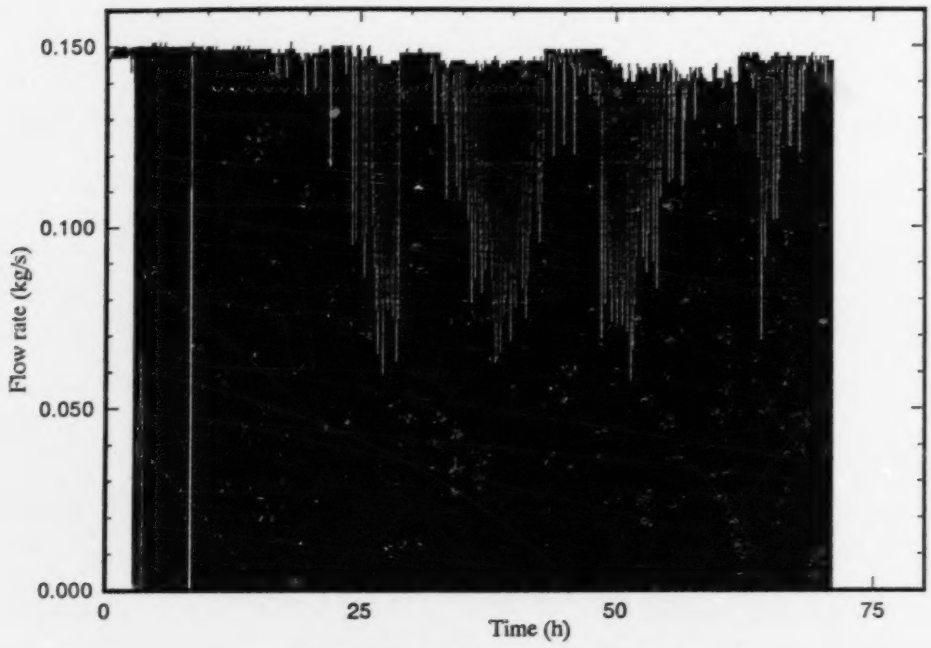

(c) Water flow rate to the heating panel

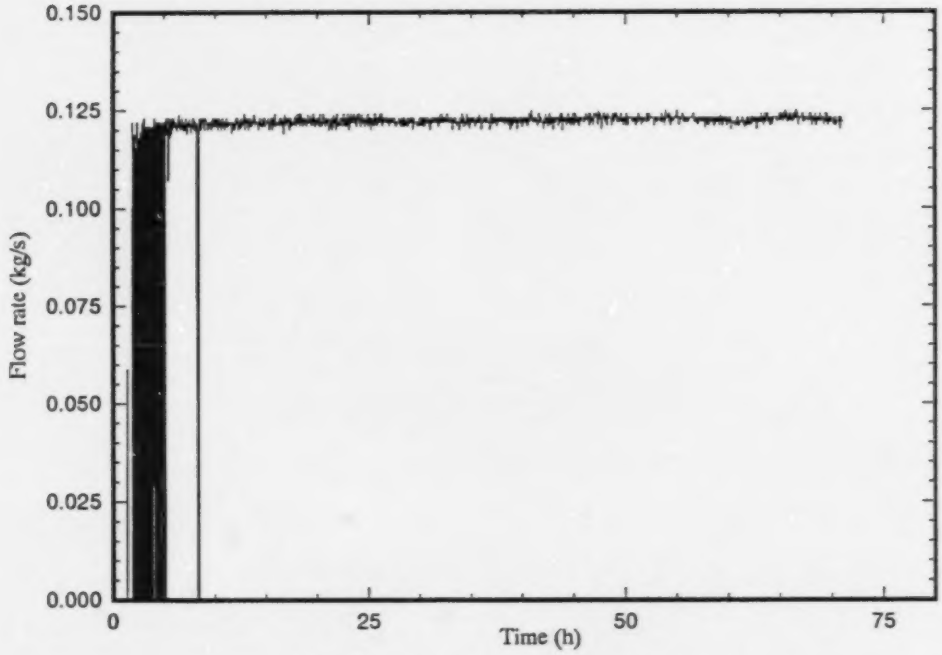

(d) Water flow rate in bypass loop 2

Figure 8.4 Control performance using a proportional control law for a step change in setpoint from 21℃ to 25℃

8.3 Conclusions

The different initial steady state basement air temperatures of 24.5°C and 21.5°C and the different magnitude of change in setpoint for the on-off and proportional control tests respectively does not make it possible to make an objective assessment of the performance of the two different control algorithms. No comparison is possible between the results of this work and the prior results of Dale and Ackerman (1990) because of the different physical configuration of water supply circuits such as the addition of bypass loop 2 used in this work.

Chapter 9
Summary and Future Work

This study has been concerned with four major areas related to the dynamics and control of hydronic floor heating systems. These are model development, numerical methods of solution for the models, comparison of the experimental and simulated dynamic response of the hydronic system installed in the one of the experimental houses at the Alberta Home Heating Research Facility, and experimental tests of two different control algorithms. A summary of the work, results and suggestions for future work based on the work in this study are as follows.

9.1 Summary

1. Models

Two simple models and a full model, have been utilized in this work. The half-pipe and one-pipe models suffer from the disadvantage of no computation of outlet water temperature and no consideration of heat loss to the soil. In order to evaluate advanced computer based control, it is important that the model provide for computation of the outlet water temperature. This is required for control strategies which employ mixing valves and flux control. Furthermore, the domain of the simple model is only a layer of gypsum cement. For these reasons, a full model was developed to represent the actual system. The characteristics of the full model are

i) three layers of materials, gypsum cement, insulation and concrete

ii) backside heat loss to the soil

iii) computation of outlet water temperature

2. Methods of Solution

The numerical methods of solution used for the simple models to obtain steady state temperature profiles and dynamic temperature responses were the grid generation and nonuniform grids method. It was found that the nonuniform grids method used less computation time and memory than grid generation approach so the nonuniform grids method was chosen for obtaining simulation results using the full model. Two different numerical techniques, the finite element and the finite difference methods in conjunction with the nonuniform grids approach were used to predict steady and unsteady state temperatures using the full model. The number of elements used in the finite element method was 6842 while the number of grid points used for the finite difference method was 19068. Since the computation time using the finite element method was about one-half of that required with the finite difference method it is recommended that the finite element method be used in any future studies.

3. Comparison of Simulated Results and Experimental Data

The simulated steady state temperature profiles and the dynamic temperature responses were found to show close agreement with the experimental data that could be collected. The series of simulations were performed to illustrate the sensitivity of the predicted temperature transient responses to any errors in parameter values and physical property values. The results showed that the parameter values of UA and h and the physical properties of the gypsum cement have a significant effect on the dynamic response of the panel surface temperature and the basement air temperature. It is thus reasonable to assume that the mismatch between the experimental dynamic response and the simulated results is due to the inaccuracy of these parameter values and possibly the physical properties of the gypsum cement.

4. Experimental Testing of Two Control Laws

Single tests of on-off and proportional control laws were implemented in the experimental house. The results showed that an overshoot of 0.5°C resulted when the

proportional control algorithm was used while there was undershoot of 0.5°C using the on-off algorithm. However, because the initial steady state basement air temperature was not the same for both tests and the magnitude of the setpoint change was different no valid conclusion concerning their relative performance is possible. Moreover, no comparison to the previous work of Dale and Ackerman (1990) is possible because the system physical configuration used in this work is different.

9.2 Recommendations for Future Work

On the basis of this study it is suggested that the following extensions of this work be given consideration for study.

1. The existing full model should be modified to accommodate a spiral type of tubing layout (cf in Figure 3.2b) so that the performance of the different tubing configurations can be evaluated by simulation.

2. The effect of the location of the tubing (spacing and depth) in the gypsum cement should be studied to establish the most suitable locations for the optimum heat output to the enclosure.

3. The full model should be modified to also handle the situation of no water flow to the circuit so that alternative control strategies/laws can be evaluated by simulation.

4. For investigation of dynamic response of the hydronic system in the upper zone of the experimental house, the full model should be extended to handle the effects of solar radiation and ambient temperature which are two major disturbances in the upper zone.

References

Algren, A.B., "Ground temperature distribution with a floor panel heating system", ASHVE Transactions, Vol.54, 1948, pp.321-338.

Algren, A.B. and Ciscel, B., "Heating panel time response study", ASHVE Transactions, Vol.55, 1949, pp.183-192.

Algren, A.B., Snyder, E.F. and Head, R.R., "Field studies of floor panel control systems - Part II", ASHVE Transactions, Vol.60, 1954, pp.135-156.

Algren, A.B., Snyder, E.F., Locke, J.S., "Field studies of floor panel control systems", ASHRAE Transactions, Vol.59, 1953, pp.173-196.

ASHRAE handbook & product directory 1977 Fundamentals, American Society of Heating, Refrigerating and Air Conditioning Engineers, Inc., third printing, 1978.

Ayres, J.M. and Levy, B.W., "Air temperature gradients in a panel heated room", ASHVE Transactions, Vol.54, 1948, pp.131-142.

Buckley, N.A., "Application of radiant heating saves energy", ASHRAE Journal, September, 1989, pp.17-26.

Dale, J.D. and Ackerman, M.Y., The performance of a radiant panel floor heating system final report, Department of Mechanical Engineering, Department Report No.77, May 1990.

Dongarra, J.J., Moler, C.B., Bunch, J.R. and Stewart, G.W., "LINPACK users' guide", 1984.

Fletcher, C.A.J., "Computational techniques for fluid dynamics, Vol II, specific techniques for different flow categories", Springer-Verlag Berlin Heidelberg, 1988, pp.46-121.

Forta-Fill® Gypsum Concrete Floor Underlayment, "Spec-data sheet", Hacker Industries, Inc., 15111 East Whittier Boulevard, Suite 475, Whittier, CA 90603, August, 1986.

Fortin, A., Fortin, M., Thi, V.C. and Camarero, R., "Simulation numèrique d'ecoulements visqueux dans une turbine hydraulique", EPM/RT-85-4, Ecole Polytechnique, Montreal, Quèbec, 1985.

Friedlander, M., "Premium heating with radiant slabs", Solar Age, April, 1986, pp.66-71.

Gerald, Curtis F., Wheatley, Patrick O., "Applied Numerical Analysis", Addison-Wesley Publishing Co., 4th ed., 1970.

Gilpin, R.R., Dale, J.D., Forest, T.W. and Ackerman, M.Y., "Construction of the Alberta home heating research facility and results for the 1979-1980 heating season", Department of Mechanical Engineering, Department Report No. 23, August 1980.

Grammling, F.J., "Methods for testing hydronic floor heating systems", ASHRAE Transactions, Vol.91, part 2a, 1985, pp.615-623.

Hogan, R.E., "Heat transfer analysis of radiant heating panels - hot water pipes in concrete slab floor", M.S. thesis, Louisiana Tech. University, 1979.

Hulbert, L.E., Nottage, H.B., Franks, C.V., "Heat flow analysis in panel heating or cooling sections: case I - uniformly spaced pipes buried within a solid slab", ASHVE Transactions, Vol.56, 1950, pp.189-204.

Humphreys, C.M., Franks, C.V. and Schutrum, L.F., "Field studies of heat losses from concrete floor panels", ASHVE Transactions, Vol.57, 1951, pp.221-232.

Hutchinson, F.W., "Response and lag in the control of panel heating systems", ASHVE Transactions, Vol.53, 1947, pp.157-176.

Hutchinson, F.W., Mills, D.L., and La Tart, L.J., "Losses from a floor type panel heating system", ASHVE Transactions, Vol.57, 1951, pp.37-50.

Incropera, Frank P., and Dewitt, David P., "Introduction to heat transfer", John Wiley & Sons, Inc., New York, 1985.

Leigh, S.B., "An experimental study of the control of radiant floor heating systems: proportional flux modulation vs. outdoor reset control with indoor temperature offset", ASHRAE Transactions, Vol.97, part 2, 1991, pp.800-808.

Leigh, S.B., "An experimental approach for evaluating control strategies of hydronic radiant floor heating systems", Ph.D. thesis, University of Michigan, 1991.

MacCluer, C.R., "Temperature variations of flux-modulated radiant slab systems", ASHRAE Transactions, Vol.95, part 1, 1989, pp.1010-1014.

MacCluer, C.R., "Analysis and simulation of outdoor reset control of radiant slab heating systems", ASHRAE Transactions, Vol.96, part 1, 1990, pp.1283-1287.

MacCluer, C.R., "The response of radiant heating systems controlled by outdoor reset with feedback", ASHRAE Transactions, Vol.97, part 2, 1991, pp.795-799.

MacCluer, C.R. and Miklavcic, M., "The temperature stability of a radiant slab-on-grade", ASHRAE Transactions, Vol.95, part 1, 1989, pp.1001-1009

Nottage, H.B., Franks, C.V., Hulbert, L.E. and Schutrum, L.F., "Heat flow analysis in panel heating or cooling sections: case II - floor slab on earth with uniformly spaced pipes or tubes at the slab-earth interface", ASHVE Transactions, Vol.59, 1953, pp.527-548.

Poly2d™ users' manual, Rheotek Inc., Cap Rouge, Quebec, 1992.

Rekken, G.M. and Associates Ltd., "Solaroll radiant floor heating", December, 1983.

Shoemaker, Richard Woolsey, "Radiant heating", McGraw-Hill Book Company, Inc. New York, 1954.

Super2d™ users' manual, Rheotek Inc., Cap Rouge, Quebec, 1992.

Zhang, Z., "An experimental study of the transient response of a radiant panel ceiling and enclosure", ASHRAE Transactions, Vol.92, part 2a, 1986, pp.85-94.

Zhang, Z. and Pate, M.B., "A new approach for designing heating panels with embedded tubes", ASHRAE Transactions, Vol.95, part 1, 1989, pp.231-238.

Appendix A

Example: Calculations for the Parameter Values Used for Simulation

1) Initial steady state (First test: shutters open) :

a) Rate of total energy input for the complete system (q_{input}):

$T_{wi} = 44.95$ °C
$T_{wo} = 41.0$ °C
$Cp_w = 4179$ J/kg°C
$\dot{m}_w = 0.149$ kg/s

$$q_{input} = \dot{m}_w \bullet Cp_w \bullet (T_{wi} - T_{wo}) = 2459.55 \text{ W}$$

b) Rate of backside heat loss to the soil (q_{loss}):

Temperatures on the top surface of the insulation at three different positions:
$T_{inu1} = 28.6$ °C
$T_{inu2} = 29.6$ °C
$T_{inu3} = 33.2$ °C

$$T_{aveu1} = \frac{T_{inu1} + T_{inu2} + T_{inu3}}{3} = 30.47 \text{ °C}$$

Temperatures on the bottom surface of the insulation at three different positions:
$T_{inb1} = 20.3$ °C
$T_{inb2} = 20.7$ °C
$T_{inb3} = 20.8$ °C

$$T_{aveb1} = \frac{T_{inb1} + T_{inb2} + T_{inb3}}{3} = 20.6 \text{ °C}$$

$Z_{p2} = 1.136$ W/m°C
$A = 46.22$ m²

$$q_{loss} = Z_{p2} \bullet A \bullet (T_{aveu1} - T_{aveb1}) = 518 \text{ W}$$

c) Rate of energy input to the enclosure (q_{up}):

$$q_{up} = q_{input} - q_{loss} = 1941.47 \text{ W}$$

d) Combined convective and radiative heat transfer coefficient (h):

$T_{surf} = 28.52$ °C
$T_r = 25.8$ °C

$$h = \frac{q_{up}}{A \bullet (T_{surf} - T_r)} = 15.45 \text{ W/m}^2\text{°C}$$

e) Heat transfer coefficient of the ceiling of the lower zone (h_{ceil}):

$Th_{foil} = 0.001$ m
$k_{foil} = 0.18$ W/m°C

$$R_{foil} = \frac{Th_{foil}}{k_{foil}} = 0.00556 \text{ m}^2\text{°C/W}$$

$R_{p2} = 2.11$ m²°C/W
$R_{joist} = 0.2$ m²°C/W
$R_{ceil} = (0.00556 + 2.11 + 0.2)$ m²°C/W = 2.3156 m²°C/W

$$h_{ceil} = \frac{1}{R_{ceil}} = 0.432 \text{ W/m}^2\text{°C}$$

f) Rate of heat loss to the upper zone (q_{ceil}):

$T_{und} = 27.3$ °C
$T_{joist} = 25.0$ °C

$$q_{ceil} = h_{ceil} \bullet A \bullet (T_{und} - T_{joist}) = 45.92 \text{ W}$$

g) Rate of heat loss to the surrounding soil (q_{s2}):

$T_r = 25.8$ °C
$T_{s2} = 6.84$ °C

$$q_{s2} = UA \bullet (T_r - T_{s2}) = 18.96 \bullet UA$$

h) Rate of heat loss to the outdoor through the flue (q_{flue}):

$T_{amb} = 9.7$ °C
ACR = 0.2/hour
H = 2.2606 m
$\rho_{air} = 1.1774$ kg/m^3
$Cp_{air} = 1005.7$ J/kg°C

$$q_{flue} = \frac{ACR}{3600} \bullet A \bullet H \bullet \rho_{air} \bullet Cp_{air} \bullet (T_r - T_{amb}) = 110.66 \text{ W}$$

i) Overall heat transfer coefficient (UA):

$$q_{up} = q_{s2} + q_{ceil} + q_{flue}$$

$$18.96 \bullet UA = q_{up} - q_{ceil} - q_{flue}$$

$$UA = \frac{1941.47 - 45.92 - 110.66}{25.8 - 6.84} = 94 \text{ W/m}^2\text{°C}$$

j) Average temperature at the bottom surface of the concrete (T_{aveco}):

$k_{p3} = 1.731$ W/m°C
$Th_{p3} = 0.1016$ m
$T_{aveb1} = 20.6$ °C

$$q_{loss} = \frac{k_{p3} \bullet A \bullet (T_{aveb1} - T_{aveco})}{Th_{p3}}$$

$$T_{aveco} = T_{aveb1} - \frac{q_{loss} \bullet Th_{p3}}{k_{p3} \bullet A} = 19.94 \text{ °C}$$

k) Thermal conductivity of the soil located under the concrete (k_{s1}):

Four soil temperature readings at 0.33 m below the concrete:
$T_{so1} = 11.94$ °C
$T_{so2} = 12.6$ °C
$T_{so3} = 13.16$ °C
$T_{so4} = 13.31$ °C

$$T_{s1} = \frac{T_{so1} + T_{so2} + T_{so3} + T_{so4}}{4} = 12.75 \text{ °C}$$

$$q_{loss} = \frac{k_{s1} \bullet A \bullet (T_{aveco} - T_{s1})}{0.3302}$$

$$k_{sl} = \frac{q_{loss} \bullet 0.3302}{A \bullet (T_{aveco} - T_{sl})} = 0.5145 \text{ W/m°C}$$

2) Initial steady state (Second test: shutters closed) :

All the calculations are the same as those in part (1).

Initial steady state values for the second test are as follows:

$\dot{m}_w = 0.152$ kg/s
$T_{wi} = 45.7$ °C
$T_{wo} = 41.5$ °C
$T_{inu1} = 30.9$ °C
$T_{inu2} = 31.7$ °C
$T_{inu3} = 34.8$ °C
$T_{inb1} = 21.9$ °C
$T_{inb2} = 22.2$ °C
$T_{inb3} = 22.6$ °C
$T_{surf} = 30.3$ °C
$T_r = 28.4$ °C
$T_{und} = 27.4$ °C
$T_{joist} = 25.2$ °C
$T_{s2} = 15.5$ °C
$T_{amb} = 9.3$ °C
$T_{so1} = 13.3$ °C
$T_{so2} = 13.31$ °C
$T_{so3} = 14.01$ °C
$T_{so4} = 14.27$ °C

The calculated parameter values are in the following:

$q_{input} = 2667.87$ W
$T_{aveu1} = 32.47$ °C
$T_{aveb1} = 22.23$ °C
$q_{loss} = 537.33$ W
$q_{up} = 2130.55$ W
$h = 24.26$ W/m²°C
$q_{ceil} = 43.93$ W
$q_{flue} = 131.27$ W
$UA = 151.577$ W/°C
$T_{aveco} = 21.55$ °C

$T_{s1} = 13.72\ °C$
$k_{s1} = 0.4903\ W/m°C$